Energy efficiency-spectral efficiency tradeoff in interference-limited wireless networks

Ahmad Mahbubul Alam

Thèse

UNIVERSITE
BRETAGNE
LOIRE

THESE INSA Rennes
sous le sceau de l'Université Bretagne Loire
pour obtenir le titre de
DOCTEUR DE L'INSA RENNES
Spécialité : Traitement du signal et de l'image

présentée par

Ahmad Mahbubul Alam

ECOLE DOCTORALE : *MATISSE*
LABORATOIRE : *IETR*

Energy efficiency-spectral efficiency tradeoff in interference-limited wireless networks

Thèse soutenue le 30.03.2017
devant le jury composé de :

Marie-Laure Boucheret
PU, INP Toulouse, Présidente
Marco Di Renzo
CR CNRS HDR, L2S Gif-sur-Yvette, Rapporteur
Jean-Marie Gorce
PU, INSA Lyon, Rapporteur
Luc Deneire
PU, Université Nice-Sophia-Antipolis, Examinateur
Jean-Yves Baudais
CR CNRS, IETR, Co-encadrant
Philippe Mary
MC, INSA Rennes, Co-encadrant
Xavier Lagrange
PU, IMT Atlantique, Directeur de thèse

Energy efficiency-spectral efficiency tradeoff in interference-limited wireless networks

Ahmad Mahbubul Alam

En partenariat avec

Dedication

To my beloved parents without whom I would not be able to come to this beautiful Earth to have a PhD. They will not read this. So if someone does not tell them, they will never know. To my wife Amena Haque and my two years old daughter Mahveen Alam for their unfailing love, patience and the sacrifice of precious time together throughout my PhD. Without them, this report could have been completed much earlier. To my boro chacha, fupu, sister Akhi and mami whom I lost in the last year of my PhD. To all who have encouraged me at any point of my life.

Acknowledgement

It is my pleasure to get the opportunity to express gratitude to all who contributed in the successful completion of my PhD thesis.

First of all, I would like to express my heartily thanks to my thesis supervisor Professor Xavier Lagrange for his constant guidance and supervision throughout the last three years. His confidence in my research work, and careful editing contributed enormously to the bringing up of this thesis. I would also like to express special thanks to my co-supervisors Dr. Philippe Mary and Dr. Jean Yves Baudais for their invaluable guidance, fruitful ideas, and generous advises throughout the whole period of my PhD. I got all kind of support from them in all difficulties I faced during my thesis.

It is also my pleasure to express my sincere thanks to the members of my thesis defence committees, Dr. Marco Di Renzo, Professor Jean-Marie Gorce. Professor Marie-Laure Boucheret and Professor Luc Deneire for reading and evaluating my manuscript that helped me to enrich my thesis.

I would like to thank all my colleagues in IETR for providing a friendly working environment and facilities to complete this thesis. I also express my gratitude to the officials and other staff members who rendered their help during the period of my thesis work. I express my gratitude particularly to Pascal Richard, Katell Kervella, Celine Laube and Aurore Gouin for their kindness help from the beginning of my thesis in all official and administrative steps.

I would like to express my thanks to my friends, and relatives including my in-laws family for their encouragement during my thesis.

I give all my love and thanks to my parents and my brother for their emotional and moral support during my thesis years.

I express my heartiest thanks to my wife for her continuous moral support during all my doctoral work. I express my love to my daughter for the joyful moments she gave me during my PhD thesis.

Contents

List of figures

List of tables

List of acronyms

ASE	Area spectral efficiency
AWGN	Additive white Gaussian noise
BB	Baseband
BPP	Binomial point process
BS	Base station
CCDF	Complementary cumulative distribution function
CCI	Co-channel interference
CDF	Cumulative distribution function
CR	Cognitive radio
CSI	Channel state information
EARTH	Energy Aware Radio and neTwork tecHnologies
EC	Energy consumption
ECG	Energy consumption gain
ECR	Energy consumption rating
ECR-VL	Variable load energy consumption rating
EE	Energy efficiency
EER	Energy efficiency rate
ERG	Energy reduction gain
ESD	Empirical spectral distribution
ETSI	European telecommunication standards institute
FDMA	Frequency division multiple access
FEC	Forward error correction
FFT	Fast Fourier transform
GSM	Global system for mobile communication

ICT	Information and communication technology
IETR	Institute of electronics and telecommunications of Rennes
ISR	Interference-to-signal ratio
ITU	International telecommunication union
iid	Independent and identically distributed
LLN	Law of large numbers
LN	Log-normal
LSD	Limit spectral distribution
LTE	Long term evolution
MIMO	Multiple input multiple output
MISO	Multiple input single output
MMSE	Minimum mean square error
MRT	Maximal ratio transmission
MU-MIMO	Multi-user multiple input multiple output
MU-MISO	Multi-user multiple input single output
NSR	Noise-to-signal ratio
OFDM	Orthogonal frequency division multiplexing
OPERA-Net	Optimizing Power Efficiency in mobile RAdio Networks
OPEX	Operational expenditures
PA	Power amplifier
PAPR	peak-to-average-power ratio
PDF	Probability density function
PGFL	Probability generating functional
PMF	Probability mass function
PPP	Poisson point process
PS	Power supply
QoS	Quality of service
RF	Radio frequency
RHS	Right hand side
RMT	Random matrix theory
RRM	Radio resource management
r.v.	Random variable
SC	Superposition coding
SDMA	Space division multiple access

SE	Spectral efficiency
SGINR	Signal-to-generating-interference-plus-noise ratio
SIMO	Single input multiple output
SINR	Signal-to-interference-plus-noise ratio
SISO	Single input single output
SLNR	Signal-to-leakage-and-noise ratio
SNR	Signal-to-noise ratio
SU-MIMO	Single-user multiple input multiple output
SVD	Singular value decomposition
TDMA	Time division multiple access
TEER	Telecommunication energy efficiency ratio
TEPN	Toward energy proportional networks
u.a.	Unit area
WiMAX	Worldwide interoperability for microwave access
ZF	Zero-forcing

Mathematical notations and variables

Mathematical notations

$\|\|\mathbf{A}\|\|_2$	Spectral norm of matrix $\mathbf{A}$
$\limsup_M \|\|\mathbf{A}\|\|_2$	limit superior of $\|\|\mathbf{A}\|\|_2$, i.e. for every $\epsilon > 0$, there exists $M_0(\epsilon)$ such that $\|\|\mathbf{A}\|\|_2 \leq \limsup_M \|\|\mathbf{A}\|\|_2 + \epsilon$ for $\forall M > M_0(\epsilon)$
$B \setminus A$	In B but not in A
$B \subset \mathbb{R}^d$	B is a subset of $\mathbb{R}^d$
$\|B\|$	Lebesgue measure of the Borel subset B
csc	Cosecant function
$\mathbb{C}$	The space of complex numbers
$\mathbb{C}^+$	$\mathbb{C} \setminus \mathbb{R}$
$\mathscr{CN}(0, \mathbf{I}_M)$	Complex normal r.v. variable with mean 0 and covariance matrix $\mathbf{I}_M$
δ_x	Dirac measure
$\delta_x(B)$	$\equiv \mathbf{1}_B(x)$
$\Delta(B)$	Intensity measure of a point process in B
$\frac{\partial \eta_{\mathrm{EE}}}{\partial \eta_{\mathrm{SE}}}$	Derivative of η_{EE} w.r.t. η_{SE}
e	Exponential function
$\mathrm{E}[X]$	Expectation of r.v. X
$\mathrm{E}_y[X]$	Expectation of X over y
$\mathrm{E}_y[X\|z]$	Expectation of X over y and conditioned on z
F	Real-valued bounded measurable function
F^Δ	Empirical cumulative distribution function of Δ, empirical spectral distribution

F_l^{Δ}	Limiting empirical cumulative distribution function of Δ, limit spectral distribution
$f(x)$	Function of x
${}_2F_1(a,b,c,z)$	Gauss hypergeometric function
$\forall$	For all
$G[f]$	Probability generating functional for f
$[\mathbf{G}_0]_k$	k-th column of $\mathbf{G}_0$
$\mathbf{I}_M$	Identity matrix of size $M \times M$
$\Im[z]$	Imaginary part of z
$\mathscr{LN}(0,\sigma)$	LN r.v. characterizing shadowing with zero mean and σ be the standard deviation in dB
M_k	k-th order moment of F^{Δ}
$\mu_{\mathbf{X}}(A)$	Empirical probability measure of the eigenvalues of $\mathbf{X}$ in A
$\mathbb{N}$	The space of natural numbers
$\binom{n}{k}$	n choose k
$n!$	Factorial of n
$\mathscr{N}(d\mu_{ik}, d^2\sigma^2)$	Normal r.v. with mean $d\mu_{ik}$ and standard deviation $d^2\sigma^2$ in natural logarithm
$(\Omega, \mathscr{F}, \mathrm{P})$	Probability space Ω with σ-field $\mathscr{F}$ and measure P
$\Longrightarrow$	Or
Φ	Point process
$\Phi(B)$	Number of points of Φ in B
$P^{!x}$	Reduced palm measure of the point process Φ
$\mathrm{P}[A]$	Probability of event A
$\prod_{x\in\Phi} f(x)$	Product of function f evaluated at a point x of the point process Φ
Q	Marcuum function that provides the CCDF of a standard normal r.v.
Q^{-1}	Inverse of the Q function
$\mathbb{R}$	The space of real numbers
$\mathbb{R}^d$	Real d-dimensional Euclidean space
$\mathbb{R}^+$	The space of non-negative real numbers
$(\mathscr{R}, \mathscr{G})$	$\mathscr{G}$ is a σ-field on $\mathscr{R}$
$\mathrm{supp}(F)$	Support of F
$\sum_{x\in\Phi} f(x)$	Sum of function f evaluated at a point x of Φ
tr ($\mathbf{X}$)	Trace of $\mathbf{X}$, sum of the elements on the main diagonal of $\mathbf{X}$
$\mathrm{var}[X]$	Variance of r.v. X

$\mathrm{var}_y[X]$	Variance of X over y
$\mathrm{var}_y[X\|z]$	Variance of X over y and conditioned on z
W_0	Positive branch of the Lambert function
W_{-1}	Negative branch of the Lambert function
$\mathbf{X}$	Matrix
$\mathbf{X}^{-1}$	Inverse of matrix $\mathbf{X}$
$\mathbf{X}^H$	Hermitian transpose of $\mathbf{X}$
$\mathbf{X}^T$	Transpose of $\mathbf{X}$
$\mathbf{X}_{ij}$	Entry (i,j) of matrix $\mathbf{X}$
$\mathbf{y}$	Column vector
$\{\cdot\}$	Elements in a set
$\mathbf{1}_B(x)$	Indicator function of $x \in B$
$\|\cdot\|$	L_2 vector norm
$\lim_{x\to\infty} f(x) = q$	$f(x)$ approaches the limit q as x approaches ∞
$\underset{a.r.}{\sim}$	Convergence in asymptotic regime

Variables

A, B	Borel subsets of $\mathbb{R}^d$
$A_{i,j}$	Coefficients of $f(v,\alpha)$ with $i+j \leq 5$
A_C	Coverage area
a	Power amplifier factor
α	Path loss exponent
$B_{i,j}$	Coefficients of $G(v,\alpha)$ with $i+j \leq 5$
b	Total power consumption at the minimum non-zero load
b_E	Bit per energy
β_I	Weighting coefficient for I% of the load
c	Non-transmission power for BB unit, PS unit and cooling
$\bar{\mathbf{D}}_{0k}$	A square diagonal matrix filled by the path losses from the 0-th BS to the active users in the network, except the k-th user
$\bar{\mathbf{D}}_{ijk}$	Square diagonal matrix filled by the path losses from the i-th BS to all active users in the network except the j-th and the k-th user
d	$\log_e 10/10$

Δ	Square diagonal matrix filled by the eigenvalues
δ_{0k}	Non-zero complex scalar corresponding to the k-th user in the 0-th cell
E_b	Energy per bit
E_n	Energy consumption of the n-th system
η_{EE}	Energy efficiency
η_{EE}^{*}	Maximum EE
$\eta_{\mathrm{EE}}^{(\epsilon)}$	ϵ-EE
η_{SE}	Spectral efficiency
η_{SE}^{*}	η_{SE} corresponding to maximum EE
$\eta_{\mathrm{SE}}^{(\epsilon)}$	ϵ-SE
$f(v,\alpha)$	ISR without shadowing
$f_s(v,\alpha)$	ISR with shadowing
$f_{r_{0k}}(r_{0k})$	PDF of r_{0k}
$G(v,\alpha)$	$\frac{\sum_{i\geq 1} r_{ik}^{-2\alpha}}{\left(\sum_{i\geq 1} r_{ik}^{-\alpha}\right)^2}$
$\mathbf{G}_0$	Concatenated non-normalized precoding vectors for the users in cell 0
$\mathbf{g}_{0k}$	Eigenvector in the eigenspace corresponding to $\lambda_{\max}$ (for the k-th user in the 0-th cell)
$\Gamma(\cdot)$	Gamma function
γ	SINR of a user in hexagonal network
$\gamma(u_0)$	SINR of a user in a cell with u_0 users in PPP network
γ_{au}	$\lim_{N_{au},M\to+\infty} \frac{N_{au}}{M}$
$\mathbf{H}_0$	Concatenated channels for the users in cell 0
$\bar{\mathbf{H}}_{0k}$	Concatenated fading channels from the 0-th BS to the active users in the network, except the k-th user
$\bar{\mathbf{H}}_{ijk}$	Concatenated fading channels from the i-th BS to all active users in the network except the j-th and the k-th user
$\mathbf{h}_{ik}$	Vector representing the complex Gaussian distributed channel between the i-th BS and the k-th user
I	Aggregated interference power
K	Frequency reuse factor
L	Propagation constant
l	Frequency reuse distance
λ_b	BS density

λ_u	User density
λ_{au}	Active user density
$\lambda_{\max}$	Maximum eigenvalue
u_{ik}	Mean of the signal received by the k-th user from the i-th BS (dB)
u_{F_n}	Mean of the numerator of $f_s(v,\alpha)$ (dB)
u_F	Mean of $f_s(v,\alpha)$ (dB)
u_N	Mean of NSR (dB)
u_γ	Mean of γ (dB)
n_k	AWGN for the k-th user
$\mu_{NL},\sigma_{NL},\mu_{FL},\sigma_{FL}$	Linear number corresponding to μ_N, σ_N, μ_F and σ_F
μ	Constant and the value is 3.5
N_{au}	Total number of active users in PPP network
n	Number of users available in a cell
P	Consumed power
P_f	Peak power
P_C	Average power consumed for A_C
P_I	Power consumption at I% of the load
P_{i}	Input power to an element
P_{o}	Output power of an element
P_{out}	Power input to an antenna
$P_{\max}$	P_{out} at the maximum load
P_{total}	Total power consumption of a BS
P_{RF}	Power consumed by RF unit
P_{BB}	Power consumed by BB unit when $M=1$
P_0	power consumption at the minimum non-zero P_{out} when $M=1$
P_{ik}	Power received by the k-th user at distance r_{ik} from the BS $i \geq 0$
P_t	Total transmit power of a BS
P_A	Average power consumption per u.a.
Φ_u	Point process for the BS group with u users
R	Achievable transmission rate
R_a	Radius of the PPP network
$R_u(u_0)$	Ergodic rate of a typical user when there are u_0 active users in the cell
$\hat{R}_u(u_0)$	Upper bound of $R_u(u_0)$
$R_{\mathrm{BS}}(u_0)$	Ergodic throughput of a BS with u_0 active users

R_{BS}	Ergodic throughput of a typical BS averaged over the number of active users
r_H	Radius of a hexagonal cell
r_{ik}	Distance from the i-th BS to the k-th user
ρ	Ratio between BS density and user density
σ^2	Variance of the signal for a user with shadowing (dB)
$\sigma^2_{F_n}$	Variance of the numerator of $f_s(v,\alpha)$ (dB)
σ^2_F	Variance of $f_s(v,\alpha)$ (dB)
σ^2_N	Variance of NSR with shadowing (dB)
σ^2_n	Noise power (dB)
σ^2_γ	Variance of γ in dB
$\bar{\Sigma}$	Singular value matrix
T_f	Maximum throughput
T_I	Throughput at I% of the load
u_i	Number of users in the i-th cell
$\mathbf{U},\mathbf{V}$	Unitary matrix
v	Normalized distance defined as r_{0k}/r_H
w	Channel bandwidth when $K=1$
$\mathbf{w}_{ij}$	Precoding vector for the j-th user in the i-th cell
x_{ij}	Transmitted symbol for the j-th user in the i-th cell
X	r.v. accounting for the random channel power gain
Y_{ik}	LN r.v. characterizing shadowing for the k-th user from BS $i \geq 0$
y_k	The signal received by the k-th user from the typical 0-th BS

Résumé étendu

Cette thèse caractérise la région d'efficacité énergétique et spectrale (EE-SE) d'un réseau cellulaire limité en interférences lorsque la consommation des circuits est prise en compte. Nous caractérisons en premier la région EE-SE d'un réseau cellulaire hexagonal avec un seul utilisateur par cellule, en considérant différentes facteurs de réutilisation de fréquence et avec ou sans masquage. La région d'efficacité énergétique et d'efficacité spectrale par unité de surface (EE-ASE) est ensuite étudiée avec des processus de Poisson ponctuels (PPP) et un réseau à entrée, sortie et utilisateur multiples (MU-MISO) utilisant un précodeur à rapport signal sur fuite plus bruit (SLNR).

Chapitre 1 : introduction

Ce chapitre présente les motivations et le contexte des études de compromis EE-SE. Cela est ensuite suivi par une description de la structure et des contribution de la thèse. Le chapitre se termine par la liste des publications relative à ces travaux de thèse.

Chapitre 2 : préliminaires mathématiques

Les travaux exposés au chapitre 5 combinent quelques résultats fondamentaux de la théorie de matrices aléatoires (RMT) et des PPP, mobilisant les outils de géométrie stochastique et plus particulièrement les processus ponctuels. Ce chapitre résume les définitions, propriétés, lemmes ou théorèmes importants de la géométrie stochastique et RMT qui seront utilisés par la suite.

Ce chapitre illustre deux des plus importants théorèmes de la littérature relative aux PPP : les théorème de Slivnyak et de Campbell. Le théorème de Slivnyak établit que la statistique d'un PPP conditionnée à un point est la même que celle du PPP en entier. L'application de ce théorème se produit dans les réseaux sans fil lorsque le conditionnement est effectué relativement à la

position de l'émetteur ou du récepteur. D'un autre côté, le théorème de Campbell est utilisé pour calculer la moyenne de la somme de fonctions évaluées à la position des point du processus ponctuel.

La transformée de Stieltjes est l'un des outils les plus importants utilisé pour résoudre les problèmes relatifs aux grandes matrices aléatoires. Dans le chapitre 5, les puissances des interférences et du signal utile sont calculées en utilisant la transformée de Stieltjes de la distribution spectrale limite (LSD) de matrices hermitiennes, qui est la transformée de Stieltjes de la distribution spectrale empirique (ESD) lorsque la taille des matrices croît. Le résultat obtenu pour la LSD des matrices de grande taille peut être utilisé pour approcher les résultats de l'ESD de matrice de taille finie. Ce chapitre présente les définitions de la transformée de Stieltjes, de la LSD et de l'ESD. Un théorème très utile de Silverstein et Bai sur la convergence de l'ESD vers la LSD est également présenté et qui sera particulièrement utile dans le chapitre 5. De plus, quelques résultats importants (lemme d'inversion de matrice, lemme de la trace, lemme de la perturbation de rang 1...) sont fournis.

Chapitre 3 : état de l'art

Dans ce chapitre, nous introduisons la SE qui est la métrique de performance conventionnelle des communications dans fil. La SE indique si le spectre est utilisé efficacement mais ne donne pas d'indication sur l'efficacité avec laquelle l'énergie est consommée. Un aperçu de la métrique la plus commune pour quantifié l'efficacité énergétique (EE) est ensuite présenté, incluant le bit par Joule qui mesure la quantité de bits distribués par le réseau par unité d'énergie consommée. Cette mesure est utilisée pour évaluer l'efficacité énergétique d'un canal AWGN dans ce chapitre, et aussi pour un réseau hexagonal dans le chapitre 4. Cependant, la métrique est normalisée par la bande passante du système pour quantifier l'EE dans le chapitre 5.

Des modèles de consommation de puissance et de réseaux sont nécessaires pour calculer l'EE et la SE. Une description détaillée des modèles de consommation linéaires, qui sont les plus communément utilisés dans la littérature, sont présentés. Ces modèles sont simples et permettent de calculer l'EE avec une précision suffisante. Principalement, la puissance consommée par l'amplificateur de puissance (PA) est proportionnelle à la puissance de sortie et la consommation des autres composants est relativement constante. Cela justifie l'approximation linéaire de la consommation des BS en fonction de la charge. Selon le modèle de consommation de puissance

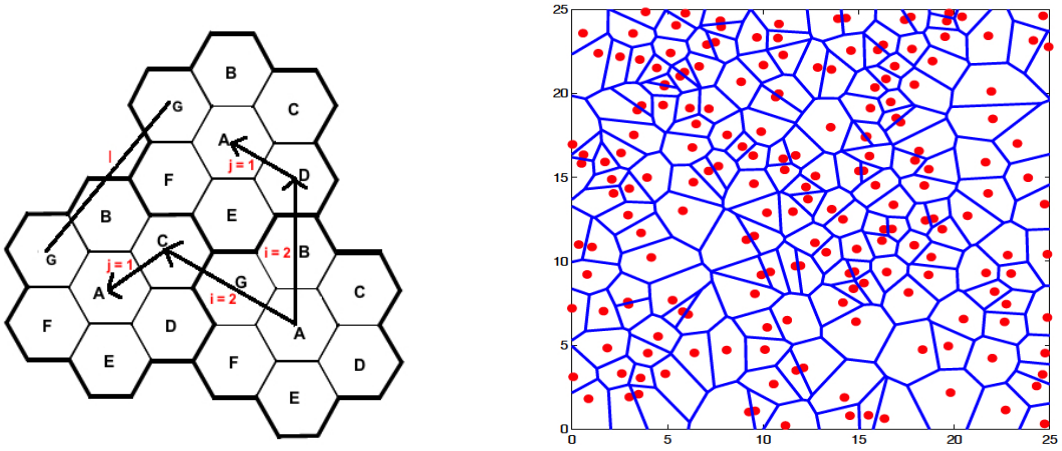

(a) Réseau cellulaire hexagonal [4] (b) Réseau PPP [5]

FIGURE 1 – Modèles réseau

linéaire, la consommation totale d'une BS peut être écrite comme

$$P_{\text{total}} = aP_t + b, \tag{1}$$

Où a est déterminé par l'efficacité du PA, P_t est la puissance d'émission et b est la consommation de puissance du circuit statique. Considérant en outre que la consommation d'énergie de l'unité d'alimentation en courant continu (PS), de l'unité de bande de base (BB) et du système de refroidissement n'est pas à l'échelle du nombre de unité de radiofréquence (RF), (1) peut être écrit comme [12]

$$P_{\text{total}} = aP_t + MP_{\text{RF}} + c, \tag{2}$$

Où M est le nombre d'unité RF, P_{RF} est la puissance consommée par unité RF et c représente la puissance de non transmission pour l'unité BB, l'unité PS et le refroidissement. Comme le montre la Fig. 1, deux types de modèles de réseau existent dans la littérature : le réseau régulier hexagonal avec des positions fixes des BS et le réseau PPP avec des positions aléatoires. Le réseau hexagonal modélise grossièrement la réalité et pose des difficultés d'analyse qui peuvent être résolues avec les réseaux PPP.

L'EE étant un sujet de recherche important, plusieurs solutions ont été proposées pour rendre les réseaux d'accès cellulaires efficacent en énergie. Un rapide survol des méthodes

dans le cadre d'un modèle à 3 couches est présenté dans ce chapitre, et sont la couche des composants, la couche des techniques de transmission et de gestion de la ressource radio et enfin la couche d'architecture cellulaire. L'amélioration de l'EE des couches les plus basses peut également améliorer l'EE des couches supérieures. L'approche au niveau des composants consiste principalement à réduire la consommation du PA. Le réseau cellulaire montre une grande variation spatiale et temporelle du trafic. La consommation d'énergie peut être réduite en adaptant les techniques de transmission, les schémas d'allocation des ressources et le nombre de points d'accès tout en maintenant la couverture souhaitée, la capacité et d'autres mesures de la qualité de service (QoS).

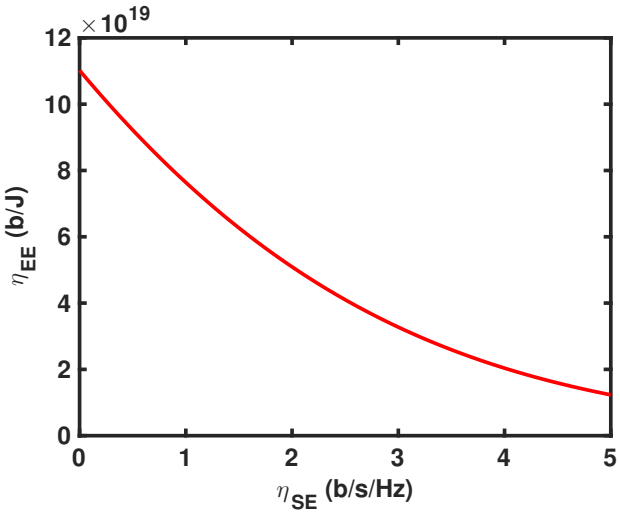

FIGURE 2 – EE vs. SE pour le canal AWGN avec P_t seulement

Nous terminons le chapitre en revisitant les caractéristiques de la relation EE-SE dans un canal AWGN avec un modèle de consommation d'énergie linéaire. Il est observé dans la Fig. 2 que l'EE décroit toujours avec l'augmentation de la SE quand seule la puissance transmise est considérée. Quand la puissance statique des circuits est prise en compte, il y a une large partie linéaire où l'EE augmente avec la SE avant de décroître, comme illustré dans la Fig. 3. Cependant, lorsque la puissance transmise domine la puissance statique, l'EE décroît avec l'augmentation de la SE. On note également que l'EE comme la SE décroissent avec l'augmentation du facteur de puissance du PA. Cependant, même si une forte valeur de la SE optimale est obtenue lorsque la puissance statique augmente, l'EE optimale reste faible.

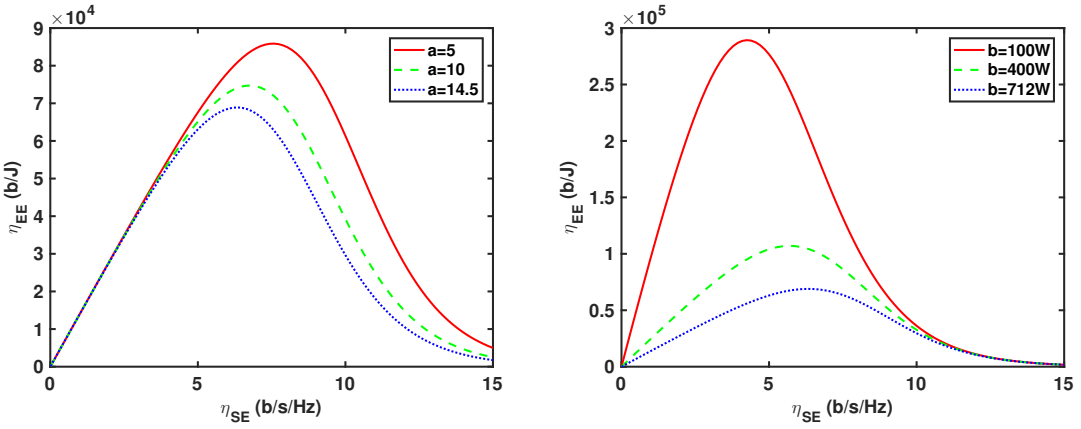

(a) $b = 712$W (b) $a = 14.5$

FIGURE 3 – EE vs. SE pour un canal AWGN en considérant la consommation d'énergie du circuit statique et dynamique

Chapitre 4 : compromis EE-SE dans un réseau cellulaire hexagonal

Dans ce chapitre, nous étudions le compromis EE-SE dans un réseau hexagonal homogène limité par les interférences, avec un seul utilisateur par cellule, en considérant le facteur de réutilisation de fréquences (FRF) et le phénomène de masquage. De plus, les BS comme les utilisateurs sont équipés d'une seule antenne. Nous obtenons une expression paramétrique du rapport interférence sur signal (ISR) pour différents FRF par une approche de régression non linéaire. L'expression de l'ESR nous permet d'analyser le compromis EE-SE pour plusieurs FRF et lorsque seul l'affaiblissement de propagation est pris en compte. Lorsque le phénomène de masquage est pris en compte en plus de l'affaiblissement de propagation, la capacité au sens de Shannon n'est pas définie et nous utilisons l'ϵ-SE et l'ϵ-SE définis comme

$$\eta_{\mathrm{SE}}^{\epsilon} = \sup\left\{E : \mathrm{P}\left[\eta_{\mathrm{SE}} < E\right] \leq \epsilon\right\} \tag{3}$$

$$\eta_{\mathrm{EE}}^{\epsilon} = \frac{\eta_{\mathrm{SE}}^{\epsilon}}{P_{\mathrm{totale}}} \tag{4}$$

avec E l'efficacité spectrale recherchée et ϵ la probabilité de coupure cible. Nous proposons une approximation des fonctions de répartition (CDF) du rapport signal sur interférence plus bruit (SINR) pour évaluer l'ϵ-EE-SE. Les expressions de l'ISR et de la CDF du SINR sont confirmés par des simulations Monte Carlo, comme illustré dans la Fig. 4.

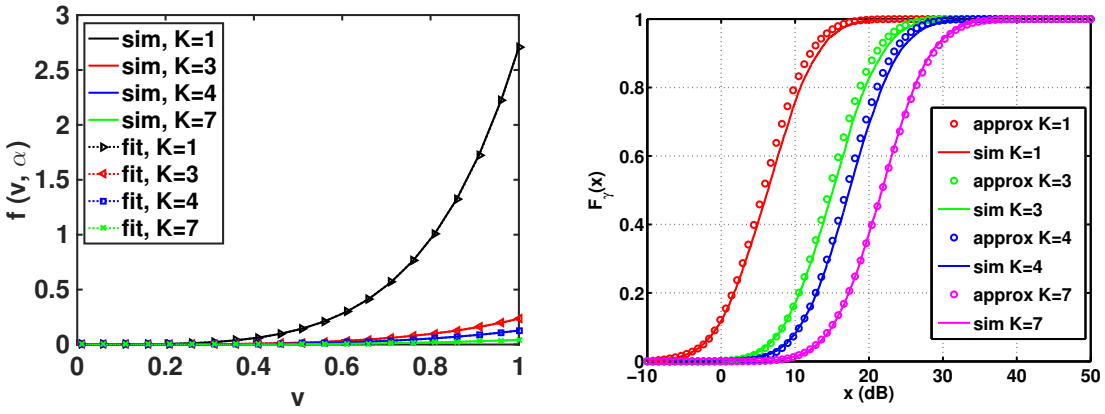

(a) $f(v,\alpha)$ vs. v à $\alpha = 3.5$

(b) CDF du SINR avec masquage

FIGURE 4 – Validation de $f(v,\alpha)$ et du CDF approché du SINR avec des simulations

.

La Fig. 5 montre les courbes de compromis EE-SE avec une large partie linéaire comme dans le cas du canal AWGN. La SE converge vers une limite donnée par le réseau limité en interférences. Il y a une faible augmentation de la SE après le compromis optimal EE-SE et avant un effondrement de l'EE lorsque la puissance transmise continue à augmenter. La Fig. 6 illustre les effets de ϵ sur la SE et l'EE optimales respectivement pour des FRF différents lorsque $v = 0.5$. Les résultats des Figs. 5 et 6 montrent qu'un FRF de 1 pour des régions proches de la BS ou un FRF plus élevé pour des régions proches du bord de la cellule optimise le compromis EE-SE quand le phénomène de masquage n'est pas considérée. De plus, un meilleur compromis EE-SE peut être obtenu avec une plus forte valeur de coupure (epsilon) lorsque le masquage est considéré. Un FRF de 1 est le meilleur choix pour une forte valeur de coupure, même à une faible distance de $v = 0.5$, à cause d'une décroissance du SINR. Cependant, un fort ϵ signifie une QoS faible donc n'est pas nécessairement souhaitable.

Chapitre 5 : compromis EE-ASE dans un réseau PPP

Nous dérivons une expression analytique de l'ASE pour un réseau cellullaire MU-MISO avec une topologie aléatoire, c.-à-d. les BS et les utilisateurs sont modélisés par des PPP homogènes et indépendants. Un précodeur SLNR est considéré en régime asymptotique, c.-à-d. avec un nombre d'antennes M et d'utilisateurs N_u qui croissent vers l'infinie. L'EE est obtenue en utilisant le modèle linéaire de la consommation dans (2). Les Figs. 7a et 7b montre le compromis EE-ASE

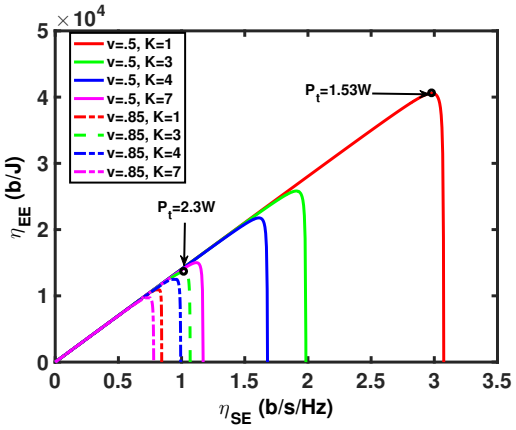

(a) Sans phénomène de masquage

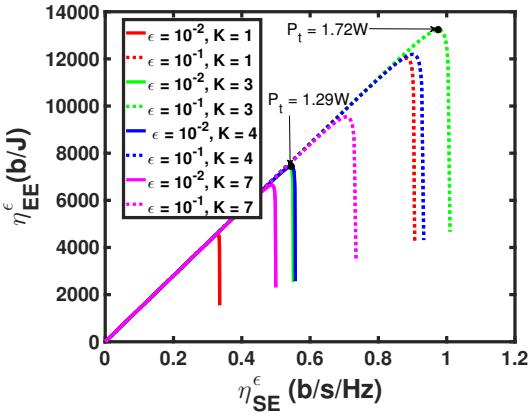

(b) Avec phénomène de masquage à $\nu = 0.5$

FIGURE 5 – Le compromis EE-SE dans un réseau hexagonal

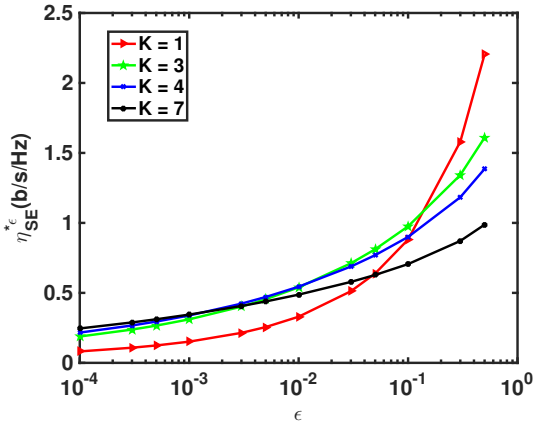

(a) Optimal ϵ-SE vs. ϵ

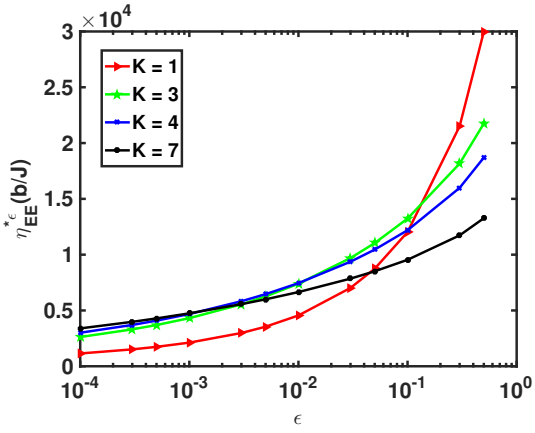

(b) Optimal ϵ-EE vs. ϵ

FIGURE 6 – Variation de ϵ-SE et ϵ-EE optimales avec ϵ à $\nu = 0.5$

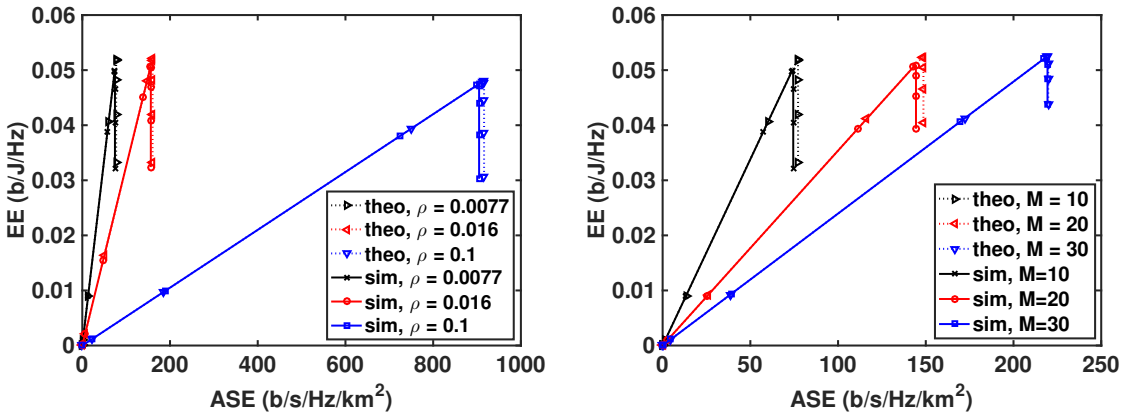

(a) $M = 10$ (b) $\rho = 0.0077$

FIGURE 7 – EE vs. ASE pour précodeur SLNR avec une densité d'utilisateurs $\lambda_u = 5 \cdot 10^{-4}$ m^{-2}, min. $N_u = 2500$

en fonction du ratio de densité BS-utilisateurs, ρ, et le nombre d'antennes M respectivement. Les expressions théoriques de l'ASE et de l'EE sont très proches des valeurs obtenues par simulation Monte Carlo, quand bien même le nombre d'antennes et d'utilisateurs sont faibles, c.à.d $M = 10$ et $N_u = 2500$ respectivement, et cela sur une large plage de valeurs de paramètres du systèmes. Les résultats montrent que le compromis ASE-EE a une large partie linéaire avant une forte décroissance de l'EE, comme pour le réseau hexagonal.

Nous comparons le compromis EE-ASE du précodeur SLNR avec un précodeur de forçage à zéro (ZF) dan la Fig. 8. Les résultats montrent que le précodeur SLNR est plus performant que le précodeur ZF, généralement étudié dans la littérature lorsque les BS sont modélisées par un PPP. Cela implique un meilleur SINR avec le précodeur SLNR qu'avec le précodeur ZF.

Les résultats numériques du précodeur SLNR montrent que déployer plus de BS ou plus d'antennes par BS augmente l'ASE lorsque la densité des utilisateur est fixe, mais le gain dépend du rapport de densité BS-utilisateurs et du nombre d'antennes. L'ASE croît linéairement avec le nombre d'antennes ou la densité des BS tant que le nombre d'utilisateurs par cellule est grand comparé au nombre d'antennes par BS, autrement le gain décroît. C'est ce qui est illustré dans la Fig. 9, où l'ASE ne croît pas linéairement avec M lorsque $\rho = 0.1$. En outre, l'ASE ne croît pas linéairement avec ρ pour $M = 30$.

Cela indique une baisse significative de l'EE avec le nombre d'antennes à $\rho = 0.1$ dans la Fig. 10a . D'un autre côté, la probabilité d'activité des BS décroît avec la densité de celles-ci.

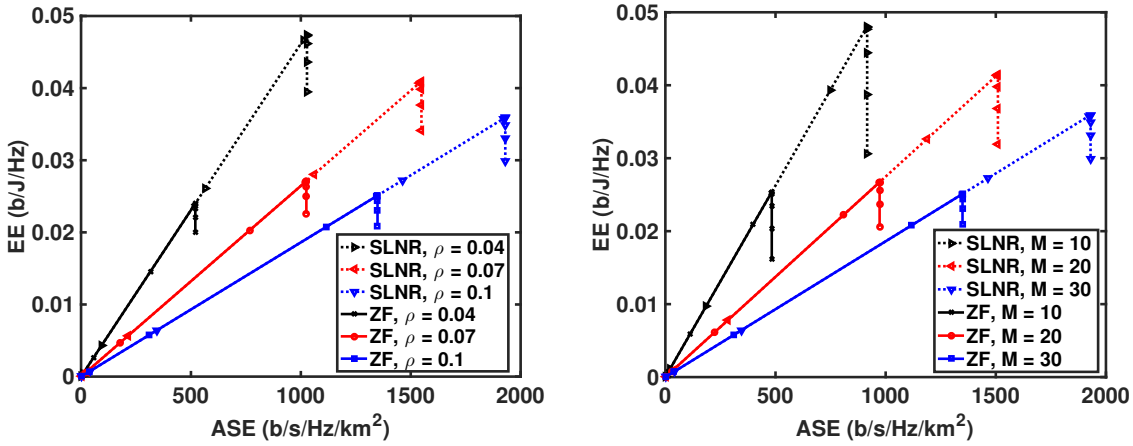

(a) $M = 30$ (b) $\rho = 0.1$

FIGURE 8 – Comparaison du compromis EE-ASE du précodeur SLNR avec précodeur ZF avec $\lambda_u = 5 \cdot 10^{-4}$ m^{-2}, le nombre maximum d'utilisateurs servi dans une cellule, $u_{\max} = M$

La conséquence est que l'EE augmente seulement lorsque l'augmentation de l'ASE domine l'augmentation de la puissance consommée par unité de surface. Cependant, la consommation d'énergie moyenne par unité de surface augmente linéairement avec la densité BS pour la plage de ρ considérée. Par conséquent, une diminution significative de l'EE est observée dans le Fig. 10b pour $M = 30$. Par ailleurs, lorsque la densité des utilisateurs augment avec un ratio de densité BS-utilisateurs fixe, l'ASE dans la région limitée par les interférences croît linéairement avec la densité des BS, c.-à-d. λ_b, alors que le débit ergodique d'un utilisateur typique reste le même. Le taux de croissante de la puissance consommée par unité de surface reste également constante car le ratio fixe de densités BS-utilisateurs conduit à une EE constante lorsque la densité de BS augmente.

Chapitre 6 : conclusions et travaux futurs

Ce chapitre présente un résumé ainsi que des extensions potentielles des travaux réalisés dans cette thèse, par exemple, développer les expressions théoriques pour le compromis EE-ASE en utilisant le précodeur minimum mean square error (MMSE) dans les réseaux PPP, étudier l'impact de la désactivation des BS, etc.

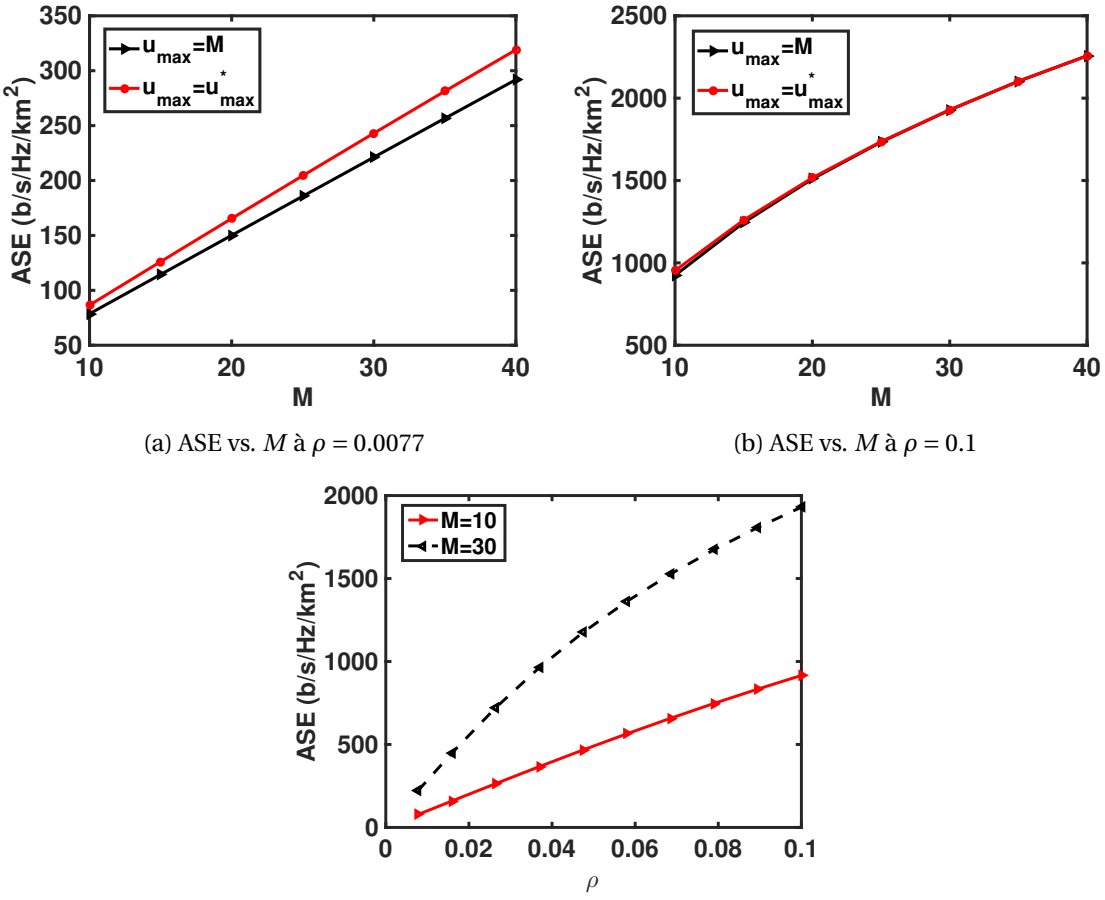

(a) ASE vs. M à $\rho = 0.0077$

(b) ASE vs. M à $\rho = 0.1$

(c) ASE vs. ρ à $u_{\max} = M$

FIGURE 9 – Effet du nombre d'antennes et ρ sur l'ASE avec $N_u = 5000$, $\lambda_u = 5 \cdot 10^{-4}$ m^{-2} et $P_t = 40$ dBm

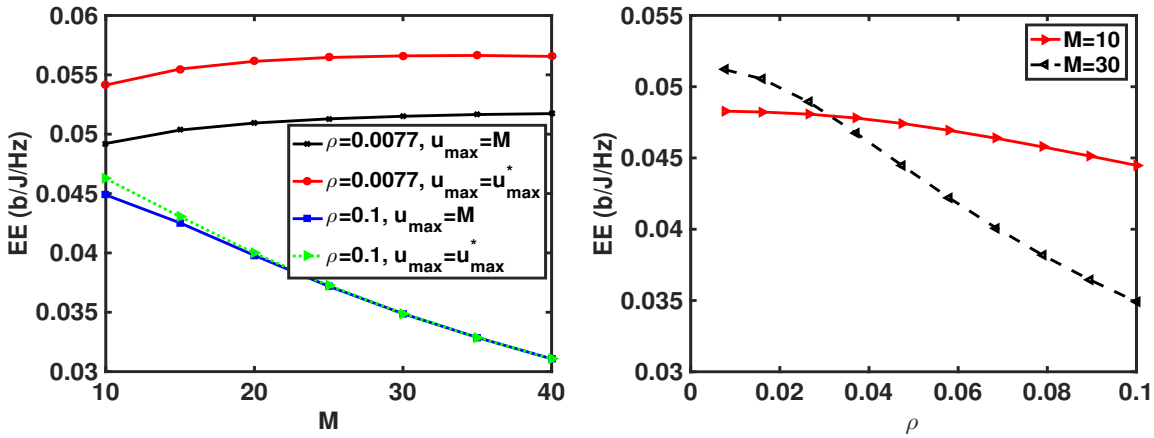

(a) EE vs. M

(b) EE vs. ρ à $u_{\max} = M$

FIGURE 10 – Variation de l'EE en fonction du nombre d'antennes et ρ avec $\lambda_u = 5 \cdot 10^{-4}$ m^{-2} and $P_t = 40$ dBm

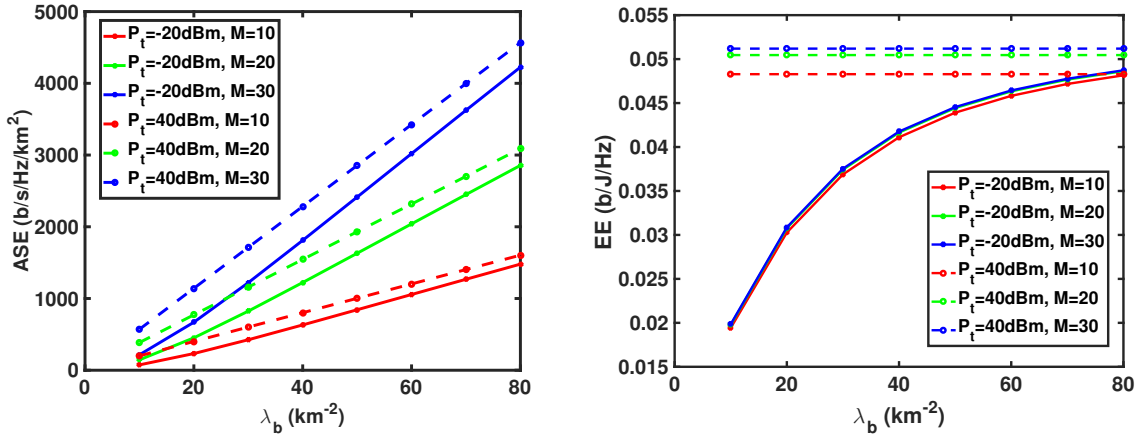

(a) ASE vs. densité des BS à $\rho = 0.0077$

(b) EE vs. densité des BS à $\rho = 0.0077$

FIGURE 11 – Variation de ASE et EE avec densité des BS à $N_u = 5000$ et $u_{\max} = M$

Chapter 1

Introduction

This thesis is focused on characterizing the energy efficiency-spectral efficiency (EE-SE) region for interference limited cellular networks considering the static power consumption. However, we also revisit the EE-SE tradeoff for an additive white Gaussian noise (AWGN) channel as a part of literature review. The original work starts with characterizing the EE-SE region of a hexagonal cellular network considering different frequency reuse factors both with and without shadowing. Subsequently, the energy efficiency-area spectral efficiency (EE-ASE) region is investigated for multi-user multiple input single output (MU-MISO) Poisson point process (PPP) network when signal-to-leakage-and-noise ratio (SLNR) precoder is used.

1.1 Background and motivation

The design and evolution of wireless networks is guided by the continuously increasing data rate demand of customers for high quality digital service. The exponentially increasing data rate requirement triggers the demand for high SE, which is a measure of how efficiently limited frequency spectrum is utilized. The deployment densification of wireless networks, i.e. micro and femto cell in long term evolution (LTE), multiple input multiple output (MIMO) technology, and reusing the frequency bandwidth over relatively small areas already appear as a suitable answer to meet that demand [13, 14].

The roll-out densification leads to an elevation of the energy consumption of communication networks. The information and communication technology (ICT) industry currently contributes to 2% of total worldwide carbon emissions, and this contribution is expected to double over the next 10 years with exponential increase in ICT sector [15]. Designing green wireless networks

has become increasingly important in order to limit the electricity bill and the greenhouse gas emission. Therefore, one of the major concerns for the next generation of wireless networks is EE, which measures how efficiently energy is used to transmit information [16, 17]. Obviously, the reduction of the energy consumption is not the only target to be pursued, and therefore the investigation of EE-SE tradeoff becomes increasingly important.

A large amount of works has been conducted to the problem of EE in wireless communications, see for instance [18] and references therein. The authors in [19] provided fundamental EE-SE tradeoff using PPP for several multiplexing technologies, i.e. time division multiple access (TDMA), frequency division multiple access (FDMA) or superposition coding (SC). However, this work does not take into account the static power consumption part, which is the predominant part for base station (BS) power consumption. EE of cellular networks taking into account practical power consumption models for BS has been a growing subject of interest for the last few years, e.g. [6, 20]. Several works have studied the EE behavior according to the roll-out density [12]. It appears that EE is an increasing function of the BS density and the number of transmit antennas only when the different components of the BS power consumption satisfy certain conditions. Since the BS static power consumption cannot be neglected, several works addressed various techniques to turn off BS in low load scenarios [21]. In [22], the authors proposed cell zooming to save energy when the network is not fully loaded. The tradeoff between EE and SE considering a practical power consumption model has been a growing subject of interest in recent years [23, 24, 25, 26, 27].

To describe the distribution of the interfering BSs, Kelif *et al.* have proposed a fluid model, which considers a continuum distribution of BS instead of a discrete summation of interfering signals [14]. This work provides a closed form expression of the interference-to-signal ratio (ISR) allowing a tractable derivation of SE and EE in hexagonal cellular networks. However, their expression is limited to frequency reuse factor 1, where the whole system bandwidth is used in each cell. Since SE is inversely proportional to the frequency reuse factor, reusing the whole system bandwidth potentially increases SE and EE as well. But the major issue in this case is the interference caused by the transmission on the same frequencies. We use a semi-analytical method to obtain an expression of ISR allowing the derivation of the EE-SE tradeoff in a regular hexagonal network when frequency reuse factor is different from 1, which has never been done in literature to the best of our knowledge. Moreover, we have proposed ϵ-SE-EE tradeoff as an outage measure for performance evaluation when shadowing is considered.

On the other hand, MIMO enables space division multiple access (SDMA) that serves multiple users in the same time-frequency resources achieving higher SE compared to the conventional

communication [28]. However, precoding must be used to mitigate the interference. Designing a precoder that maximizes the output signal-to-interference-plus-noise ratio (SINR) for each user is desired, but this is a challenging task. A suboptimal and more tractable precoder is zero-forcing (ZF), which is based on nulling the intra-cell interferences [29, 30, 31]. Although ZF performs well in high signal-to-noise ratio (SNR) regime, its performance deteriorates in low SNR regime. Another drawback of this precoder is that it imposes a restriction on the minimum number of transmit antennas at BS [32]. Sadek *et al.* have proposed SLNR as an alternative optimization metric for designing precoder, which has a closed form solution [33]. In contrast to zero-forcing solution, this precoder does not impose any restriction on the number of BS antennas and also considers the influence of noise [33].

Although there have been numerous works based on SLNR precoder [33, 34, 32, 35], these works did not consider multi-cell environment and also ignored the network geometry while computing the precoder. We investigate the performance of the SLNR precoder for cellular network taking into account non-homogeneous average SNR due to large scale fading, i.e. path loss, and also the interference created on the other-cell users. We consider a spatial PPP network model, which is more tractable compared to the hexagonal grid model. Although the PPP model is extensively used in literature, works in [29, 36, 30, 31] have used either the maximal ratio transmission (MRT) or ZF precoder for tractability. We develop the analytical expressions of ASE and EE in a PPP cellular network when SLNR precoder is used, using random matrix theory (RMT) and stochastic geometry.

1.2 Structure of the thesis and contributions

This thesis is a part of the project titled toward energy proportional networks (TEPN) of Cominlabs Labex, and is carried out at the institute of electronics and telecommunications of Rennes (IETR) in Rennes, France. The manuscript is organized as follows :

Chapter 2 reviews important definitions, properties, lemmas, theorems, etc. from stochastic geometry and RMT that are used later in Chapter 5, which combines some fundamental results from RMT to PPP leveraging the tools from stochastic geometry.

Chapter 3 first defines SE, which is the traditional performance metric for wireless communications. SE indicates how efficiently a frequency spectrum is used. An overview of the most common energy metrics used to quantify EE is presented next. Energy metrics provide insight on how efficiently the energy is consumed. Two kinds of network models exist in literature: regular hexagonal networks with fixed BS positions and PPP networks with random BS positions. A short

description of these models is provided next. A detailed description of linear power consumption models, which are the most commonly used in literature, is discussed afterwards. These models are simple and have the ability to calculate EE with reasonable accuracy. We also describe the general propagation model for the whole thesis, and also an overview of the precoding techniques used for MU-MISO networks. Since EE is an important research topic, several researchers have proposed many energy efficient solutions. A brief survey of these methods in a three-layer stack, and well-known research projects are also presented in this chapter. Finally, we revisit the EE-SE tradeoff for an AWGN channel first taking into account only the transmit power. The study is then extended considering the static circuit power consumption. EE-SE tradeoff for different power amplifier (PA) factors and static circuit power consumptions are also analyzed.

In Chapter 4, EE-SE region in a hexagonal cellular network for different frequency reuse factors both with and without shadowing consideration is characterized. A parametric expression of ISR for different frequency reuse factors is obtained when only the path loss is considered allowing a tractable derivation of SE and EE. The expressions of ISR are obtained with a curve fitting approach, and are expressed as function of the normalized distance of the user and path loss exponent. On the other hand, ϵ-SE and ϵ-EE are proposed to characterize the EE-SE tradeoff when shadowing is considered along with the path loss. To allow the study of EE-SE tradeoff with shadowing, an analytical expression of the cumulative distribution function (CDF) of SINR is obtained and validated by Monte Carlo simulations. EE-SE region with and without shadowing for different frequency reuse factors is investigated when a user is at various distances. For the shadowing case, the effect of ϵ on the EE-SE tradeoff is also investigated.

It is well known that for a single link AWGN channel SE and EE are two quantities varying towards opposite directions when static power consumption is neglected or when it is not the predominant factor [37]. However, a linear part where EE increases with SE also exists in the EE vs. SE curves when static power consumption is taken into account. It is observed that the EE-SE tradeoff curves for the hexagonal cellular network also have a large linear part as seen for the AWGN channel when static power consumption is considered. However, the EE decreases very sharply after reaching the optimal points, since the network is homogeneous and interference-limited. It is shown that a frequency reuse equal to 1 for regions close to BS and higher reuse factors in region closer to the cell edge optimizes the EE-SE tradeoff. Moreover, better EE-SE tradeoff can be achieved with higher value of ϵ when shadowing is considered. But higher ϵ causes a lot of outage in the system and therefore should be set according to a certain quality of service (QoS) to meet. Moreover, frequency reuse factor 1 is the best choice for a very high value of outage, even at a moderate distance, due to significant SINR decrease in shadowing

environment.

In Chapter 5, EE-ASE region is investigated for a MU-MISO cellular network with random topology, i.e. BSs and users are modelled by two independent homogeneous PPP, when SLNR precoder is used. The precoder is derived based on maximizing SLNR using the generalized Rayleigh quotient theorem. Although BSs are not totally random in reality, they are modelled by a PPP to facilitate the tractability. An expression of the mean SINR is derived for a typical user in asymptotic regime, i.e. number of antennas and number of users grow to infinity, using RMT and stochastic geometry. ASE is calculated based on the expression of the mean SINR, and EE is derived afterwards using a linear power consumption model. The analytical expressions of ASE and EE provide useful insights in addition to saving the time to run extensive Monte Carlo simulations. EE-ASE tradeoff is then investigated for different number of BS antennas and BS density with constant user density, using theoretical expressions and Monte Carlo simulations. The theoretical expressions of ASE and EE are found to be tight with the results obtained through Monte Carlo simulations, even for moderate values of the number of antennas and users in the network, and for a wide range of system parameters. The results also show that the EE-ASE tradeoff curves have a large linear part before a sharply decreasing EE, as observed for hexagonal network.

EE-ASE tradeoff with SLNR is then compared with ZF precoder. SLNR is observed to outperform the ZF precoder, which is typically used in literature when BS and users are modelled by PPP. This implies a better SINR at user of interest for SLNR compared to ZF. In addition, the effect of system parameters, i.e. maximum number of allowed users in a cell, number of BS antennas, BS density with constant user density and constant BS-user density ratio, on ASE and EE is investigated using the SLNR precoder. Numerical results show that deploying more BS or a large number of BS antennas increase ASE, but the gain depends on the BS-user density ratio and on the number of antennas when user density is fixed. EE increases only when the increase in ASE dominates the increase of the power consumption per unit area (u.a.). On the other hand, when user density increases, ASE can be improved by deploying more BS without sacrificing EE and the ergodic rate of the users.

Chapter 6 provides the conclusions and future perspectives of our works.

1.3 Publications

1.3.1 Journal paper

[J1] **Ahmad Mahbubul Alam**, Philippe Mary, Jean-Yves Baudais, and Xavier Lagrange. Asymptotic Analysis of Area Spectral Efficiency and Energy Efficiency in PPP Network with SLNR Precoder. Accepted in IEEE Transactions on Communications (TCOM).

1.3.2 Conference papers

[C1] **Ahmad Mahbubul Alam**, Philippe Mary, Jean-Yves Baudais, and Xavier Lagrange. Energy Efficiency-Spectral Efficiency Tradeoff in Interference-Limited Wireless Networks with Shadowing. *In IEEE 82nd Vehicular Technology Conference: VTC2015-Fall*, volume 82, pp. 1-5, 2015.

[C2] **Ahmad Mahbubul Alam**, Philippe Mary, Jean-Yves Baudais, and Xavier Lagrange. Energy Efficiency-Area Spectral Efficiency Tradeoff in PPP Network with SLNR Precoder. *In IEEE 17th International Workshop on Signal Processing Advances in Wireless Communications: SPAWC2016*, volume 17, pp. 1-6, 2016.

Chapter 2

Mathematical preliminaries

2.1 Stochastic geometry

Performance of cellular networks depends largely on the locations of BSs and users. The user locations are usually random. However, locations of the BSs can either be fixed as in Chapter 4 or random as modelled in Chapter 5. Stochastic geometry is a tool used to capture the spatial randomness of the network nodes, and enables to study the behaviour of wireless networks averaged over random spatial realizations. Our work in Chapter 5 includes modelling the network nodes by PPP leveraging the tools from stochastic geometry, particularly the point process theory. We review important definitions, properties and theorems related to point processes from [38, 1].

2.1.1 Point process

A point process is a random collection of points and plays a fundamental role in the description of the network geometry. A point process can be defined as

Definition 2.1. *(Point process) A point process is a countable random collection of points that reside in some measure space, usually the Euclidean space* $\mathbb{R}^d$ *[38]. The point process is alternatively defined as [1]*

$$\Phi = \sum_{i=1}^{\infty} \delta_{x_i},$$

where δ_x *is the Dirac measure such that* $\delta_x(B) = \mathbf{1}_B(x)$ *for* $B \subset \mathbb{R}^d$*, where* B *is a Borel subset.*

We will focus on the two dimensional Euclidean space $\mathbb{R}^2$ since BSs and users in Chapter 5 are modelled by two point processes located in a two-dimensional circular disc.

Definition 2.2. *(Intensity measure)[38] The intensity measure of a point process* Φ *is equal to the average number of points in a set* $B \subset \mathbb{R}^d$ *and is expressed as*

$$\Delta(B) = \mathrm{E}[\Phi(B)].$$

For example, intensity measure of the BS and user processes in a subset area of $\mathbb{R}^2$ in Chapter 5 are respectively the average number of BSs and users in that area.

Definition 2.3. *(Homogeneous point process)[1] A point process* $\Phi = \{x_n\}$ *is called homogeneous if* $\Phi_x = \{x_n + x\}$ *has the same distribution as* Φ *for all* $x \in \mathbb{R}^d$*, i.e.,*

$$\mathrm{P}(\Phi \in B) = \mathrm{P}(\Phi_x \in B).$$

The intensity measure of a homogeneous point process can be written as

$$\Delta(B) = \lambda |B|,$$

where $|B|$ is the Lebesgue measure and λ is the density of the point process Φ. A homogeneous point process has a constant density. Therefore, the intensity measure of such process is proportional to the Lebesgue measure, which assigns a measure to the subsets of d-dimensional Euclidean space $\mathbb{R}^d$. For the two dimensional network considered in Chapter 5, Lebesgue measure corresponds to area, and densities of the BSs and users are defined as the average number of the processes per u.a. Both BSs and users are homogeneous point processes since their intensity measures are proportional to the area.

Two of the most important point processes are binomial point process (BPP) and PPP, which are descried in the following.

2.1.2 Binomial point process [1]

$\Phi = \{x_n\}$ is a BPP if the number of points is fixed, and the points are identically and independently distributed on a compact set $B \subset \mathbb{R}^d$. Φ is a uniform BPP only if the points are uniformly

distributed. The probability of having $k < n$ nodes in $A \subset B$ of a uniform BPP is

$$\mathrm{P}\Big(\Phi\big(A\big) = k\Big) = \binom{n}{k}\left(\frac{|A|}{|B|}\right)^k\left(1-\frac{|A|}{|B|}\right)^{n-k},$$

where $|A|$ and $|B|$ represent the Lebesgue measures corresponding to set A and B respectively. Note that the number of points in $\Phi(A)$ and $\Phi(B)$ are not independent since the total number of points is fixed. Due to this dependence, it is usually difficult to analyze the performance of cellular networks when the nodes are designed as points of BPP. However, PPP can be obtained as a limit of BPP when $|B| \to \infty$ keeping $n^{-1}|B|$ constant.

2.1.3 Poisson point process [1]

PPP is the most widely used point process. The characteristics of a homogeneous PPP of density λ are:

- the number of points in any $B \subset \mathbb{R}^d$ is a Poisson random variable (r.v.) with mean $\lambda|B|$ and can be characterized by the probability distribution function (PDF)

$$\mathrm{P}\Big(\Phi\big(B\big) = n\Big) = e^{-\lambda|B|}\frac{(\lambda|B|)^n}{n!}, \tag{2.1}$$

- the number of points in disjoint sets are independent r.vs.

PPP is more tractable compared to BPP due to the independence property. Hence, PPP is more widely used to model the nodes in wireless networks, e.g. BSs and users are modelled by two independent homogeneous PPPs in Chapter 5. PPP has the following interesting properties:

Property 2.1. *(Superposition) The superposition of the independent PPPs Φ_k with density λ_k is another PPP with density $\lambda = \sum_k \lambda_k$.*

Property 2.2. *(Independent thinning) Selecting a point of the PPP with probability p independently of the other points results in another PPP with density $p\lambda$. This is known as independent thinning.*

In Chapter 5, number of active users in different cells are considered to be independent and BSs are divided into subsets based on the number of active users in the cells. Hence, the BS groups are considered as thinned PPPs created by independent thinning from the process of all BSs. Moreover, the density of BSs is the sum of the densities of the BS groups following the superposition property.

Property 2.3. *(Conditional property) Conditioned on the number of points of Φ in a compact set $B \subset \mathbb{R}^d$, the distribution of $\Phi(A)$ for $A \subset B$ is BPP characterized by*

$$\mathrm{P}\Big(\Phi\big(A\big) = k | \Phi\big(B\big) = n\Big) = \binom{n}{k} \left(\frac{|A|}{|B|}\right)^k \left(1 - \frac{|A|}{|B|}\right)^{n-k}.$$

Proof.

$$\mathrm{P}\Big(\Phi\big(A\big) = k | \Phi\big(B\big) = n\Big) = \frac{\mathrm{P}\Big(\Phi\big(A\big) = k, \Phi\big(B\big) = n\Big)}{\mathrm{P}\Big(\Phi\big(B\big) = n\Big)} \\ \frac{\mathrm{P}\Big(\Phi\big(A\big) = k, \Phi\big(B \setminus A\big) = n-k\Big)}{\mathrm{P}\Big(\Phi\big(B\big) = n\Big)}. \tag{2.2}$$

Since the number of points in the disjoint sets A and $B \setminus A$ are independent according to the characteristic of PPP, (2.2) can be written as

$$\mathrm{P}\Big(\Phi\big(A\big) = k | \Phi\big(B\big) = n\Big) = \frac{\mathrm{P}\Big(\Phi\big(A\big) = k\Big)\mathrm{P}\Big(\Phi\big(B \setminus A\big) = n-k\Big)}{\mathrm{P}\Big(\Phi\big(B\big) = n\Big)}. \tag{2.3}$$

Using (2.1), (2.3) can be expressed as

$$\begin{aligned} \mathrm{P}\Big(\Phi\big(A\big) = k | \Phi\big(B\big) = n\Big) &= \frac{e^{-\lambda|A|}\frac{(\lambda|A|)^k}{k!}\, e^{-\lambda|B\setminus A|}\frac{(\lambda|B\setminus A|)^{n-k}}{(n-k)!}}{e^{-\lambda|B|}\frac{(\lambda|B|)^n}{n!}} \\ &= \frac{n!}{k!(n-k)!}\left(\frac{|A|}{|B|}\right)^k \left(\frac{|B \setminus A|}{|B|}\right)^{n-k} \\ &= \binom{n}{k}\left(\frac{|A|}{|B|}\right)^k \left(1 - \frac{|A|}{|B|}\right)^{n-k}. \end{aligned} \tag{2.4}$$

□

Since we consider an infinite network in Chapter 5, both the number of BSs and number of users converge to their intensity measures according to law of large number (LLN). Therefore, Bss and users can be characterized also by two BPPs according to the conditional property mentioned.

2.1.4 Function of point process

Mean of sum and product of functions evaluated at the points of a point process have wide applications in wireless communications, and they are described in the following.

Theorem 2.1. *(Campbell's theorem)[38] If Φ is a point process on $\mathbb{R}^d$ with intensity measure Δ and $f : \mathbb{R}^d \mapsto \mathbb{R}$ is a measurable function, then the random sum*

$$S = \sum_{x \in \Phi} f(x)$$

is a r.v. with mean

$$\mathrm{E}[S] = \int_{\mathbb{R}^d} f(x)\Delta(dx),$$

provided that the right hand side (RHS) is finite. If Φ has a density λ,

$$\mathrm{E}[S] = \int_{\mathbb{R}^d} f(x)\lambda(x)dx.$$

When Φ is homogeneous, Campbell's theorem can be written as

$$\mathrm{E}[S] = \lambda \int_{\mathbb{R}^d} f(x)dx.$$

In Chapter 5, Campbell's theorem is applied over the groups of interfering BS to calculate the mean of the aggregated inter-cell interference powers from each group. The measurable function in this context is the inter-cell interference power from a BS within the group.

Theorem 2.2. *(Probability generating functional (PGFL))[1] The PGFL of the point process Φ is defined as*

$$G\big[f\big] = \mathrm{E}\Big[\prod_{x \in \Phi} f(x)\Big],$$

where $f(x) : \mathbb{R}^d \to [0,\infty)$ is measurable. The PGFL of a PPP is

$$G\big[f\big] = e^{-\int_{\mathbb{R}^d}(1-f(x))\Delta(dx)}.$$

PGFL is very useful to evaluate the Laplace transform of $\sum_{x\in\Phi} f(x)$, which can be expressed as

$$\mathrm{E}\left[e^{-s\sum_{x\in\Phi} f(x)}\right] = \mathrm{E}\left[\prod_{x\in\Phi} e^{-sf(x)}\right] = G\left[e^{-sf(x)}\right].$$

Most of the works in literature dealing with PPP networks consider exponential distribution for the desired signal power since it allows them to use PGFL and leads to simple analytical expressions for the coverage probability, i.e. complementary CDF (CCDF) of the SINR, and ergodic rate, i.e. rate averaged over the fast fading and the network geometry [39, 40, 41, 42]. Since the distributions of the signal powers are unknown due to the consideration of SLNR precoding at BSs in Chapter 5, PGFL cannot be applied to calculate the ergodic rate. This makes the calculation of the ergodic rate of a typical user in a PPP network difficult when SLNR precoder is used. Therefore, we follow a different approach to calculate the ergodic rate in Chapter 5.

2.1.5 Slivnyak's theorem

Slivnyak's theorem is regarded as one of the striking properties of PPP. The theorem can be stated as

Theorem 2.3. *[38] The reduced palm distribution equals the distribution of the PPP itself and can be written as*

$$\mathrm{P}^{!x} = \mathrm{P},$$

where P *is the distribution of the PPP, and* $\mathrm{P}^{!x}$ *is the reduced Palm probability, defined as the distribution of the PPP conditioned to have a point at* $x \in \mathbb{R}^d$.

The application of palm distribution arises in a wireless network when a condition is put on either the transmitter or the receiver's position. Slivnyak's theorem states that the law of $\Phi - \delta_x$ conditioned to have a point at $x \in \mathbb{R}^d$ is the same as the law of Φ. For a homogeneous PPP, the theorem says

$$\mathrm{E}\Big[\sum_{y\in\Phi\setminus\{x\}} f(y)\Big] = \lambda \int_{\mathbb{R}^d} f(y)\,dy.$$

In Chapter 5, while Campbell's theorem is applied over the groups of interfering BS to calculate the mean of the aggregated inter-cell interference powers from each, we condition on the location of

the typical connected BS, and the desired signal power is not taken into account in the calculation of the aggregated inter-cell interference power. This is allowed by Slivnyak's theorem.

2.2 Random matrix theory

Deriving the achievable rate region in multiple antenna systems is an intractable problem, and RMT has been introduced for analyzing such systems [43]. When random matrices grow large with a given ratio between the number of rows and the number of columns, empirical spectral distribution (ESD) of the large dimensional matrices converges to deterministic functions. The results obtained for ESD of large dimensional matrices can be used to approximate the results for ESD of finite size matrices. There are a number of powerful and appealing theorems on the convergence of eigenvalue distribution of large dimensional matrices to deterministic functions. This section provides the definitions and basic tools related to RMT used in Chapter 5, which are reproduced mostly from [43] unless otherwise mentioned.

Definition 2.4. *(Random matrix) An $N \times n$ matrix $\mathbf{Y}$ is a random matrix if it is a matrix valued r.v. on some probability space $(\Omega, \mathscr{F}, \mathrm{P})$ with entries in some measurable space $(\mathscr{R}, \mathscr{G})$, where $\mathscr{F}$ is a σ-field on Ω with probability measure P and $\mathscr{G}$ is a σ-field on $\mathscr{R}$.*

Here Ω is the sample space, i.e. set of all possible outcomes, $\mathscr{F}$ is a set of events and P is the probability of the events. In the context of our work, the space $\mathscr{R}$ can be either $\mathbb{R}$ or $\mathbb{C}$ since we encounter both real and complex r.vs.

Definition 2.5. *(Empirical probability measure of eigenvalues) Let $\mathbf{X} \in \mathbb{C}^{N\times N}$ be a Hermitian matrix with real eigenvalues $\lambda_1, \lambda_2, \cdots, \lambda_N$. The empirical probability measure of the eigenvalues of $\mathbf{X}$ is defined as*

$$\mu_{\mathbf{X}}(A) = \frac{1}{N}\sum_{i=1}^{N} \mathbf{1}_A(\lambda_i).$$

This definition implies that empirical probability measure of eigenvalues of a matrix is the proportion of the realization of the eigenvalues in a set.

Definition 2.6. *(Empirical spectral distribution) ESD of the matrix $\mathbf{X} \in \mathbb{C}^{N\times N}$ is defined as the empirical CDF of its eigenvalues, and is expressed as*

$$F^{\Delta}(x) = \mu_{\mathbf{X}}\Big(\big(-\infty, x\big]\Big) = \frac{1}{N}\sum_{i=1}^{N} \mathbf{1}_{\lambda_i \le x}(x),$$

where $\Delta = \text{diag}(\lambda_1, \lambda_2, \cdots, \lambda_N)$ *represents a square diagonal matrix filled by the eigenvalues.*

The definition implies that ESD is the proportion of the eigenvalues less than or equal to x.

Definition 2.7. *(Limit spectral distribution) If* $F^{\Delta}(x)$ *converges in distribution towards a non random distribution function* $F_l^{\Delta}(x)$ *as* $N \to \infty$*, then the function* $F_l^{\Delta}(x)$ *is called the limit spectral distribution (LSD) of* $\mathbf{X}$ *when* $F_l^{\Delta}(x)$ *exists.*

It is often sufficient to have convergence of $F^{\Delta}(x)$ in distribution to $F_l^{\Delta}(x)$ for all x where $F_l^{\Delta}(x)$ is continuous to obtain relevant results. In Chapter 5, eigen decomposition is applied to Hermitian matrices of size equal to the number of BS antennas. ESD of the matrix is random function for small number of BS antennas, but converges to a non-random function following Theorem 2.4 stated further below in the document, as the number of BS antennas tends to infinity. The non-random function is called LSD.

Definition 2.8. *(Moment of ESD) The* k*-th order moment of* F^{Δ} *can be expressed as*

$$M_k = \int_{-\infty}^{\infty} \lambda^k dF^{\Delta}(\lambda) = \frac{1}{N} \sum_{i=1}^{N} \lambda_i^k = \frac{1}{N} \text{tr}\left(\mathbf{X}^k\right),$$

where tr $(\mathbf{X}^k)$ represents the trace of $(\mathbf{X}^k)$, i.e. the sum of the elements on the main diagonal of $\mathbf{X}^k$.

2.2.1 Stieltjes transform

Stieltjes transform is one of the most important tools used to solve the problems related to large random matrices. Marcěnko and Pastur first used Stieltjes transform approach to find the distribution of the eigenvalues of random matrices [44].

Definition 2.9. *(Stieltjes transform) Let* F *be a real-valued bounded measurable function with support* $\text{supp}(F) \subset \mathbb{R}$*. Then the Stieltjes transform of* F *for* $z \in \mathbb{C} \setminus \text{supp}(F)$ *is defined as*

$$m_F(z) = \int_{\text{supp}(F)} \frac{1}{\lambda - z} dF(\lambda).$$

Study of large dimensional random matrices is simplified due to the Stieltjes transform. For

the Hermitian matrix $\mathbf{X} \in \mathrm{C}^{N\times N}$, we can write

$$\begin{aligned} m_{F^{\Delta}}(z) &= \int_{\mathbb{R}} \frac{1}{\lambda - z} dF^{\Delta}(\lambda) \\ &= \frac{1}{N}\mathrm{tr}\Big(\big(\Delta - z\mathbf{I}_N\big)^{-1}\Big) \\ &= \frac{1}{N}\mathrm{tr}\Big(\big(\mathbf{X} - z\mathbf{I}_N\big)^{-1}\Big). \end{aligned}$$

Therefore, working with the Stieltjes transform simplifies to working with trace of the matrix $(\mathbf{X} - z\mathbf{I}_N)^{-1}$. Stieltjes transform has been used in communications engineering problems in a large extent [45, 46, 47, 48].

In Chapter 5, average quantities are calculated from the Stieltjes transform of LSD of positive semidefinite matrices, which are the limiting Stieltjes transform of ESD as the size of the matrices grow large. Since the eigenvalues of positive semidefinite matrices are non-negative, Stieltjes transforms are analytic over $\mathbb{C} \setminus \mathbb{R}^{+}$.

2.2.2 Lemmas and theorem

Some basic lemmas, and a theorem on the convergence of the ESD of random matrices with asymptotically large dimensions to LSD are used in this thesis.

Lemma 2.1. *(Matrix inversion lemma)[49] Let $\boldsymbol{A}$ be an invertible matrix of size $M \times M$. Then, for any vector $\boldsymbol{y} \in \mathbb{C}^M$ and scalar $\tau \in \mathbb{C}$ for which $\boldsymbol{A} + \tau \boldsymbol{y}\boldsymbol{y}^H$ is invertible,*

$$\mathbf{y}^H(\mathbf{A} + \tau\mathbf{y}\mathbf{y}^H)^{-1} = \frac{\mathbf{y}^H\mathbf{A}^{-1}}{1 + \tau\mathbf{y}^H\mathbf{A}^{-1}\mathbf{y}}.$$

Lemma 2.2. *(Trace lemma) [50, 51] Let $\boldsymbol{y} = [y_1, \cdots, y_M]^T$ be an $M \times 1$ vector where the y_m are iid complex Gaussian r.vs. with unit variance. If $\boldsymbol{A}$ is an $M \times M$ matrix independent of $\boldsymbol{y}$ and* $\limsup_M ||\mathbf{A}||_2 \leq \infty$*, then*

$$\frac{1}{M}\left(\mathbf{y}^H\mathbf{A}\mathbf{y} - \mathrm{tr}(\mathbf{A})\right) \xrightarrow{M\to+\infty} 0,$$

where $||\mathbf{A}||_2$ is the spectral norm of matrix $\mathbf{A}$ and $\limsup_M ||\mathbf{A}||_2$ is the limit superior of $||\mathbf{A}||_2$, i.e. for every $\epsilon > 0$, there exists $M_0(\epsilon)$ such that $||\mathbf{A}||_2 \leq \limsup_M ||\mathbf{A}||_2 + \epsilon$ for $\forall M > M_0(\epsilon)$.

Lemma 2.3. *(Rank-1 perturbation lemma) [52] Let, $z \in \mathbb{C}^{+}$, $v = \Im[z]$, $\mathbf{A}$ and $\mathbf{B}$ are $N \times N$ matrix*

with $\mathbf{B}$ *be Hermitian and* $\mathbf{r} \in \mathbb{C}^N$. *Then*

$$\left|\mathrm{tr}\Big(\big(\mathbf{B}-z\mathbf{I}_N\big)^{-1}-\big(\mathbf{B}+\mathbf{r}\mathbf{r}^H-z\mathbf{I}_N\big)^{-1}\Big)\mathbf{A}\right| = \left|\frac{\mathbf{r}^H\big(\mathbf{B}-z\mathbf{I}_N\big)^{-1}\mathbf{A}\big(\mathbf{B}-z\mathbf{I}_N\big)^{-1}\mathbf{r}}{1+\mathbf{r}^H\big(\mathbf{B}-z\mathbf{I}_N\big)^{-1}\mathbf{r}}\right| \leq \frac{||\mathbf{A}||_2}{v}$$

for $z<0$,

$$\left|\mathrm{tr}\Big(\big(\mathbf{B}-z\mathbf{I}_N\big)^{-1}-\big(\mathbf{B}+\mathbf{r}\mathbf{r}^H-z\mathbf{I}_N\big)^{-1}\Big)\mathbf{A}\right| \leq \frac{||\mathbf{A}||_2}{|z|}.$$

This lemma with $z<0$ is used a number of times in Chapter 5. However, $\mathbf{A}$ is an identity matrix in the context of our work implying a spectral norm equal to one. We now state Theorem 2.4, which is used in Chapter 5, and is very important result for us.

Theorem 2.4. *[47] Let* $\mathbf{B}=\frac{1}{N}\mathbf{H}\mathbf{D}\mathbf{H}^H$, *where* $\mathbf{H}\in\mathbb{C}^{N\times n}$ *contains iid complex entries with* $\mathrm{E}\Big[\mathbf{H}_{11}-\mathrm{E}\big[\mathbf{H}_{11}\big]\Big]^2=1$ *where* $\mathbf{H}_{11}$ *denotes the element of the first column and first row of the matrix* $\mathbf{H}$, $\mathbf{D}\in\mathbb{C}^{n\times n}$ *be an Hermitian positive semi-definite matrix and independent of* $\mathbf{H}$. *Moreover, ESD of* $\mathbf{D}$, *denoted as* $F^{\mathbf{D}}$, *converges in distribution to* $F_l^{\mathbf{D}}$ *on* $[0,\infty)$ *as* $n\to\infty$, *and the ratio* $\frac{n}{N}\to\gamma_{au}\in(0,\infty)$ *as* $n,N\to\infty$. *Then ESD of* $\mathbf{B}$ *surely converges in distribution to* $F_l^{\mathbf{B}}$ *such that for* $z\in\mathbb{C}^+$, $m_{F_l^{\mathbf{B}}}(z)$ *is the unique solution of*

$$m_{F_l^{\mathbf{B}}}(z)=-\left(z-\gamma_{au}\int\frac{t}{1+tm_{F_l^{\mathbf{B}}}(z)}dF_l^{\mathbf{D}}(t)\right)^{-1}. \tag{2.5}$$

In the context of Chapter 5, $\mathbf{H}$ represents the concatenated fading channels with iid entries of mean zero and variance one, N and n respectively represent the number of BS antennas and number of active users in the network which grow to infinity keeping a constant ratio between them, $\mathbf{D}$ represents a diagonal matrix filled by functions of path losses which are non-negative real entries and also independent of $\mathbf{H}$.

Chapter 3

State of the art

3.1 Introduction

Mobile communication has experienced a tremendous evolution since the introduction of global system for mobile communication (GSM) in 1980's. The major breakthrough in mobile communication took place in 2007 when the amount of data traffic exceeded the amount of voice traffic [53]. Number of mobile subscribers overtook the number of fixed broadband subscriptions in 2008 [54]. The driving force behind this rapid growth was the introduction of mobile internet that caused a paradigm shift from low bandwidth services, e.g. voice and short message, to bandwidth hungry data services. Global mobile penetration rate is forecasted to reach 100% after 2020 [54]. Moreover, internet of things will potentially increase the number of connected devices leading to a massive traffic increase in future.

The massive traffic increase is accompanied by increased energy consumption. Energy cost for running a network constitutes almost 50% of the operational expenditures (OPEX) of the operators [55]. Mobile network traffic is envisioned to increase exponentially leading to an exponential increase in the energy cost in contrast to the increase of the revenue, as shown in Fig. 3.1. Reducing the energy consumption is critical to lowering the OPEX from an operator's perspective. Another important consequence of increasing energy consumption is the increase of carbon-dioxide (CO_2) emissions that has a devastating impact on climate change [56, 57]. Since energy saving and environmental protection become inevitable needs, focus of research in wireless communications is shifting to EE oriented design. However, around 60% of the energy required for the operation of a cellular network is consumed at BSs, as can be seen in Fig. 3.2. Therefore, the most energy-efficient designs are targeted to reduce the energy consumption in

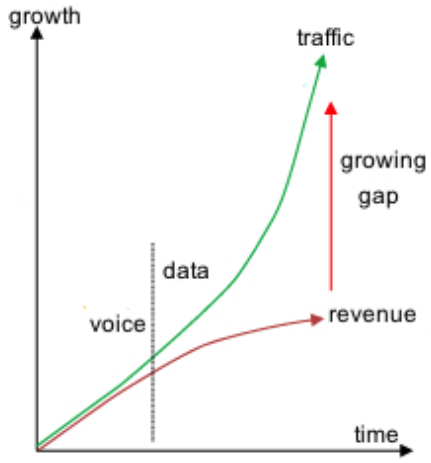

Figure 3.1 – Growth of mobile network traffic and revenue [2]

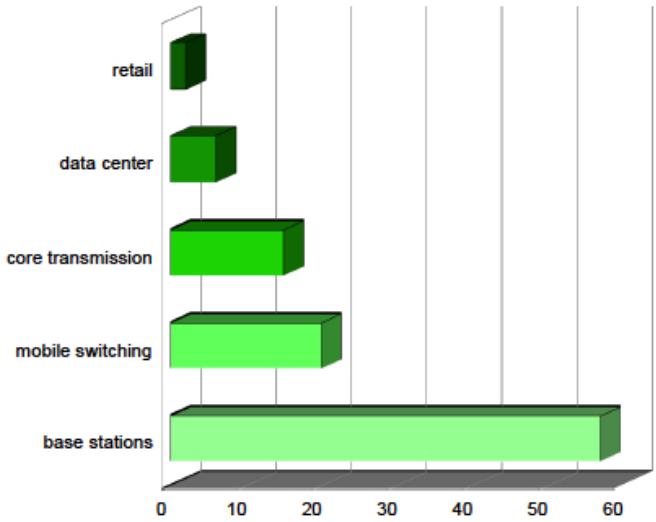

Figure 3.2 – Percentage of power consumption in a cellular network [3]

the wireless access part of a cellular network.

SE has been considered as the main criterion to optimize the performance in wireless communication systems for a long time. In this chapter, this metric is defined first, and an overview of the most common energy metrics available in literature is presented next. This is followed by the description of the two most common state of the art cellular network models. Since the total power consumption of the BSs has a close relation with the metrics quantifying the EE, linear BS power consumption models commonly used in literature are presented afterwards. A general propagation model for the whole thesis, and also an overview of the precoding techniques used for MU-MISO systems are provided. Next, a detailed survey of the research approaches and projects aiming to reduce the energy consumption is provided. The chapter ends with a revisit of the fundamental EE-SE tradeoff for an AWGN channel.

3.2 Performance metrics

SE has driven the wireless system design in the past decades due to the high data rate demand of multimedia services. It indicates how efficiently frequency spectrum is used, but fails to provide any insight on how efficiently the energy is consumed. The fast growing data traffic volume and dramatic expansion of network infrastructures inevitably trigger tremendous escalation of energy consumption in wireless networks. Hence, EE is quickly becoming one of the key performance metrics to evaluate wireless communication systems together with SE that has been traditionally used.

3.2.1 Spectral efficiency

SE is defined as the achievable transmission rate per unit bandwidth and expressed in b/s/Hz as

$$\eta_{\mathrm{SE}} = \frac{R}{w}, \tag{3.1}$$

where R is the achievable transmission rate in b/s, also known as the capacity, over a communication channel with bandwidth w Hz. The achievable transmission rate of an AWGN channel has been computed by Shannon in [58]. We use η_{SE} as the performance metric for the AWGN channel in this chapter, and also for the hexagonal network in Chapter 4 when only path loss is considered. The Shannon capacity is not adapted to describe the performance of a system in shadowing environment when the transmitters have no channel state information (CSI). When shadowing is considered in Chapter 4, we define ϵ-SE, adapted from the ϵ-outage capacity definition in [59].

The ϵ-SE is defined as the largest SE E such that the probability of SE being below E is less than or equal to ϵ and can be expressed as

$$\eta_{\mathrm{SE}}^{(\epsilon)} = \sup\left\{E : \mathrm{P}\left[\eta_{\mathrm{SE}} < E\right] \leq \epsilon\right\}. \tag{3.2}$$

On the other hand, the performance metric used in Chapter 5 is ASE, i.e. average sum of the ergodic rate of users in b/s/Hz per u.a., since we are interested on the total sum rate, not the individual rate.

The capacity region of the multiple access and broadcast channel in a single cell network has been characterized in [60, 61, 62] and [63, 64, 65, 66, 67, 68] respectively. On the other hand, cellular network consists of multiple cells, and cells having the same set of frequencies interfere with each other. The common practice to obtain R in the interference-limited cellular networks is to consider the inter-cell interferences as noise [69], as considered in Chapter 4 and Chapter 5.

3.2.2 Energy metrics

Energy metrics are introduced in order to assess and compare the energy consumption of different telecommunication networks and equipments [70]. These metrics are useful in setting long term research target to achieve more energy efficient solutions. The energy consumption of the telecommunication networks can be attributed to the operational energy and to the embodied energy. The operational energy represents the energy consumed due to the actual run-time operation of the network and equipments. On the other hand, the embodied energy represents the energy consumed to manufacture and deploy the system [20]. Energy metrics given by various standardization bodies mainly quantify the operational energy. Therefore, in the following, an overview of the energy metrics is provided taking only the operational energy consumption into account.

Energy metrics can be divided into component, equipment and network level metrics [71]. While component and equipment level metrics are used to evaluate the energy consumption of a component within an equipment and the equipment respectively, network level metrics assess the consumption of a network as a whole. The efficiency of a PA is a component level metric, which is defined as [71],

$$\eta = \frac{P_{\mathrm{o}}}{P_{\mathrm{i}}}, \tag{3.3}$$

where P_{o} is the effective output power and P_{i} is the input power. Another component level

metric corresponding to PA is peak-to-average-power ratio (PAPR), i.e. the ratio between the peak output power and the average output power, whose reduction ensures a better amplifier efficiency [72].

Energy consumption rating (ECR) of an equipment is an equipment level metric and can be expressed in J/b as [73]

$$\text{ECR} = \frac{P_f}{T_f}, \tag{3.4}$$

where P_f is the peak power in Watts (W) and T_f is the maximum throughput in b/s. The lower ECR, the less energy is consumed to transport the same amount of data. ECR metric is developed with the aim to compare EE of the network equipments from different manufacturers. However, this metric can be used to measure EE of networks also [70]. The definition of ECR fits only for full load and hence, variable load ECR (ECR-VL) is introduced to consider the dynamic nature of the traffic. ECR-VL can be expressed as [70]

$$\text{ECR} - \text{VL} = \frac{\sum_I \beta_I P_I}{\sum_I \beta_I T_I} \tag{3.5}$$

with β_I, P_I and T_I be the weighting coefficient, power consumption and throughput respectively at $I \in \{0, 10, 30, 50, 100\}$ percent of the load. The weighting coefficients are selected such that $\sum_I \beta_I = 1$. Having the best peak efficiency assumed by ECR does not necessarily mean that the equipment has the best power management capabilities, as measured by ECR-VL. The telecommunication energy efficiency ratio (TEER) is another equipment level metric, which is defined as [70]

$$\text{TEER} = \frac{\text{useful work}}{\text{power}}, \tag{3.6}$$

where 'useful work' varies with the type and function of the equipment, and 'power' is the average power over the duration of the measurement test.

A network level metric is power per area, which is defined in W/m^2 as [74]

$$\rho = \frac{P_C}{A_C}, \tag{3.7}$$

where P_C is the average power consumed in the network, and A_C is the coverage area. Energy per unit area expressed in J/m^2 is another network level metric which relates the energy consumed

in a network to the area covered. Both these network level metrics allow to compare various deployment strategies, e.g. heterogeneous networks with overlapping cells, cells with variables sizes. Since a network is coverage limited at low loads, these metrics are particularly relevant when the traffic is low. International telecommunication union (ITU) suggested a network level metric for wireless access networks that is defined in J/b/m^2/subscriber as the power per number of subscribers, per throughput and per area [70]. This metric is relevant for capacity limited systems since it takes the number of subscribers and the throughput into account.

Energy metrics are further classified into absolute metrics and relative metrics [70]. While absolute metrics measure the actual EE of a component, equipment or a network, relative metrics quantify EE w.r.t. references. Absolute metrics can be further classified into EE metrics and energy consumption (EC) metrics [3]. While the EE metrics express the ratio of the performed work over the consumed energy, EC metrics are defined as the opposite. However, both of these metrics contain exactly the same information. Energy per bit is the most common EC metric in literature, particularly used for theoretical studies [75, 76, 77, 78]. This metric is defined as the ratio between the consumed power and the bit rate, and can be measured in J/b as

$$E_b = \frac{P}{R}, \tag{3.8}$$

where P is the consumed power. The bit per energy is an EE metric which measures the amount of bits delivered per unit energy consumed, and can be expressed in b/J as [79]

$$b_E = \frac{1}{E_b} = \frac{R}{P}. \tag{3.9}$$

This metric has been extensively used in literature, e.g. wireless sensor and ad-hoc networks [80, 81, 82], cooperating BSs [83], AWGN channels [84]. The metric b/J/Hz relates the number of transferred bits with the energy consumed in the network and the bandwidth [85, 86]. This metric can be obtained from b_E by normalizing w.r.t. bandwidth. An EE metric derived from ECR is the energy efficiency rate (EER), which is defined in b/J as [70]

$$\text{EER} = \frac{1}{\text{ECR}} \tag{3.10}$$

and fits only for full load.

On the other hand, energy consumption gain (ECG) and energy reduction gain (ERG) are the two most commonly used relative metrics. These metrics are useful only to compare systems

with same characteristics. ECG is defined as [87]

$$\text{ECG} = \frac{E_1}{E_2}, \tag{3.11}$$

where E_1 and E_2 are the energy consumption of the reference system and the system under consideration respectively. On the other hand, ERG is defined as [87]

$$\text{ERG} = \frac{E_1 - E_2}{E_2}.$$

To summarize, it is necessary to have reliable energy metrics to evaluate energy saving techniques and their performance in practical systems. Due to the difference among various communication systems and different QoSs required, a single metric is not sufficient and hence multitude of criteria have been developed. In this thesis, EE metrics are used since our interest lies in measuring the performance of the network per energy consumption. EE metrics have higher values when energy consumption is reduced. We use b_E to evaluate EE for the AWGN channel in this chapter and also for the hexagonal network in Chapter 4. However, the normalized bandwidth EE is used in Chapter 5.

3.3 Cellular network models

Cellular network is based on the concept of replacing a single cell with high power BS by several cells with low power BSs for higher system capacity [4]. The region over which the signal strength of a BS is above a minimum threshold is the coverage area of BS, also known as cell. On the side of the network models existing in literature, we can find two kind of works: the work considering regular hexagonal networks with fixed BS positions [88, 89, 90, 91] and the researches dealing with PPP to model the BS distribution, e.g. [19, 29, 30, 31] among others.

3.3.1 Hexagonal network

Among the shapes that could be considered for the geometry of a cell in regular networks, hexagon covers the maximum area and hence this pattern has been widely used to model the cellular deployment. In hexagonal network, the whole system bandwidth is divided and allocated to a number of cells. The set of cells among which the whole system bandwidth is divided constitutes a regular pattern. This regular pattern is called the cluster and this is repeated throughout the whole network. Fig. 3.3 is an example of hexagonal cellular network with three clusters.

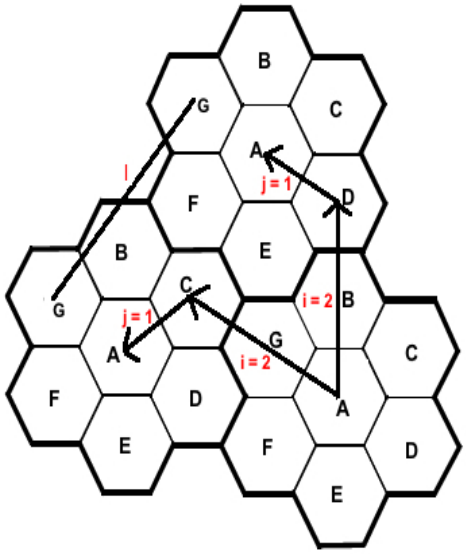

Figure 3.3 – Hexagonal cellular network [4]

Cells in different clusters having the same frequencies are called the co-channel cells, and are marked with the same letters in Fig. 3.3. Number of cells in a cluster is defined as the frequency reuse factor, which is given by

$$K = i^2 + ij + j^2, \quad i \geqslant 0, j \geqslant 0, \tag{3.12}$$

where i and j are non-negative integers. For example, K is 7 in Fig. 3.3 since there are seven cells in a cluster. The nearest co-channel neighbours of a particular cell can be obtained first by moving i cells along any chain of hexagons and secondly, turning 60 degrees counter-clockwise and moving j cells, as illustrated in the figure for cell A with $i = 2$ and $j = 1$. The distance between any two nearest co-channel cells is known as the frequency reuse distance. Since all the clusters in Fig. 3.3 are neighbouring to each other, any two cells marked with the same letter are the nearest co-channel cells, and the distance between them is the frequency reuse distance. If r_H is the radius of the hexagonal cell, then the distance between two adjacent cell centers is $\sqrt{3}r_H$ and the frequency reuse distance is

$$l = \sqrt{3K}r_H. \tag{3.13}$$

Interference between co-channel cells due to the transmission on the same frequency is known as the co-channel interference (CCI). Hexagonal network model is used in Chapter 4.

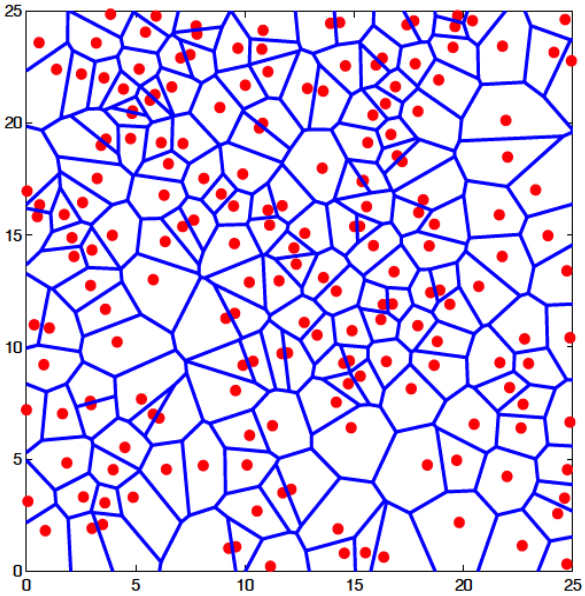

Figure 3.4 – Poisson homogeneously distributed BSs [5]

3.3.2 PPP network

Since the regular hexagonal network is highly idealized and not very tractable, Andrews *et al.* have introduced a more tractable model in [5] by considering BSs as a PPP. In nearest-neighbour cell association model [5, 92], i.e. each user connects to its nearest BS, the coverage area of a BS is the set of points belonging to $\mathbb{R}^2$ which are the closest from this BS than any other. This association rule leads to Voronoi tesselation [93], as shown in Fig. 3.4. The proposed model better captures the increasingly opportunistic and dense placement of BSs in urban cellular networks with highly variable coverage area. The main weakness is that BSs in some cases are located very close to each other but with a significant coverage area [5]. However, the strength of this model can be stated as the independent positions of the BSs leveraging the tools from stochastic geometry, natural inclusion of different cell sizes and shapes, and the lack of edge effects [5]. The assumption that BSs are positioned completely at random has turned the PPP model more tractable compared to the hexagonal network model. PPP model is adopted for our works in Chapter 5.

3.4 BS power consumption models

Sophisticated power consumption models are required to calculate EE accurately in thereby. Power consumption model of a BS must incorporate the power consumed by its components since considering only the transmit power leads to wrong conclusions for designing energy efficient systems [94, 95].

3.4.1 Components of a BS

As shown in Fig. 3.5, a BS is comprised of a baseband (BB) unit and one or more transceivers. Each transceiver consists of a radio frequency (RF) unit, a PA and an antenna connected through a feeder cable. In addition, BS contains a power supply (PS) unit that comprises the mains supply and the DC-DC unit. Moreover, a cooling system is also present to protect the telecommunications equipments from damage due to heat.

PA amplifies the low output power from the RF block into a signal with high enough power for transmission. It is one of the most power consuming components. Current wireless standards, i.e.

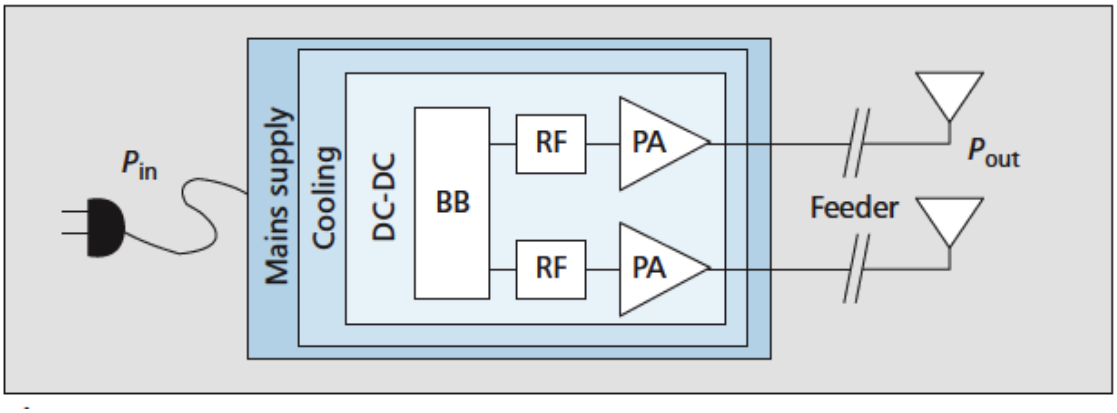

Figure 3.5 – Components of a BS [6]

LTE, LTE-advanced, worldwide interoperability for microwave access (WiMAX), adopt orthogonal frequency division multiplexing (OFDM) with high PAPR forcing PA to operate in a linear region instead of the most efficient operating point near the saturation [16]. Operating in the linear region reduces the adjacent channel interference, but gives rise to the power consumption of PA.

RF unit comprises a receiver and a transmitter for uplink and downlink communications respectively. At the transmitter side, digital output signal from the BB unit is first converted to

analog signal followed by an up-conversion in RF signal with sufficient signal amplification [9]. BB unit carries out digital signal processing, e.g. channel coding, decoding, signal detection, digital pre-distortion (only in the downlink for micro/macro BSs), modulation, demodulation, filtering, fast Fourier transform (FFT), inverse FFT for OFDM, etc. [9]. The silicon technology, which is anticipated to be replaced by a new generation every two years, significantly affects the power consumption of the BB unit.

Mains supply unit performs the AC-DC conversion and connects to the power grid, while DC-DC unit works as a battery backup. On the other hand, cooling depends largely on environmental conditions. Power saving can be achieved by allowing as much natural cooling as possible to reduce the air conditioning. However, active cooling is relevant only for macro BSs, while smaller BSs can be cooled naturally [6].

3.4.2 Linear power consumption models

Since the RF output power per transmit antenna, P_{out} is measured at the input of the antenna element, losses due to the antenna interface are usually not included in the calculation of the total power consumption of a BS. Traditionally PAs are located far from the antenna incurring significant power loss in the feeder cables. The effect of the feeder cable can be approximated by an efficiency term, i.e. ratio between the output power and input power, considering that the power consumption by the feeder cable scale with P_{out} [16]. The power consumption of each PA is proportional to the power input to the feeder cable. Besides, the losses incurred by the cooling system, mains supply and DC-DC unit scale linearly with the power consumption of the other components, and the effects can be approximated by efficiency terms [16].

Putting all pieces together, total power consumption of a BS at maximum load, i.e. $P_{\text{out}} = P_{\text{max}}$, can be expressed as [16]

$$P_{\text{total}} = M \frac{\frac{P_{\text{max}}}{\eta_{\text{PA}}\eta_{\text{feed}}} + P_{\text{RF}} + P_{\text{BB}}}{\eta_{\text{DC}}\eta_{\text{MS}}\eta_{\text{cool}}}, \tag{3.14}$$

where M is the number of transceiver chains, P_{max} is the maximum P_{out}, P_{RF} is the power consumed by RF unit, and P_{BB} is the power consumed by BB unit when M is one. Moreover, η_{PA}, η_{feed}, η_{DC}, η_{MS} and η_{cool} are the efficiencies of PA, feeder cable, DC-DC unit, mains supply and the active cooling system respectively. Note that the total power consumption scales with the number of transceiver chains, i.e. M.

Mainly the power consumption of PA scales with the output power, i.e. P_{out}, and the con-

sumption of the other components is comparatively static, as shown by the authors in [6]. This justifies a linear approximation of the BS power consumption model at variable load [6]:

$$P_{\text{total}} = M(aP_{\text{out}} + P_0), \tag{3.15}$$

where $0 < P_{\text{out}} \leq P_{\max}$, a is the slope of the load-dependent power consumption, determined by the efficiency of PA and known as the PA factor, and P_0 represents the power consumption with a single transceiver at the minimum non-zero P_{out}. Writing $P_t = MP_{\text{out}}$ and $b = MP_0$, (3.15) can be expressed as

$$P_{\text{total}} = aP_t + b. \tag{3.16}$$

This model is extensively used in literature because of its simplicity [90]. We use this model to calculate EE in Chapter 4. Considering further that the power consumption of the PS unit, BB unit and cooling system do not scale with the number of transceiver chains, (3.16) can be written as [12]

$$P_{\text{total}} = aP_t + MP_{\text{RF}} + c, \tag{3.17}$$

where c represents the non-transmission power for BB unit, PS unit and cooling. This power consumption model is used in Chapter 5 to calculate EE. Since BSs in the hexagonal network considered in Chapter 4 have a single antenna, (3.16) and (3.17) are equivalent in that case.

3.5 Propagation model

Radio signal propagated through wireless channel is impaired by path loss, shadowing, multipath, fading, etc. An accurate but tractable propagation model is required to calculate the power at the receiver. Taking into account all the impairments of a wireless channel, power received by the typical k-th user at distance r_{ik} from the BS $i \geq 0$ can be written as [96]

$$P_{ik} = P_t L X r_{ik}^{-\alpha}, \tag{3.18}$$

where P_t is the transmit power, L is the propagation constant, X is a random variable accounting for the random channel power gain and $r_{ik}^{-\alpha}$ is the path loss with α being the path loss component. Due to the singularity at the origin, propagation model in (3.18) is an unbounded model, which

is valid only for calculating the received power at the far field [97]. This model is widely used in literature due to its simplicity and mathematical tractability. We use this model throughout the whole thesis to calculate the received power. However, the parameters of the model vary for different scenario and will be mentioned when the model is applied.

3.6 Precoding techniques

Different precoding techniques are used at BSs with multiple antennas in order to increase the desired signal power, while reducing the interference or leakage to other users. This is done by sending the same data signal with different amplitudes and phases from different antennas such that they add coherently at the desired user, but destructively at the other users [7]. Precoding enables global utilization of all spectral resources removing the need for frequency reuse technique. Dirty paper coding is based on non-linear interference pre-cancellation, and it is capacity achieving for a single cell [98]. However, deploying it in real-time systems is difficult due to high complexity of decoding and the required knowledge of all interfering signals at transmitter. On the other hand, optimal precoding technique is yet not known for multicell scenario [99]. Although the linear precoders, e.g. MRT, ZF, SLNR, are suboptimal in the capacity-sense, they are practically more feasible because of low complexity and robustness to channel uncertainty.

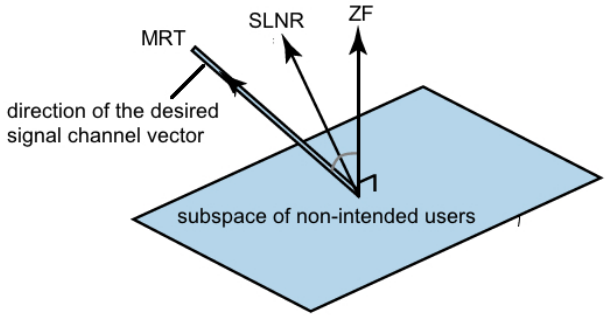

Figure 3.6 – Directions of the linear precoding vectors [7]

MRT precoder maximizes the SNR by aligning the precoding vector with the channel vector of the desired user [100]. This precoder does not consider the leakage created on other users, and is optimal in the low SNR regime. On the other hand, ZF technique is based on nulling the interference generated at non-intended users and can be achieved by selecting precoding vectors

that are orthogonal to the channel vectors of the non-intended users [101, 102]. Therefore, the ZF precoder is available only when the number of BS antennas is greater than the number of users to whom no leakage is created. ZF is the optimal precoder in the high SNR scenarios where inter-user interference greatly dominates the noise term in the SINR expression [103].

SLNR precoder creates a balance between the two extremes, i.e. maximizing the desired signal power and minimizing the interference generated at other users, by maximizing the ratio between the desired signal power and the interference power that leaks to non-intended users plus the noise power at the desired user [101]. The principle of SLNR precoding has been used by different authors in literature and was first used by the authors in [33]. An equivalent metric, known as the signal-to-generating-interference-plus-noise-ratio (SGINR), is used in [104]. The maximization of the SLNR or SGINR is a generalized eigenvalue problem, and hence also named as the generalized eigenvalue based beamformer in [105]. This precoder combines the benefit of MRT at low SNR with the benefit of ZF at high SNR. Furthermore, SLNR always exists while ZF is only possible under certain conditions.

Fig. 3.6 illustrates the directions of MRT, ZF and SLNR precoding vectors. As illustrated in the figure, precoding vector for MRT follows the direction of the channel vector of the desired user, ZF precoding vector is orthogonal to the channel of non-intended users, and SLNR balances between these extremes and moves between them depending on the SNR. In Chapter 5, performance of the SLNR precoder in terms of EE-ASE tradeoff is compared with ZF considering a PPP network, and better performance is achieved for the SLNR precoder. However, the non-intended users for the precoders are not the same. While ZF considers only the intra-cell interference, the SLNR precoder takes into account leakage to the active users in the other cells also.

3.7 Energy efficient research approaches

Since EE is an important research topic, several researchers have proposed many solutions to design energy efficient networks. We present a brief survey of these methods in a three-layer stack where lower layers serve the upper layers to increase their attainable EE. The layers from the bottom are component layer, transmission techniques and radio resource management layer, and the cellular architecture layer as illustrated in Fig. 3.7.

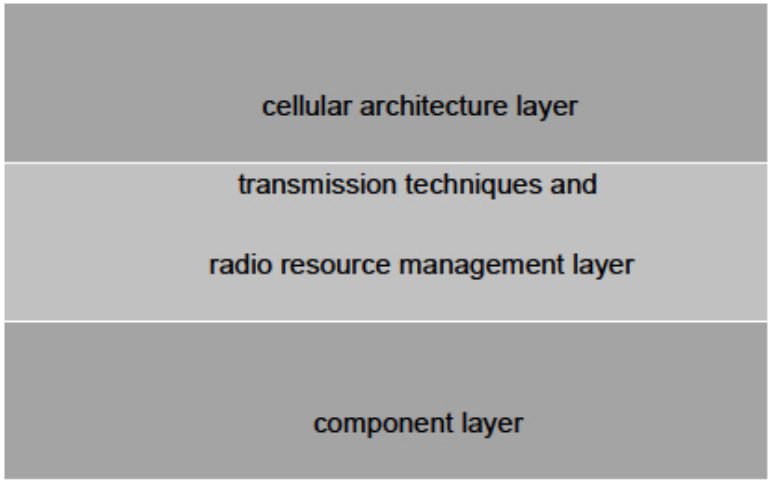

Figure 3.7 – Layered energy efficient approaches

3.7.1 Component layer

Since BSs consume the maximum portion of the total energy consumption in a cellular system, component level approach mainly considers energy savings in BSs. PA has a great potential for energy saving since it consumes the largest portion of the energy consumption in a BS, as shown in Fig. 3.8. Hence, a lot of works exist in literature that aim at increasing the PA efficiency

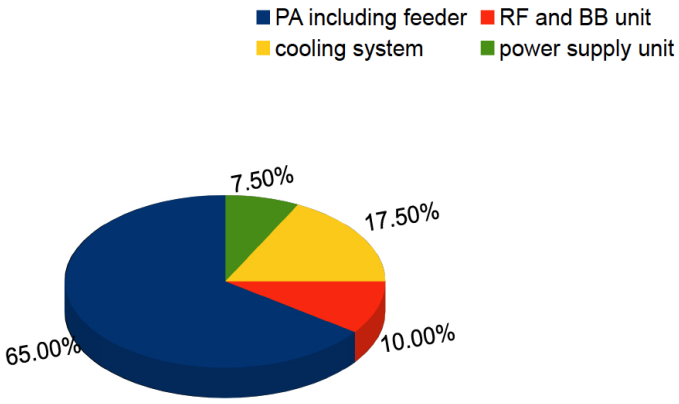

Figure 3.8 – Distribution of power consumption in BSs [8]

[106, 107, 108, 109]. Improving the efficiency of a PA by the reduction of PAPR has been discussed in [11]. Among others, amplifiers with different architectures and features, e.g. class J amplifier,

switched mode power amplifier, etc., are proposed in literature which have higher efficiencies compared to the conventional Doherty amplifier [110]. Authors in [111, 110] have proposed a new BS architecture with the transceivers decoupled from the BB unit and mounted at the same physical location as the antenna element. Compared to the traditional architecture, the new one simplifies the installation, reduces the feeder loss and energy required for cooling due to more fresh air cooling. Switching off the transceivers when there is no traffic is a promising technique to improve EE [10], as considered in Chapter 5.

3.7.2 Transmission techniques and radio resource management layer

Cellular access networks have been traditionally designed targeting performance maximization at full load. However, the daily traffic shows high variations between peak and off-peak values with long periods of low loads. Moreover, only 20% of BSs carries 80% of traffic even during the busy hour resting the network under-utilized most of the time in most of the space [112]. As

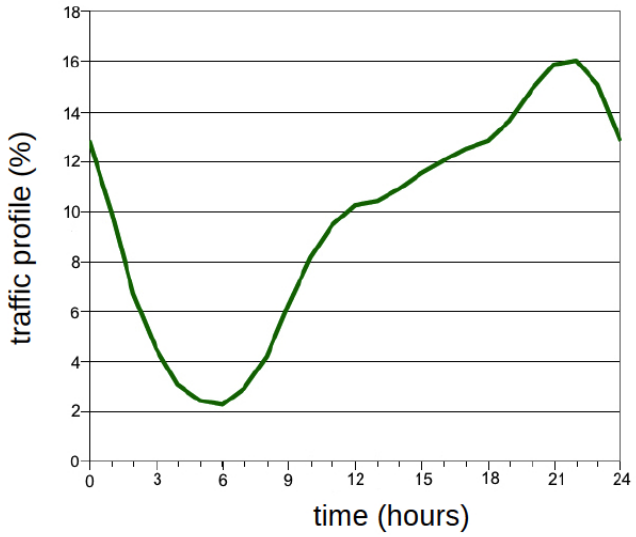

Figure 3.9 – Daily data traffic profile for cellular systems in Europe [9]

illustrated in Fig. 3.9, a large difference exists between busy and quiet hours in the daily data traffic profile, i.e. percentage of active mobile broadband subscribers, in Europe. Moreover, only 16% of the mobile broadband subscribers are active even in peak hours. The large spatial and temporal traffic variation would not be issues if the power consumption of BSs was proportional to their load. But this is not the case due to the large static circuit power consumption into

BS. The energy consumption of cellular networks can be reduced by adapting transmission techniques and resource allocation schemes to the load.

Unlike the conventional radio resource management (RRM) techniques aiming at achieving higher data rates, energy aware resource allocation schemes target to utilize the resources of the network, i.e. bandwidth, time, space, power, etc., to maximize EE without compromising the QoS. The insights on relation among these resources guide practical system designs towards a green evolution. Relation among the resources is often a tradeoff, i.e. one cannot be improved without reducing other. The authors in [113] have identified four fundamental tradeoffs of EE with network performance, i.e. deployment cost, SE, bandwidth, delay, for a network with AWGN channels. However, our focus is only on the EE-SE tradeoff and we revisit the relation for an AWGN channel at the end of this chapter. The aim is to differentiate the EE-SE characteristics achieved for interference limited multi-cell networks in Chapter 4 and Chapter 5 from noise-limited AWGN channel.

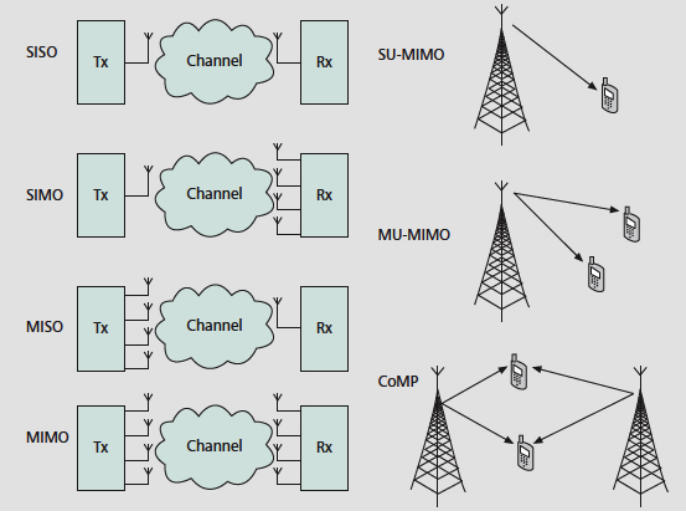

Figure 3.10 – MIMO and CoMP [10]

On the other hand, several transmission techniques, e.g. MIMO, adaptive antennas, Coordinated MultiPoint transmission (CoMP), advanced retransmission techniques, have emerged as the possible ways to meet the high data rate demand. Single input single output (SISO), single input multiple output (SIMO), and MISO are special cases of MIMO, which can also be used with single user and multiple users to form single-user MIMO (SU-MIMO) and multi-user MIMO (MU-MIMO) [10], as it has been summarized in Fig. 3.10. Despite the fact that these techniques

have potential to increase the data rate, their EE is still an open issue because of the increase of circuit energy consumption [10]. EE of MIMO for short-range transmission has been found to be lower than single antenna when static circuit power consumption is considered by both and none of them adopt adaptive modulation techniques [114, 115, 116, 117]. However, a balance between the energy used for transmission and circuit energy consumption can be achieved adapting the modulation order resulting in higher EE for MIMO [95]. Adapting the number of antennas to the traffic variation can further increase EE [115, 117].

Andrews *et al.* have studied EE in a PPP cellular network considering the ZF precoder and shown that EE is an increasing function of the number of transmit antennas only when the different components of the BS power consumption satisfy certain conditions [86]. However, ZF precoder performs worse than the SLNR precoder in terms of EE-ASE tradeoff [118]. EE of CoMP is potentially better compared to the conventional single BS transmission scheme due to the spatial diversity induced by coordinated BSs [119]. Among other works, tradeoff between number of retransmissions and longer packets with forward error correction (FEC) is evaluated, and an energy-efficient algorithm combining FEC and automatic repeat request scheme is proposed in [120]. Furthermore, the authors in [121] have shown how OFDM can improve EE when combined with adaptive modulation techniques.

3.7.3 Cellular architecture layer

To reduce the consumption of circuit energy, cellular networks should be dimensioned with as few nodes as possible while maintaining the desired coverage, capacity and other QoSs. Wireless access network is dimensioned for peak hour traffic as mentioned earlier, and deployment of new architectures, e.g. small cells, relays, repeaters, etc., has been recently considered as a way to meet the high data rate requirement. Although they save transmit power due to lower path loss, the circuit energy consumption is increased [122, 123]. The authors of [124] studied the tradeoff between transmit power and circuit power consumption by evaluating the area power consumption of different deployment scenarios for a minimum received power at the cell edge. They concluded that large cell deployments are more energy efficient than the small cell deployments due to the large circuit power consumption by the latter.

Since mobile traffic shows significant variations in spatial and temporal domain leading to significant energy loss in low load scenarios, one potential approach to save energy is to adapt the network to the dynamic load variation via switching off BSs and cell zooming, as investigated in [125, 126, 127, 128]. Cell zooming is a technique in which a cell under heavy load reduces its size

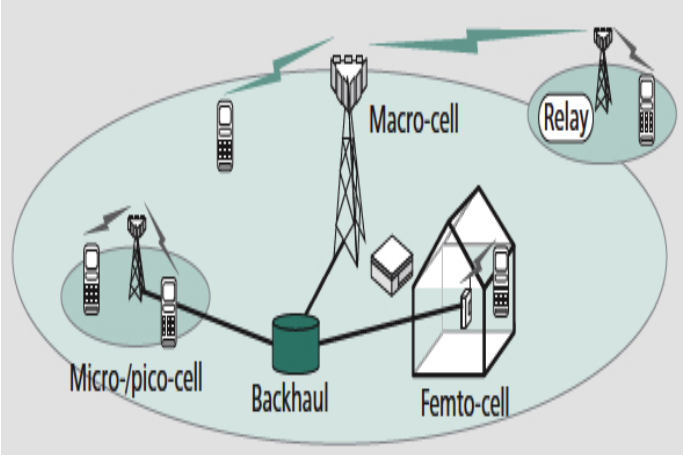

Figure 3.11 – Heterogeneous network deployment with relay for coverage extension [11]

through power control and the users are handed off to the neighbouring cells [129]. Deployment of heterogeneous network of small cells with overlay macro cell, as illustrated in Fig. 3.11, can save a huge amount of energy when combined with switching off BSs and cell zooming techniques [130, 131]. Macro cell can provide a low bit rate but high coverage to users, while BSs with smaller cell sizes can be utilized to provide high bandwidth connections when needed. Lower amount of transmit power is required by the small cells to transmit at shorter propagation distances. Besides, the small cells can be switched off during low traffic period leading to a huge energy saving. EE of different femto cell deployments has been studied in [132, 133, 134, 111, 135] and joint macro-femto cell deployment has been shown to consume more energy in contrast to traditional macro-only network for medium and high femtocell densities [132]. Relays provide coverage for areas that would otherwise be shaded or that would necessitate the use of extremely strong transmit powers. Enhanced concepts include relays that are switched on only when users are present in the area handled by them. EE of different relay schemes, i.e. amplify and forward, decode and forward, block Markov coding, are compared with that of direct transmission in [78].

All these layers can be benefited through employing cognitive radio (CR) techniques, which can adapt the transmission parameters, resource allocation and also network layout to different channel and traffic conditions [136]. CR can optimizes the usage of available spectrum causing less required power to achieve the same data rate, which can lead to better EE-SE tradeoff [8]. CR can also be used to mitigate interference resulting in energy saving. Several applications of CR for green radio, e.g. tuning the direction of power radiated from sector antenna, have been given in [137].

3.8 International research projects

EE has been an interesting research topic in recent years among the network operators, vendors, academia and the regulatory and standardization bodies, e.g. ITU, the 3rd generation partnership project (3GPP), European telecommunication standards institute (ETSI). Many projects have been initiated over the last decades in order to reduce the energy consumption. Majority of the works in literature have been concentrated on battery driven systems, e.g. mobile terminals, wireless ad-hoc and sensor networks [138, 114, 94]. However, many international research projects, e.g. Optimizing Power Efficiency in mobile RAdio Networks (OPERA-Net), mobile VCE Green-Radio, Energy Aware Radio and neTwork tecHnologies (EARTH), Green-touch, have been started over the last few years which have dealt with EE of cellular networks.

EARTH project started in January 2010 with the aim to decrease the energy consumption of the 4^{th} Generation mobile network by half while sustaining the growth in data traffic [122]. EARTH follows a holistic approach targeting the whole system from an EE perspective. Energy efficiency evaluation framework (E^3F) is an important contribution of EARTH that discusses the network modelling, EE performance metrics, energy aware RRM techniques, network architecture and coverage extension devices [74]. GreenTouch is a consortium of leading ICT industry, academic and non-governmental research experts. The project has analyzed the fundamental limits of global communication systems with the target to deliver architecture, specifications and roadmaps to increase the network EE by a factor of 1000 by 2015 from the level in 2010 [139]. The consortium concluded in 2015 and has been successful in its mission to improve the EE of communication networks by the factor it targeted [140]. The project GREAT from Huawei has identified, analysed and modelled the tradeoff among the fundamental resources, e.g. power, energy, spectrum and bandwidth, latency, deployment cost, for mobile networks [141]. Among the other projects, Mobile VCE Green Radio started in 2007 in the UK. This project has aimed at developing green radio architectures focusing mostly on BS design issues, and targeted to achieve 100 times energy reduction of the current wireless networks by 2020 [142]. OPERA-Net, a project led by France telecom, proposed energy saving solutions through cell-size breathing and sleep modes based on traffic loads [143]. This project started in June 2008 and ended on May 2011. The project TEPN, in which the thesis takes place, aims at making the network energy consumption proportional to the actual load, i.e. number of served users, requested bandwidth, by taking intelligent decisions, e.g. switching on and off network components [144]. This project started in 2013 and expected to end in 2017.

3.9 EE-SE tradeoff in AWGN channel

3.9.1 Fundamental EE-SE tradeoff without static power consumption

According to the Shannon's formula, the achievable transmission rate in b/s for AWGN channel is

$$R = w\log_2\left(1+\frac{P_{0k}}{wN_0}\right), \tag{3.19}$$

where w is the channel bandwidth in Hz, P_{0k} is the power received by the typical k-th user from the typical 0-th transmitter expressed in W, and N_0 is the noise spectral density in W/Hz. When noise is the only impairment, P_{0k} is equal to the transmit power P_t, and other parameters in (3.18) are one. Inserting (3.19) with $P_{0k} = P_t$ into (3.1), SE in b/s/Hz can be expressed as

$$\eta_{\text{SE}} = \frac{R}{w} = \log_2\left(1+\frac{P_t}{wN_0}\right). \tag{3.20}$$

Considering bit per energy definition from (3.9) as the energy metric and using (3.20), EE can be

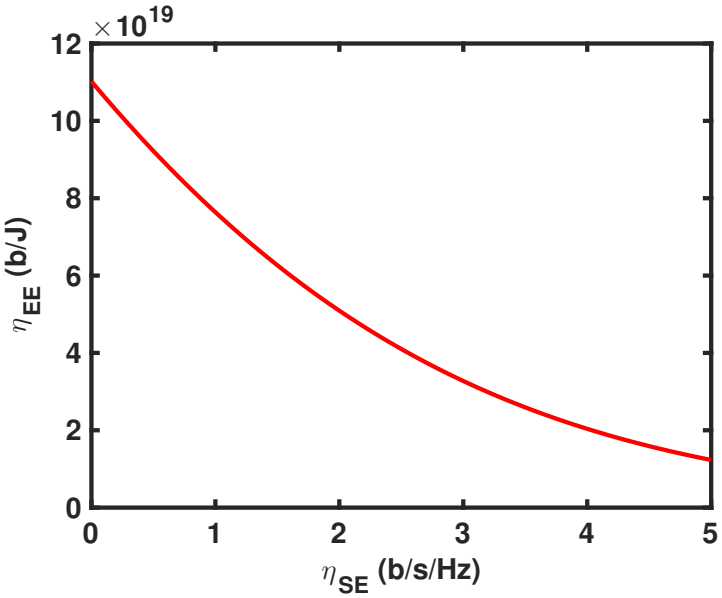

Figure 3.12 – EE vs. SE for AWGN channel considering only the transmit power with $N_0 = -168.83$ dBm/Hz

expressed as

$$\eta_{\text{EE}} = \frac{R}{P_t} = \frac{\eta_{\text{SE}}}{(2^{\eta_{\text{SE}}} - 1)N_0}. \tag{3.21}$$

The EE-SE tradeoff for an AWGN channel considering only the transmit power is shown in Fig. 3.12 for $N_0 = -168.83$ dBm/Hz. As observed in this figure, EE vs. SE curve is a Pareto front tradeoff, i.e. EE decreases if SE increases, when only P_t is considered. Moreover, maximum EE and minimum SE are obtained when the system is in bandwidth limited regime, i.e. w tends to infinity leading to $\lim_{w\to\infty} w\log_2\left(1+\frac{P_t}{wN_0}\right) = \frac{P_t}{N_0}\log_2 e$.

3.9.2 EE-SE tradeoff with static power consumption

EE-SE region for the AWGN channel is characterized by considering the linear power consumption model introduced in (3.16):

$$P_{\text{total}} = aP_t + b. \tag{3.22}$$

When path loss is considered, the power received by the typical k-th user at distance r_{0k} from the typical 0-th transmitter is

$$P_{0k} = P_t\left(\frac{r_{0k}}{r_0}\right)^{-\alpha}, \tag{3.23}$$

where r_0^α is the propagation constant equal to L in (3.18) and random channel power gain X is 1. Using (3.23), (3.19) and (3.20), SE in b/s/Hz can be written as

$$\eta_{\text{SE}} = \log_2\left(1 + \frac{P_t\left(\frac{r_{0k}}{r_0}\right)^{-\alpha}}{wN_0}\right). \tag{3.24}$$

Using (3.22) and inserting the value of P_t from (3.24), EE in b/J can be written as

$$\eta_{\text{EE}} = \frac{w\eta_{\text{SE}}}{aP_t + b} = \frac{w\eta_{\text{SE}}}{a\left(2^{\eta_{\text{SE}}} - 1\right) wN_0\left(\frac{r_{0k}}{r_0}\right)^{\alpha} + b}. \tag{3.25}$$

Fig. 3.13a and Fig. 3.13b respectively depict the effects of the PA factor, i.e. a, and static power consumption, i.e. b, on the EE-SE tradeoff. Parameters for all the remaining plots in this chapter are set according to Table 3.1 unless otherwise mentioned. The value of r_0 is calculated

from COST-231 Hata model for suburban areas considering a carrier frequency at 1800 MHz, BS antenna effective height of 30m and mobile station antenna effective height of 3m [145]. It can

Parameter	Value
w	10 MHz
N_0	-168.83 dBm/Hz
r_{0k}	0.5 km
r_0	1.7×10^{-4} km
α	3.5

Table 3.1 – Parameters for the AWGN channel with static power consumption

be observed that the EE-SE tradeoff curves have large linear parts, where EE increases with SE before reaching to a optimal point beyond which SE cannot be increased without decreasing EE. This large linear part is due to the large amount of energy spent in static power consumption, i.e. b, and is defined as circuit power dominated region. EE starts decreasing when SE is further increased resulting in transmission power dominated region.

Fig. 3.13a shows the EE-SE tradeoff for $a \in \{5, 10, 14.5\}$ [74] when b is 712 W [74]. The results demonstrate that increasing the PA factor decreases EE implying the fact that PA is inefficient when a is large. Total power consumption increases as a becomes higher, but SE does not depend on it resulting in lower EE when a is increased. Besides, the transmission power dominated region starts for a smaller value of P_t when a is large. This causes the optimal point to move towards a lower SE when a is higher.

Fig. 3.13b illustrates the EE-SE tradeoff for $b \in \{100\text{W}, 400\text{W}, 712\text{W}\}$ when a is 14.5. The results demonstrate that increasing b decreases EE. This is due to the fact that the total power consumption increases as static power consumption becomes higher, but SE remains unchanged resulting in lower EE when b is increased. However, the circuit power dominates over a greater value of transmit power causing the optimal point to move towards a higher SE when b increases.

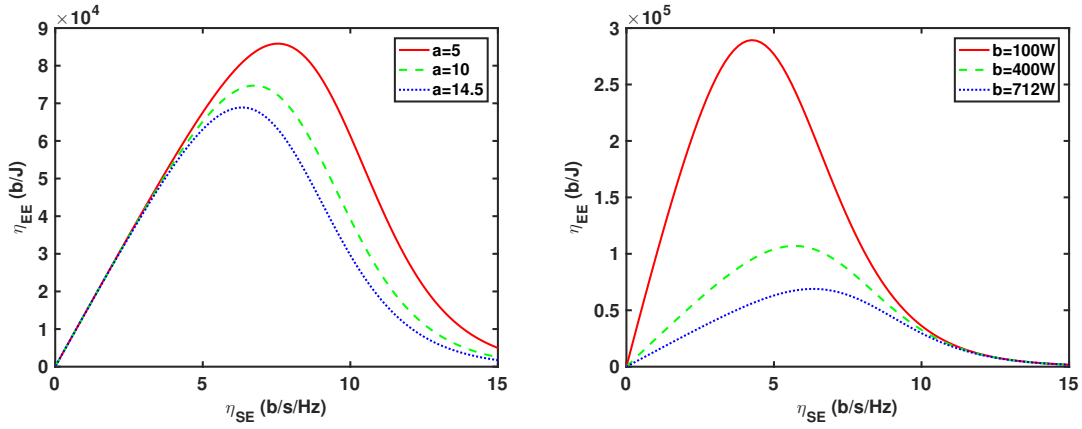

(a) EE vs. SE for different a at $b = 712$ W

(b) EE vs. SE for different b at $a = 14.5$

Figure 3.13 – EE vs. SE for AWGN channel considering static circuit power consumption

Let η_{SE}^* be SE when EE is maximum. Derivative of EE in (3.25) w.r.t. SE can be written as

$$\frac{\partial \eta_{\text{EE}}}{\partial \eta_{\text{SE}}} = \frac{\partial}{\partial \eta_{\text{SE}}} \left(\frac{w\eta_{\text{SE}}}{a\left(2^{\eta_{\text{SE}}}-1\right) wN_0 \left(\frac{r_{0k}}{r_0}\right)^{\alpha} + b} \right)$$
$$= w\left(a\left(2^{\eta_{\text{SE}}}-1\right) wN_0 \left(\frac{r_{0k}}{r_0}\right)^{\alpha} + b\right)^{-1} + w\eta_{\text{SE}}(-1)\left(a\left(2^{\eta_{\text{SE}}}-1\right) wN_0 \left(\frac{r_{0k}}{r_0}\right)^{\alpha} + b\right)^{-2} awN_0 \left(\frac{r_{0k}}{r_0}\right)^{\alpha} 2^{\eta_{\text{SE}}} \log_e 2. \tag{3.26}$$

Since $\frac{\partial \eta_{\text{EE}}}{\partial \eta_{\text{SE}}} = 0$ when EE is maximum, nulling (3.26) and inserting $\eta_{\text{SE}} = \eta_{\text{SE}}^*$, we obtain

$$w\left(a\left(2^{\eta_{\text{SE}}^*}-1\right) wN_0 \left(\frac{r_{0k}}{r_0}\right)^{\alpha} + b\right)^{-1} = \eta_{\text{SE}}^* \left(a\left(2^{\eta_{\text{SE}}^*}-1\right) wN_0 \left(\frac{r_{0k}}{r_0}\right)^{\alpha} + b\right)^{-2} aw^2 N_0 \left(\frac{r_{0k}}{r_0}\right)^{\alpha} 2^{\eta_{\text{SE}}^*} \log_e 2. \tag{3.27}$$

Dividing both sides of (3.27) by $aw^2 N_0 \left(\frac{r_{0k}}{r_0}\right)^{\alpha} \left(a\left(2^{\eta_{\text{SE}}^*}-1\right) wN_0 \left(\frac{r_{0k}}{r_0}\right)^{\alpha} + b\right)^{-2} \neq 0$, we can write

$$2^{\eta_{\text{SE}}^*} - 1 + \frac{b}{awN_0 \left(\frac{r_{0k}}{r_0}\right)^{\alpha}} = \eta_{\text{SE}}^* 2^{\eta_{\text{SE}}^*} \log_e 2$$
$$\implies \frac{b}{awN_0 \left(\frac{r_{0k}}{r_0}\right)^{\alpha}} - 1 = \left(\eta_{\text{SE}}^* \log_e 2 - 1\right) 2^{\eta_{\text{SE}}^*}. \tag{3.28}$$

The negative branch of the Lambert function[1], denoted as W_{-1}, ranges from $W_{-1}(-1/2) = -1$ to $W_{-1}(0^-) = -\infty$. On the other hand, positive branch of the Lambert function, denoted as $W_0(z)$, is ≥ -1 for $z > 0^-$. Solving (3.28) for η_{SE}^*, we obtain

$$\eta_{\text{SE}}^* = \log_2 e \left(1 + W_0 \left[\frac{1}{e} \left(\frac{b}{a w N_0 \left(\frac{r_{0k}}{r_0} \right)^{\alpha}} - 1 \right) \right] \right). \tag{3.29}$$

W_0 is considered due to the fact that SE cannot be negative. With (3.25), maximum EE is

$$\eta_{\text{EE}}^* = \frac{w \eta_{\text{SE}}^*}{a(2^{\eta_{\text{SE}}^*} - 1) w N_0 \left(\frac{r_{0k}}{r_0} \right)^{\alpha} + b}. \tag{3.30}$$

Using (3.24), the transmit power corresponding to maximum EE can be expressed as

$$P_t^* = (2^{\eta_{\text{SE}}^*} - 1) w N_0 \left(\frac{r_{0k}}{r_0} \right)^{\alpha}. \tag{3.31}$$

Figs. 3.14a, 3.14b and 3.14c respectively illustrate the variation of η_{SE}^*, η_{EE}^* and P_t^* w.r.t. a labelled on static circuit power consumption, i.e. b. It is observed that η_{SE}^*, η_{EE}^* and P_t^* decreases when a increases. This implies that the lowest a is desirable to achieve the best EE-SE tradeoff, but this is achieved with higher transmit power. The results also show that increasing the static power consumption increases η_{SE}^* and P_t^* while decreasing η_{EE}^*.

3.10 Conclusion

In this chapter, we have first provided the state of the art performance metrics, cellular network and BS power consumption models. The general propagation model for the whole thesis is also described. Moreover, we illustrated the linear precoding techniques applied at multi-antenna BSs. A detailed survey of the research approaches and projects that aim at improving EE was also given. Finally, we have revisited the characteristic of EE-SE relation in AWGN channel first by considering only the transmit power and then using the linear power consumption model. It is observed that EE is always decreasing with SE when only the transmit power is accounted. However, there is also a large linear part where EE increases with SE when the static circuit power is taken into account. The results also illustrate that both optimal EE and SE decrease as

[1] Inverse of the function $f(z) = ze^z$ with z be any complex number can be written as $z = f^{-1}(ze^z) = W(ze^z)$, where W denotes the Lambert function

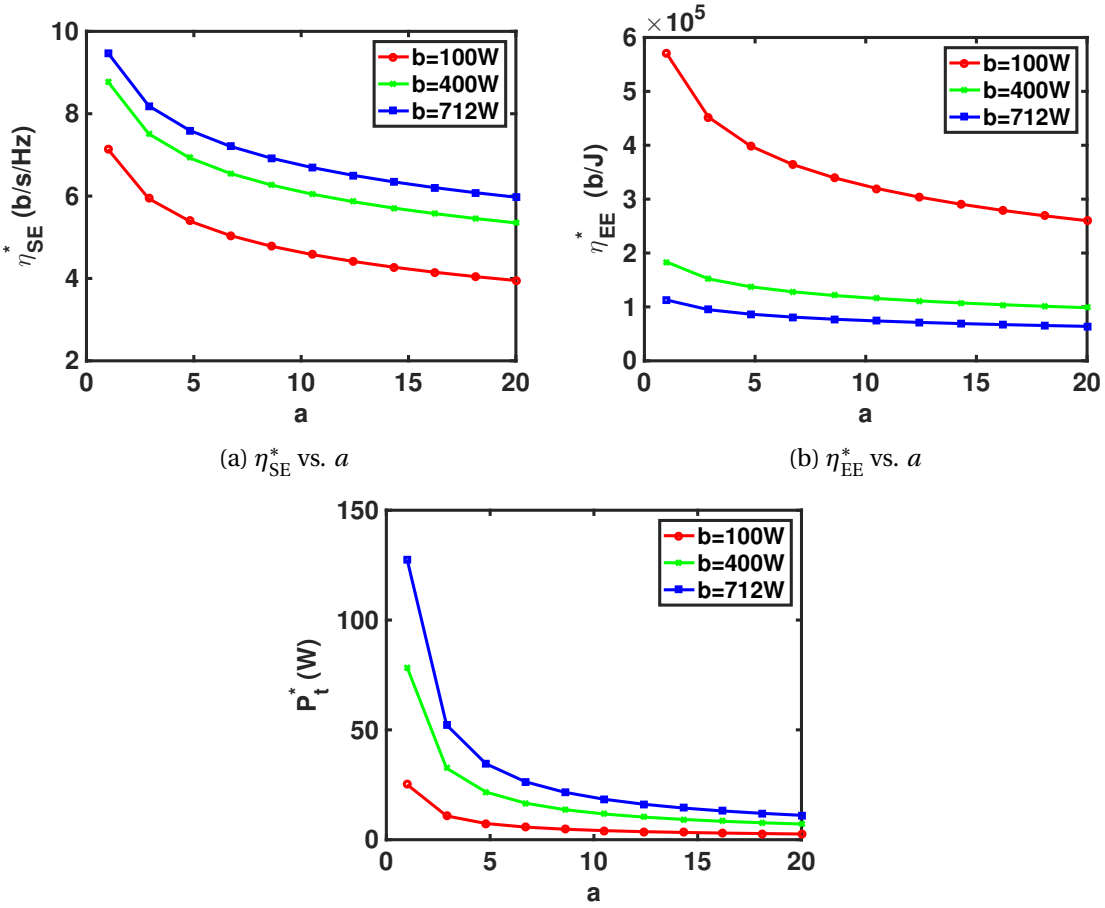

(a) η^*_{SE} vs. a

(b) η^*_{EE} vs. a

(c) P^*_t vs. a

Figure 3.14 – Variation of η^*_{SE}, η^*_{EE} and P^*_t with a for different b

the PA factor increases. Besides, although higher optimal SE is achieved when the static power consumption is increased, the optimal EE becomes lower.

.

Chapter 4

EE-SE tradeoff in a hexagonal cellular network

4.1 Introduction

This chapter deals with the EE-SE tradeoff in a downlink regular hexagonal cellular network.[1] The CDF of SINR is higher in a regular network compared to PPP network and hence, it is better for an operator to be as close as possible to the hexagonal model [5]. We assume a TDMA, FDMA or orthogonal FDMA (OFDMA) type of access leading to a perfect orthogonality between radio resources of a cell. Hence, there is no intra-cell interference. On the other hand, the decrease of signal power with distance allows to reuse the same frequency at spatially separated locations. Reusing the frequency bandwidth over relatively small geographical areas is necessary for the efficient use of the available bandwidth, which potentially increases SE as well as EE. But the major issue in this case is CCI among the co-channel cells.

When the cell size and the BS transmit power are the same for all BSs, then CCI depends only on the ratio between the frequency reuse distance and cell radius, which is equal to $\sqrt{3K}$ as obtained from (3.13). If K is increased, then the effective distance between the co-channel cells increases and CCI decreases. However, since the number of cells in a cluster increases, available bandwidth in a cell decreases. This has a negative effect on SE as well as on EE. It is not clear whether the increase of available bandwidth or the increase of interference has the dominating effect on the EE-SE tradeoff. The aim of this chapter is to study the effect of different frequency reuse factors, i.e. K, on the EE-SE tradeoff both with and without shadowing when the users are

[1] This work has led to the publication [C1], cf. 1.3.2

at different locations in the cell.

To describe the distribution of the interfering BSs, Kelif *et al.* have proposed a model, known as fluid model [14]. A closed form expression of ISR is derived using the model allowing a tractable derivation of outage probability in hexagonal cellular networks. The expression for ISR provided by Kelif *et al.* is limited to the case where the system bandwidth is reused in each cell. We obtain a parametric expression of ISR for various reuse cases with a curve fitting approach. The parametric expressions of ISR allow us to derive the EE-SE tradeoff for several frequency reuse factors when non negligible static circuitry power consumption is assumed and path loss dependent channel modelling is considered. On the other hand, although SE is generally taken as equal to the Shannon capacity when only the path loss is taken into account, the capacity in Shannon's sense is not defined when shadowing is considered. We propose the ϵ-EE-SE tradeoff when shadowing is considered. The definition depends on the outage capacity achievable and its corresponding EE, and is particularly useful when long-term fading is present. We determine the CDF of SINR allowing to study the EE-SE tradeoff when shadowing is taken into account.

The results show that when static power consumption into the BS is considered, the EE-SE tradeoff has a large linear part before a sharp decreasing. Our results also illustrate that using the whole system bandwidth in each cell optimizes the EE-SE tradeoff only when a user is close to the BS. Moreover, better EE-SE tradeoff in the shadowing environment is achieved for higher ϵ implying higher outage in the system, and hence, should be set according to the desired QoS.

4.2 System model

A downlink regular hexagonal cellular network with different frequency reuse factors is considered. BSs are placed at the center of the cells and both BSs and users are equipped with a single antenna. Users are connected to the nearest BS. Transmit power of all BSs is the same that makes the network homogeneous causing the EE-SE study of a single cell valid for all the other cells in the network. The linear power consumption model introduced in (3.16) is considered for BSs :

$$P_{\text{total}} = aP_t + b. \tag{4.1}$$

We assume that the parameters of the power consumption model corresponds to a resource block allocated to a user.

The power received by the typical k-th user at distance r_{ik} from BS $i \geq 0$ considering shadow-

ing along with path loss is

$$P_{ik} = P_t \left(\frac{r_{ik}}{r_0} \right)^{-\alpha} Y_{ik}, \tag{4.2}$$

where r_0^α is the propagation constant given by L in (3.18) which has the same value as for the AWGN channel, Y_{ik}, given by X in (3.18), is a log-normal (LN) r.v. characterizing shadowing denoted as $Y_{ik} \sim \mathscr{LN}(0,\sigma)$, with zero mean and σ as standard deviation in dB. The factor $P_t\left(\frac{r_{ik}}{r_0}\right)^{-\alpha}$ is the received power related with path loss and represents the average received power in shadowing condition. The user receives interference from all BSs having the same frequency sub-band as the connected BS. The connected BS is set for $i = 0$ without loss of generality, and the power received by the k-th user at distance r_{0k} from the connected BS is

$$P_{0k} = P_t \left(\frac{r_H v}{r_0} \right)^{-\alpha} Y_{0k}, \tag{4.3}$$

where $v = r_{0k}/r_H$ is the normalized distance with $0 \leq v \leq 1$. Let $I = \sum_{i\geq 1} P_{ik}$ the interference power aggregated from BS i ($i \geq 1$) to the k-th user and σ_n^2 the noise power on the total bandwidth available to the user. Then, the SINR of the user is

$$\gamma = \frac{P_{0k}}{\sigma_n^2 + I} = \frac{1}{\frac{\frac{w}{K} N_0}{P_{0k}} + \frac{I}{P_{0k}}}, \tag{4.4}$$

where w is the bandwidth of a resource block allocated to a user when frequency reuse factor is one and N_0 is the noise spectral density.

The ISR with shadowing depends on the r.v. Y_{ik} and can be written as

$$f_s(v,\alpha) = \frac{I}{P_{0k}} = \sum_{i\geq 1} \left(\frac{r_{ik}}{r_H v} \right)^{-\alpha} \frac{Y_{ik}}{Y_{0k}}. \tag{4.5}$$

We also study the EE-SE tradeoff without shadowing consideration, which is equivalent to work with the average received power in shadowing environment. The ISR without shadowing consideration, noted as $f(v,\alpha)$, is simply [14]

$$f(v,\alpha) = \frac{I}{P_{0k}} = \sum_{i\geq 1} \left(\frac{r_{ik}}{r_H v} \right)^{-\alpha}. \tag{4.6}$$

4.3 EE-SE tradeoff without shadowing

Considering a frequency reuse factor K, the available frequency for a user is w/K and the Shannon SE in b/s/Hz is

$$\eta_{\mathrm{SE}} = \frac{1}{K}\log_2\left(1+\gamma\right). \tag{4.7}$$

Inserting the value of γ from (4.4), and using (4.6), (4.7) can be written as

$$\eta_{\mathrm{SE}} = \frac{1}{K}\log_2\left(1+\frac{1}{\frac{\frac{w}{K}N_0}{P_{0k}}+f(v,\alpha)}\right). \tag{4.8}$$

When shadowing is not considered, (4.3) can be written as $P_{0k} = P_t\left(\frac{r_H v}{r_0}\right)^{-\alpha}$. Inserting the value of P_{0k} in (4.8), we get

$$\begin{aligned}
&\frac{1}{\frac{\frac{w}{K}N_0}{P_t\left(\frac{r_H v}{r_o}\right)^{-\alpha}}+f(v,\alpha)} = 2^{K\eta_{\mathrm{SE}}}-1\\
&\Leftrightarrow \frac{P_t\left(\frac{r_H v}{r_o}\right)^{-\alpha}}{\frac{w}{K}N_0} = \frac{1}{\frac{1}{2^{K\eta_{\mathrm{SE}}}-1}-f(v,\alpha)}\\
&\Leftrightarrow P_t = \frac{\left(\frac{r_H v}{r_o}\right)^{\alpha}\frac{w}{K}N_0(2^{K\eta_{\mathrm{SE}}}-1)}{1-f(v,\alpha)(2^{K\eta_{\mathrm{SE}}}-1)}.
\end{aligned} \tag{4.9}$$

Since EE is defined as

$$\eta_{\mathrm{EE}} = \frac{w\eta_{\mathrm{SE}}}{aP_t+b}, \tag{4.10}$$

inserting the value of P_t from (4.9), (4.10) can be expressed as

$$\eta_{\mathrm{EE}} = \frac{w\eta_{\mathrm{SE}}}{a\frac{\left(\frac{r_H v}{r_0}\right)^{\alpha}\frac{w}{K}N_0(2^{K\eta_{\mathrm{SE}}}-1)}{1-f(v,\alpha)(2^{K\eta_{\mathrm{SE}}}-1)}+b}. \tag{4.11}$$

4.3.1 Parametric expression of $f(v,\alpha)$

A pragmatic approach is adopted and a parametric expression of $f(v,\alpha)$ given in (4.6) is obtained for K equal to 1, 3, 4 and 7 for α ranging from 2.5 to 4 by fitting the Monte Carlo simulations

performed over the random position of a user in the cell of interest. A location is chosen randomly

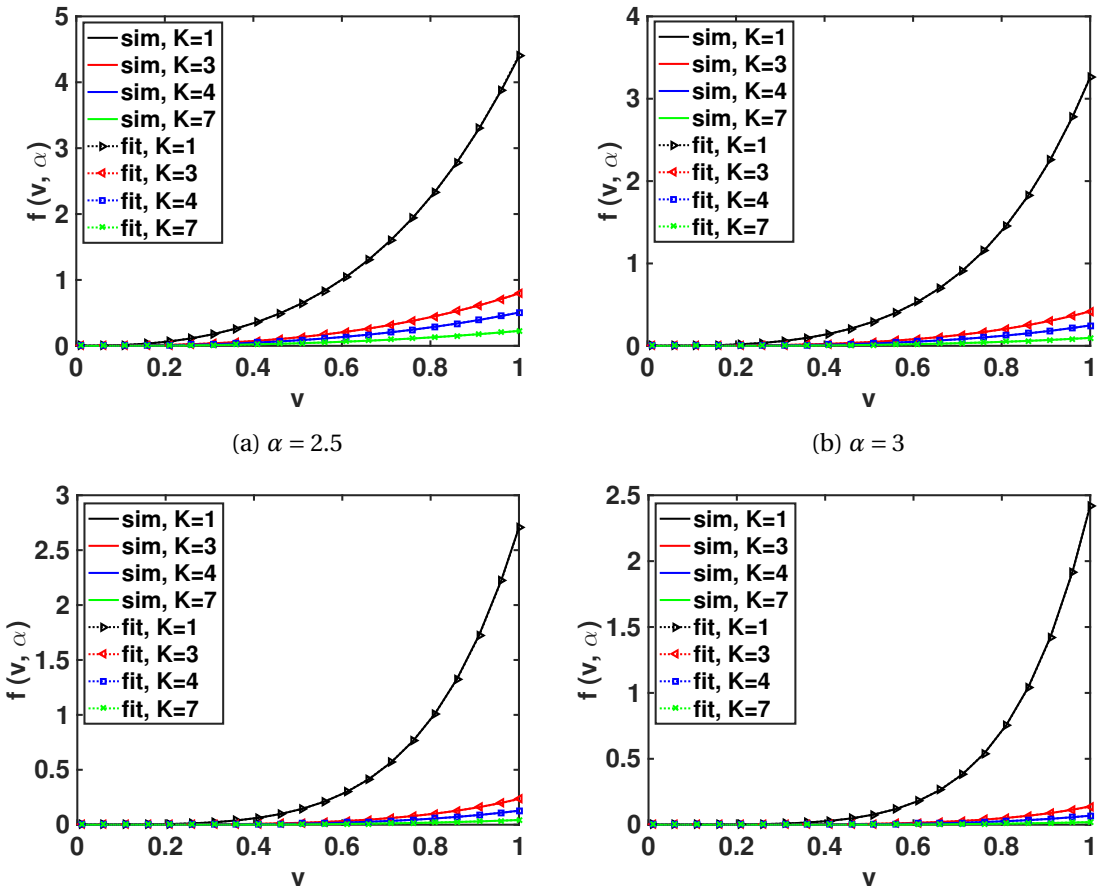

(a) $\alpha = 2.5$ (b) $\alpha = 3$

(c) $\alpha = 3.5$ (d) $\alpha = 4$

Figure 4.1 – Fitting of the parametric expressions of $f(v,\alpha)$ with simulations for $K = \{1,3,4,7\}$ and $\alpha = \{2.5,3,3.5,4\}$

.

with uniform distribution in the cell of interest with $r_H = 0.5$ km at each snapshot and $f(v,\alpha)$ is computed applying (4.6). Following the multiple linear regression model, a general expression of $f(v,\alpha)$ for different frequency reuse factors is obtained afterwards as follows:

$$f(v,\alpha) = e^{\sum_{i+j\leq 5} A_{i,j} (\log_e v)^i \alpha^j}. \tag{4.12}$$

The values of the coefficients $A_{i,j}$ for different K are provided in Table 4.1. The simulated and the fitted values match very well, which can be observed in Fig. 4.1. The maximum value of the relative error, considering all the simulations, is 0.75% depicting a perfect match between the simulation and the parametric expression. It can also be observed that the ISR is higher for lower frequency reuse factor. Moreover, the ISR increases as the user moves away from the BS, and this is extremely significant for K=1, since it experiences more interference. The tractable closed-form of this semi-analytical expression enables us to avoid performing Monte Carlo simulations to study the EE-SE tradeoff for different frequency reuse factors.

Coefficients	$K=1$	$K=3$	$K=4$	$K=7$
$A_{5,0}$	0.0043	0.0025	0.0015	0.0009
$A_{0,5}$	0.0018	0.0006	0.0003	0.0002
$A_{4,1}$	0.0098	0.0049	0.0031	0.0018
$A_{1,4}$	0.0007	-0.0001	-0.0001	-0.00004
$A_{3,2}$	0.0022	0.0022	0.0014	0.0009
$A_{2,3}$	-0.0034	-0.0005	-0.0003	-0.0001
$A_{4,0}$	0.0286	0.0169	0.0105	0.0064
$A_{0,4}$	-0.0254	-0.009	-0.0054	-0.0031
$A_{3,1}$	0.0961	0.0386	0.0251	0.0143
$A_{1,3}$	-0.026	-0.001	-0.0003	0.0001
$A_{2,2}$	0.0546	0.0226	0.0144	0.0079
$A_{3,0}$	-0.0078	0.0166	0.0105	0.0075
$A_{0,3}$	0.0944	0.0421	0.0236	0.0124
$A_{2,1}$	0.1996	0.0675	0.0468	0.0276
$A_{1,2}$	0.276	0.061	0.0379	0.0191
$A_{2,0}$	-0.2363	-0.0434	-0.0282	-0.0131
$A_{0,2}$	0.2685	0.0824	0.0843	0.0732
$A_{1,1}$	0.7172	0.9695	0.9929	1.0046
$A_{1,0}$	-0.0106	-0.0189	-0.0215	-0.0179
$A_{0,1}$	-2.6125	-2.1043	-2.0724	-2.1864
$A_{0,0}$	5.6798	4.1574	3.7802	3.4321

Table 4.1 – Coefficients of $f(\nu,\alpha)$

4.3.2 Numerical results on EE-SE tradeoff without shadowing

In this subsection, we provide some numerical results to illustrate the effect of the frequency reuse factor on the EE-SE tradeoff. The parameters for all the plots remaining in this chapter are

set according to Table 4.2 unless otherwise mentioned.

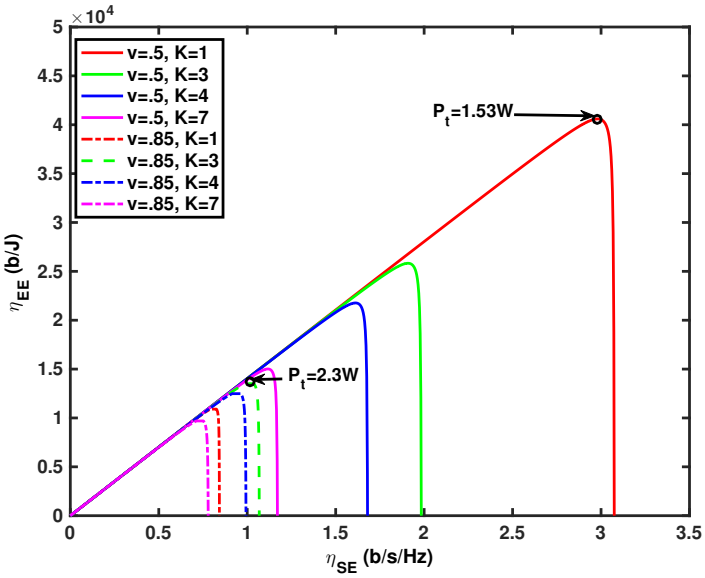

Figure 4.2 – EE-SE tradeoff without shadowing

Parameter	Value
w	10 MHz
N_0	-168.83 dBm/Hz
r_0	1.7×10^{-4} km
r_H	0.5 km
a	14.5 [74]
b	712 W [74]
α	3.5

Table 4.2 – Parameters for the plots with and without shadowing

Fig. 4.2 depicts the effects of K on the EE-SE tradeoff without shadowing. Static circuit power dominates for low value of SE, and EE increases linearly with the SE as seen also for the AWGN channel. Therefore, EE can be increased without sacrificing the SE for this linear portion of the EE-SE tradeoff curves. Afterwards, EE decreases due to the transmission power domination. Thus, there exists an optimal EE-SE tradeoff, which has to be obtained. However, since the network is homogeneous, i.e. all BSs have the same transmit power, and interference limited, SE converges towards the limit $\frac{1}{K}\log_2\left(1+\frac{1}{\mathrm{ISR}}\right)$ with a small increase of P_t after the optimal point is

reached. This results in sharp decrease of EE when P_t is further increased which is not observed in case of AWGN channel.

While the optimal frequency reuse factor in Fig. 4.2 is $K = 3$ for $\upsilon = 0.85$, it is 1 for $\upsilon = 0.5$. This behavior is based on the characteristic of (4.7). Since SE is inversely proportional to K, it increases for lower K resulting in higher EE for a particular P_t. On the other hand, noise power increases for lower K because of higher available bandwidth. Moreover, ISR is also higher for lower K as can be observed from Fig. 4.1. Therefore, the SINR is decreasing for the given transmit power as K is decreasing. The ISR decrease is extremely significant for $K = 1$ compared to the other values of K when $\upsilon = 0.85$ as can be seen in Fig. 4.1. This causes $K = 3$ to be the best choice at this distance. For a particular K, the decrease of SINR, due to high ISR as the user moves away from BS, results in lower SE and EE. We determine EE, SE and P_t corresponding to the optimal point in the next section.

4.3.3 Determination of EE, SE and P_t corresponding to optimal point

Derivative of EE in (4.11) w.r.t. SE is

$$\begin{aligned}\frac{\partial \eta_{\mathrm{EE}}}{\partial \eta_{\mathrm{SE}}} &= \frac{\partial}{\partial \eta_{\mathrm{SE}}} \frac{w\eta_{\mathrm{SE}}}{a\frac{\left(\frac{r_H \upsilon}{r_0}\right)^{\alpha}\frac{w}{K}N_0(2^{K\eta_{\mathrm{SE}}}-1)}{1-f(\upsilon,\alpha)(2^{K\eta_{\mathrm{SE}}}-1)}+b} \\ &= w\frac{\left(a\frac{\left(\frac{r_H \upsilon}{r_0}\right)^{\alpha}\frac{w}{K}N_0(2^{K\eta_{\mathrm{SE}}}-1)}{1-f(\upsilon,\alpha)(2^{K\eta_{\mathrm{SE}}}-1)}+b\right)-\eta_{\mathrm{SE}}\left(a\left(\frac{r_H \upsilon}{r_0}\right)^{\alpha}\frac{w}{K}N_0\frac{K\log_e 2\, 2^{K\eta_{\mathrm{SE}}}}{(1-f(\upsilon,\alpha)(2^{K\eta_{\mathrm{SE}}}-1))^2}\right)}{\left(a\frac{\left(\frac{r_H \upsilon}{r_0}\right)^{\alpha}\frac{w}{K}N_0(2^{K\eta_{\mathrm{SE}}}-1)}{1-f(\upsilon,\alpha)(2^{K\eta_{\mathrm{SE}}}-1)}+b\right)^2}. \end{aligned} \tag{4.13}$$

When EE is maximal, η^*_{EE}, (4.13) equals to 0. Let η^*_{SE} be the optimal SE for which η_{EE} is maximum providing $\frac{\partial \eta_{\mathrm{EE}}}{\partial \eta_{\mathrm{SE}}}|_{\eta^*_{SE}} = 0$. Nulling (4.13), and using the change of variable $y = 2^{K\eta^*_{SE}} - 1$,

we can write

$$\frac{\left(a\frac{\left(\frac{r_H v}{r_0}\right)^{\alpha}\frac{w}{K}N_0 y}{1-f(v,\alpha)y}+b\right)-\frac{1}{K}\log_2(y+1)\left(a\left(\frac{r_H v}{r_0}\right)^{\alpha}\frac{w}{K}N_0\frac{K\log_e 2\,(y+1)}{\left(1-f(v,\alpha)y\right)^2}\right)}{\left(a\frac{\left(\frac{r_H v}{r_0}\right)^{\alpha}\frac{w}{K}N_0 y}{1-f(v,\alpha)y}+b\right)^2}=0$$

$$\Leftrightarrow\left(a\frac{\left(\frac{r_H v}{r_0}\right)^{\alpha}\frac{w}{K}N_0 y}{1-f(v,\alpha)y}+b\right)-\frac{1}{K}\log_2(y+1)\left(a\left(\frac{r_H v}{r_0}\right)^{\alpha}\frac{w}{K}N_0\frac{K\log_e 2\,(y+1)}{\left(1-f(v,\alpha)y\right)^2}\right)=0$$

$$\Leftrightarrow\frac{y}{1-f(v,\alpha)y}-\log_2(y+1)\frac{\log_e 2\,(y+1)}{\left(1-f(v,\alpha)y\right)^2}=-\frac{b}{a\left(\frac{r_H v}{r_0}\right)^{\alpha}\frac{w}{K}N_0}. \tag{4.14}$$

Multiplying both sides of (4.14) by $1-f(v,\alpha)y\neq 0$,

$$y-\frac{\log_2(y+1)(y+1)\log_e 2}{1-f(v,\alpha)y}=-\frac{b\left(1-f(v,\alpha)y\right)}{a\left(\frac{r_H v}{r_0}\right)^{\alpha}\frac{w}{K}N_0}. \tag{4.15}$$

There is no closed form expression for y. We obtained η_{SE}^* by solving (4.15) numerically. Using (4.9), the transmit power corresponding to η_{SE}^* can be written as

$$P_t^*=\frac{\left(\frac{r_H v}{r_0}\right)^{\alpha}\frac{w}{K}N_0(2^{K\eta_{SE}^*}-1)}{1-f(v,\alpha)(2^{K\eta_{SE}^*}-1)}. \tag{4.16}$$

Using (4.11), η_{EE}^* can be written as

$$\eta_{EE}^*=\frac{w\eta_{SE}^*}{a\frac{\left(\frac{r_H v}{r_0}\right)^{\alpha}\frac{w}{K}N_0\left(2^{K\eta_{SE}^*}-1\right)}{1-f(v,\alpha)\left(2^{K\eta_{SE}^*}-1\right)}+b}. \tag{4.17}$$

Fig. 4.3 illustrates the variation of η_{SE}^*, η_{EE}^* and P_t^* with frequency reuse factor. The results show that the optimal frequency reuse factor in terms of η_{SE}^* and η_{EE}^* is 1 for $v=0.5$, while it is 3 for $v=0.85$ and $v=1$. Besides, $K=1$ is the worst at $v=1$, while this is not the case when v is equal to 0.85. This is due to fact that the increase of ISR becomes extremely significant for $K=1$ when the user moves closer to the cell edge. On the other hand, ISR becomes lower as K is increased and requires higher P_t^* for the convergence of SE towards the limit, as it can be

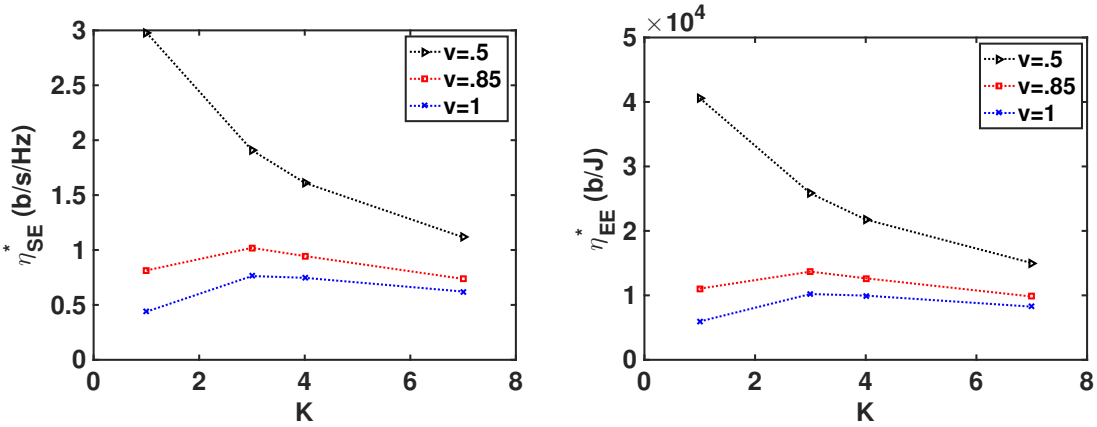

(a) η^*_{SE} vs. K

(b) η^*_{EE} vs. K

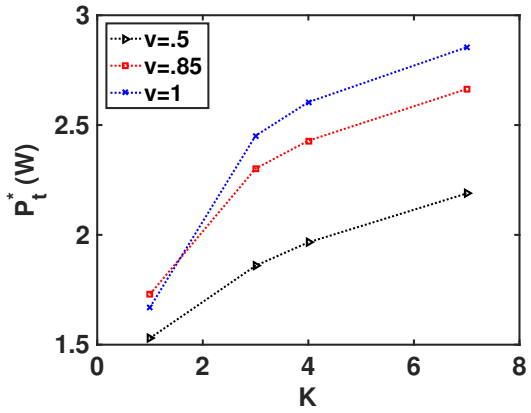

(c) P^*_t vs. K

Figure 4.3 – Variation of η^*_{SE}, η^*_{EE} and P^*_t with K

illustrated by (4.8). This results in higher P_t^* as K is increased.

4.4 ϵ-EE-SE tradeoff with long term shadowing

Since SE is an increasing function of γ, inserting (4.7) into (3.2), ϵ-SE can be expressed as

$$\begin{aligned}\eta_{\mathrm{SE}}^{(\epsilon)} &= \sup\left\{E : \mathrm{P}\left[\frac{1}{K}\log_2\left(1+\gamma\right) < E\right] \le \epsilon\right\} \\ &= \sup\left\{E : \mathrm{P}\left[\gamma < \left(2^{KE}-1\right)\right] \le \epsilon\right\} \\ &= \sup\left\{E : F_\gamma\left(2^{KE}-1\right) \le \epsilon\right\}, \end{aligned} \tag{4.18}$$

where F_γ denotes the CDF of γ. Outage EE or ϵ-EE is then defined using (4.10) as

$$\eta_{\mathrm{EE}}^{(\epsilon)} = \frac{w\eta_{\mathrm{SE}}^{(\epsilon)}}{aP_t+b}. \tag{4.19}$$

In order to characterize the EE-SE tradeoff, CDF of γ is needed to be computed first.

4.4.1 CDF of γ

The SINR of the k-th user at distance v from BS with shadowing consideration can be expressed using (4.4), (4.3), and (4.5) as

$$\gamma = \left(\frac{\frac{w}{K}N_0}{P_t\left(\frac{r_H v}{r_0}\right)^{-\alpha}Y_{0k}} + f_s(v,\alpha)\right)^{-1}. \tag{4.20}$$

Each term of the sum in the numerator of $f_s(v,\alpha)$ is a LN r.v. Therefore, we can write $\log_e(r_{ik}^{-\alpha}Y_{ik}) \sim \mathcal{N}(d\mu_{ik}, d^2\sigma^2)$, where $d = \log_e 10/10$ and $\mu_{ik} = \frac{1}{d}\log_e\left(r_{ik}^{-\alpha}\right)$. Numerator of $f_s(v,\alpha)$ is sum of LN r.vs., and can be approximated by a LN r.v. according to the Fenton-Wilkinson method [146]. Therefore, we can write $\log_e\left(\sum_{i\ge1} r_{ik}^{-\alpha}Y_{ik}\right) \sim \mathcal{N}\left(d\mu_{Fn}, d^2\sigma_{Fn}^2\right)$, where [146]

$$\begin{aligned} d\mu_{Fn} &= \log_e\left(\sum_{i\ge1} e^{d\mu_{ik}}\right) + \frac{d^2\sigma^2}{2} - \frac{d^2\sigma_{Fn}^2}{2} \\ &= \log_e\left(\sum_{i\ge1} r_{ik}^{-\alpha}\right) + \frac{d^2\sigma^2}{2} - \frac{d^2\sigma_{Fn}^2}{2} \end{aligned} \tag{4.21}$$

and

$$d^2\sigma_{Fn}^2 = \log_e\left[\left(e^{d^2\sigma^2}-1\right)\frac{\sum_{i\geq 1} e^{2d\mu_{ik}}}{\left(\sum_{i\geq 1} e^{d\mu_{ik}}\right)^2}+1\right]$$
$$= \log_e\left[\left(e^{d^2\sigma^2}-1\right)\frac{\sum_{i\geq 1} r_{ik}^{-2\alpha}}{\left(\sum_{i\geq 1} r_{ik}^{-\alpha}\right)^2}+1\right]. \tag{4.22}$$

The ratio of two LN r.v. is a LN r.v. with mean and variance equal to the difference of the means and sum of the variances respectively. Therefore, $f_s(\nu,\alpha)$ is a LN r.v. and is noted as $\mathscr{LN}(\mu_F,\sigma_F)$ with

$$d\mu_F = d\mu_{Fn} - \log_e r_{0k}^{-\alpha} \tag{4.23}$$

and

$$d^2\sigma_F^2 = d^2\sigma_{Fn}^2 + d^2\sigma^2. \tag{4.24}$$

Inserting (4.21) into (4.23), we get

$$d\mu_F = \log_e\left(\sum_{i\geq 1} r_{ik}^{-\alpha}\right) + \frac{d^2\sigma^2}{2} - \frac{d^2\sigma_{Fn}^2}{2} - \log_e r_{0k}^{-\alpha}. \tag{4.25}$$

Inserting $r_{0k} = r_H\nu$ and (4.6) into (4.25), we can write

$$\mu_F = \frac{1}{d}\left(\log_e f(\nu,\alpha) + \frac{d^2\sigma^2}{2} - \frac{d^2\sigma_{Fn}^2}{2}\right). \tag{4.26}$$

using (4.22), (4.26) can be expressed as

$$\mu_F = \frac{1}{d}\left(\log_e f(\nu,\alpha) + \frac{d^2\sigma^2}{2} - \frac{1}{2}\left(\log_e\left[\left(e^{d^2\sigma^2}-1\right)G(\nu,\alpha)+1\right]\right)\right), \tag{4.27}$$

where $G(\nu,\alpha) = \frac{\sum_{i\geq 1} r_{ik}^{-2\alpha}}{\left(\sum_{i\geq 1} r_{ik}^{-\alpha}\right)^2}$. Inserting (4.22) into (4.24), we obtain

$$\sigma_F = \sqrt{\frac{1}{d^2}\log_e\left[\left(e^{d^2\sigma^2}-1\right)G(\nu,\alpha)+1\right] + \sigma^2}. \tag{4.28}$$

Parametric expressions of $G(\nu,\alpha)$ are obtained for various frequency reuse factors in the same

way as was done for $f(\upsilon,\alpha)$ and they have the same general form as follows:

$$G(\upsilon,\alpha)=e^{\sum\limits_{i+j\leq 5} B_{i,j}(\log_e \upsilon)^i \alpha^j}. \tag{4.29}$$

The values of the coefficients $B_{i,j}$ for different K are provided in Table 4.3. The maximum value of

Table 4.3 – Coefficients of $G(\upsilon,\alpha)$

Coefficients	$K=1$	$K=3$	$K=4$	$K=7$
$B_{5,0}$	-0.0038	0.0048	0.0022	0.0019
$B_{0,5}$	-0.007	-0.0031	-0.0021	-0.0014
$B_{4,1}$	-0.0118	0.004	0.002	0.0025
$B_{1,4}$	-0.0006	0.0007	0.0005	0.0002
$B_{3,2}$	-0.0093	-0.0028	-0.002	-0.0003
$B_{2,3}$	0.0068	-0.0002	-0.0004	-0.0003
$B_{4,0}$	0.0048	0.0519	0.0256	0.0181
$B_{0,4}$	0.1169	0.0578	0.0405	0.0268
$B_{3,1}$	-0.048	0.0657	0.0388	0.0305
$B_{1,3}$	0.0404	-0.0098	-0.0085	-0.0044
$B_{2,2}$	-0.1412	-0.0187	-0.0108	0.0015
$B_{3,0}$	0.2167	0.1574	0.0766	0.0432
$B_{0,3}$	-0.7086	-0.413	-0.3002	-0.2041
$B_{2,1}$	0.4045	0.3293	0.2027	0.1167
$B_{1,2}$	-0.5395	0.0109	0.0222	0.0279
$B_{2,0}$	0.3355	0.0131	-0.0209	-0.021
$B_{0,2}$	1.554	1.2898	0.9783	0.6955
$B_{1,1}$	2.1089	0.522	0.3008	0.1318
$B_{1,0}$	-1.1807	-0.4013	-0.2474	-0.1178
$B_{0,1}$	0.9219	-0.7917	-0.6697	-0.5189
$B_{0,0}$	-10.702	-7.7232	-7.2845	-6.9271

the relative error considering all the simulations is about 3%. This small relative error indicates a good match between the simulations and the parametric expressions, which can also be observed in Fig. 4.4.

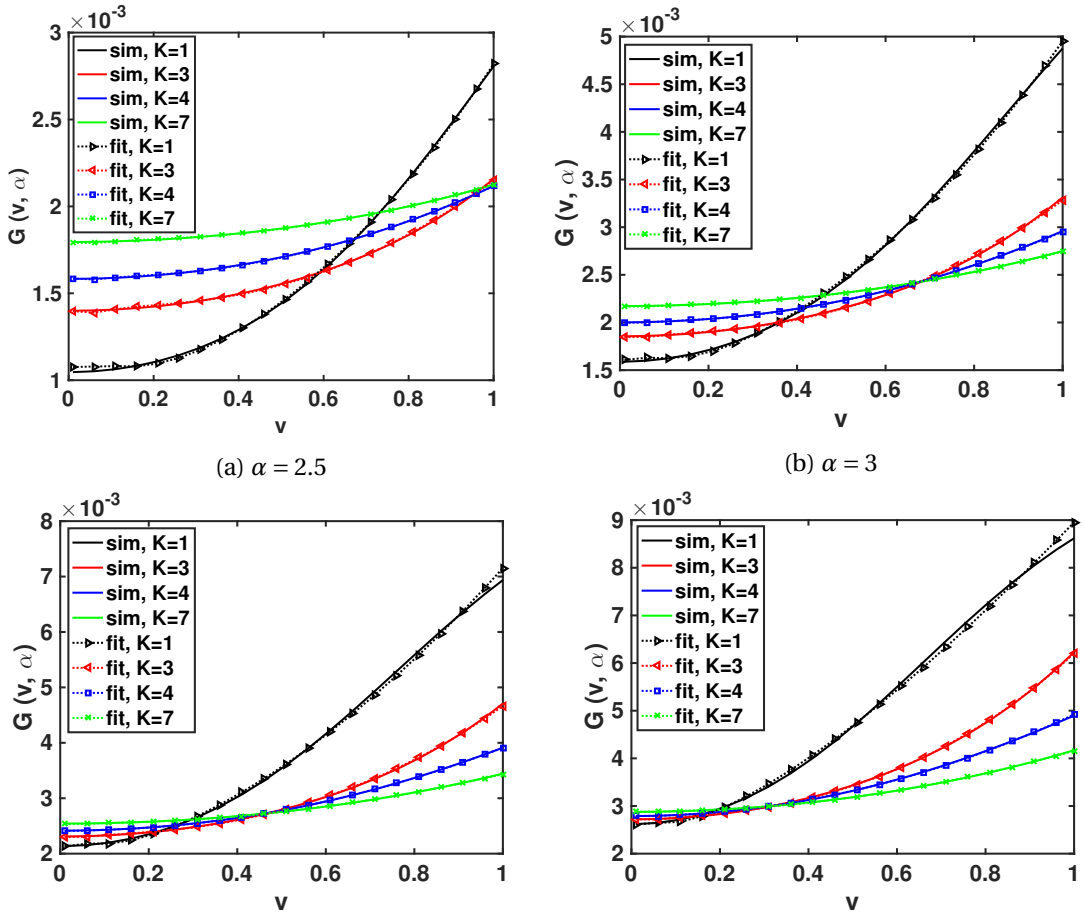

(a) $\alpha = 2.5$

(b) $\alpha = 3$

(c) $\alpha = 3.5$

(d) $\alpha = 4$

Figure 4.4 – Fitting of parametric expressions of $G(v,\alpha)$ with simulations for $K = \{1,3,4,7\}$ and $\alpha = \{2.5,3,3.5,4\}$

.

We approximate $\frac{\frac{w}{K}N_0}{P_t\left(\frac{r_H v}{r_0}\right)^{-\alpha}Y_{0k}} \sim \mathscr{LN}(\mu_N, \sigma_N)$ with

$$\begin{cases} \mu_N = 10\log_{10}\left(\frac{w}{K}N_0\right) - 10\log_{10}\left(P_t\left(\frac{r_H v}{r_0}\right)^{-\alpha}\right) \\ \sigma_N = \sigma \end{cases} \tag{4.30}$$

Since the sum of two LN r.v. can be approximated by a LN r.v. and the inverse of a LN r.v. is also LN [147], we can write $\gamma \sim \mathscr{LN}(\mu_\gamma, \sigma_\gamma)$. If μ_{NL}, σ_{NL}, μ_{FL} and σ_{FL} are the parameters in linear units corresponding to μ_N, σ_N, μ_F and σ_F respectively, then μ_γ and σ_γ can be written as [146]

$$\begin{cases} \mu_\gamma = \frac{1}{2d}\log_e\left(\frac{{\sigma_{NL}}^2+{\sigma_{FL}}^2}{(\mu_{NL}+\mu_{FL})^2}+1\right) - \frac{1}{d}\log_e\left(\mu_{NL}+\mu_{FL}\right) \\ \sigma_\gamma = \frac{1}{d}\sqrt{\log_e\left(\frac{{\sigma_{NL}}^2+{\sigma_{FL}}^2}{(\mu_{NL}+\mu_{FL})^2}+1\right)} \end{cases} \tag{4.31}$$

where

$$\begin{cases} \mu_{NL} = e^{d\mu_N + d^2\sigma^2/2}, \quad \mu_{FL} = e^{d\mu_F + d^2{\sigma_F}^2/2} \\ \sigma^2_{NL} = e^{2d\mu_N + d^2\sigma^2}\left(e^{d^2\sigma^2}-1\right) \\ \sigma^2_{FL} = e^{2d\mu_F + d^2{\sigma_F}^2}\left(e^{d^2{\sigma_F}^2}-1\right) \end{cases} \tag{4.32}$$

The CDF of γ can now be expressed as

$$F_\gamma(x) = 1 - \mathrm{P}(\gamma > x) = 1 - \mathrm{P}\left(\frac{10\log_{10}(\gamma)-\mu_\gamma}{\sigma_\gamma} > \frac{10\log_{10}(x)-\mu_\gamma}{\sigma_\gamma}\right). \tag{4.33}$$

Since $\left(\frac{10\log_{10}(\gamma)-\mu_\gamma}{\sigma_\gamma}\right)$ is a standard normal r.v., (4.33) can be expressed as

$$F_\gamma(x) = 1 - Q\left(\frac{10\log_{10}(x)-\mu_\gamma}{\sigma_\gamma}\right), \tag{4.34}$$

where $Q(x)$ is the Marcuum function that provides the CCDF of a standard normal r.v. X. Fig. 4.5 validates the approximations regarding CDF of SINR. In this figure, CDF of γ is plotted from Monte Carlo simulations performed for $v = 0.5$ and $\sigma = 5$ dB, and compared to the analytical approximation (4.34). An excellent match can be observed validating the approximations, and the maximum relative error is less than 2%.

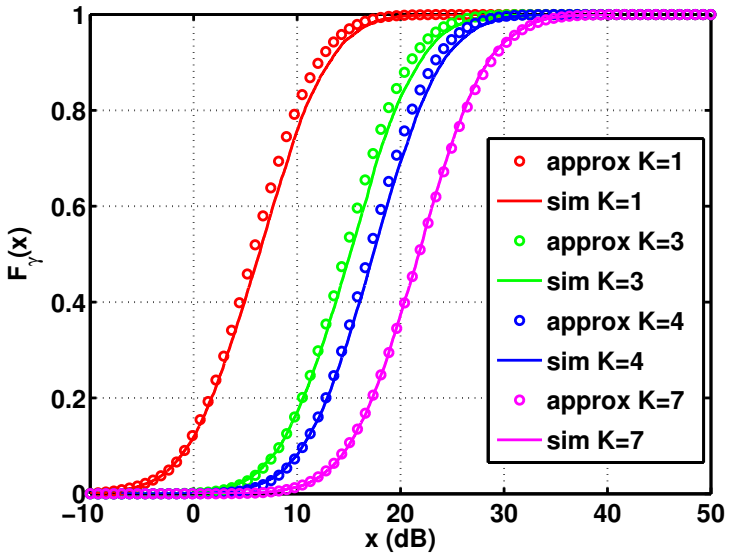

Figure 4.5 – Comparison of the approximated CDF of the SINR with simulations

4.4.2 Calculation of $\eta_{\mathrm{SE}}^{(\epsilon)}$ and $\eta_{\mathrm{EE}}^{(\epsilon)}$

Using (4.34), we can write ϵ-SE from (4.18) as

$$\eta_{\mathrm{SE}}^{(\epsilon)} = \sup\left\{E : 1 - Q\left(\frac{10\log_{10}\left(2^{KE}-1\right)-\mu_\gamma}{\sigma_\gamma}\right) \leq \epsilon\right\}. \tag{4.35}$$

Solving $1 - Q\left(\frac{10\log_{10}\left(2^{KE}-1\right)-\mu_\gamma}{\sigma_\gamma}\right) = \epsilon$ yields $\eta_{\mathrm{SE}}^{(\epsilon)}$ providing

$$E = \frac{1}{K}\log_2\left(10^{\frac{\sigma_\gamma Q^{-1}(1-\epsilon)+\mu_\gamma}{10}} + 1\right), \tag{4.36}$$

where Q^{-1} is the inverse of the Q function and E represents the ϵ-SE. Afterwards, $\eta_{\mathrm{EE}}^{(\epsilon)}$ can be obtained by inserting the value of ϵ-SE into (4.19).

4.4.3 Numerical results on EE-SE tradeoff with shadowing

In this subsection, we provide some numerical results to illustrate the effect of frequency reuse factors and ϵ on the EE-SE tradeoff when shadowing is considered. Throughout this subsection, we set $\sigma = 5$ dB.

Fig. 4.6 depicts the effects of K on the EE-SE tradeoff with shadowing. The EE-SE tradeoff has a large linear part before a sharp decreasing when η_{SE} is increasing as also observed in the case without shadowing. For a particular P_t and K, η_{SE} increases as ϵ increases leading to higher values of η_{EE}. However, high ϵ causes lot of outage in the system, which is not necessarily desirable, and hence the value should be set according to a certain QoS to meet. From Fig. 4.6a, it can be observed that $K = 3$ allows the highest EE and SE when $v = 0.5$ due to the significant SINR decrease in shadowing environment when $K = 1$. When the user moves further from the BS, e.g. $v = 0.85$, $K = 7$ achieves the best performance as observed in Fig. 4.6b. However, $K = 1$ performs the worst due to the extreme increase of ISR at this distance.

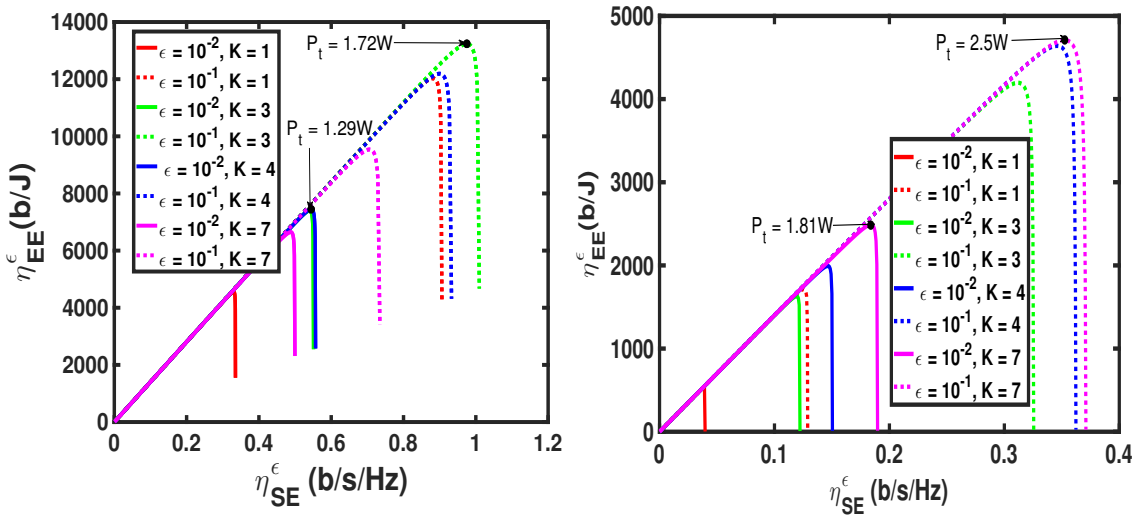

(a) $v = 0.5$

(b) $v = 0.85$

Figure 4.6 – EE-SE tradeoff with long term shadowing

Figs. 4.7 and 4.8 are labelled on K and illustrate the effects of ϵ on the optimal SE and EE respectively for $v = \{0.25, 0.5, 0.85\}$. Both optimal SE and EE increases when ϵ is increased, as also seen in Fig. 4.6. The results also show that $K = 1$ attains the highest optimal SE and EE at $v = 0.25$ for a wide range of ϵ, while it performs the worst at $v = 0.85$ due to the significant SINR decrease at this distance. Moreover, although $K = 1$ allows the best optimal EE-SE tradeoff at $v = 0.5$ without shadowing as can be seen in Fig. 4.2, SINR decreases more significantly in shadowing environment for $K = 1$ causing it to be the best choice only for very high outage value. Hence, higher values of K are preferred when shadowing is considered to maintain high level of QoS.

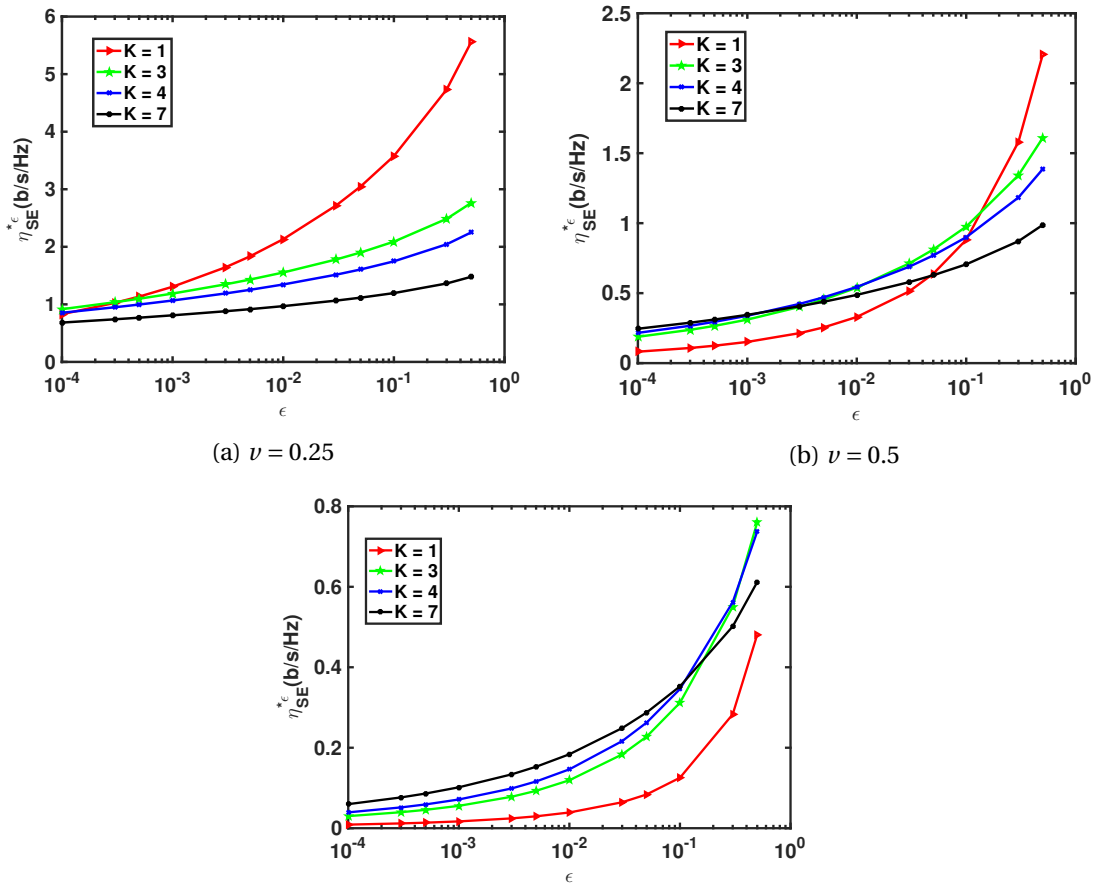

(a) $\nu = 0.25$

(b) $\nu = 0.5$

(c) $\nu = 0.85$

Figure 4.7 – Optimal ϵ-SE vs. ϵ

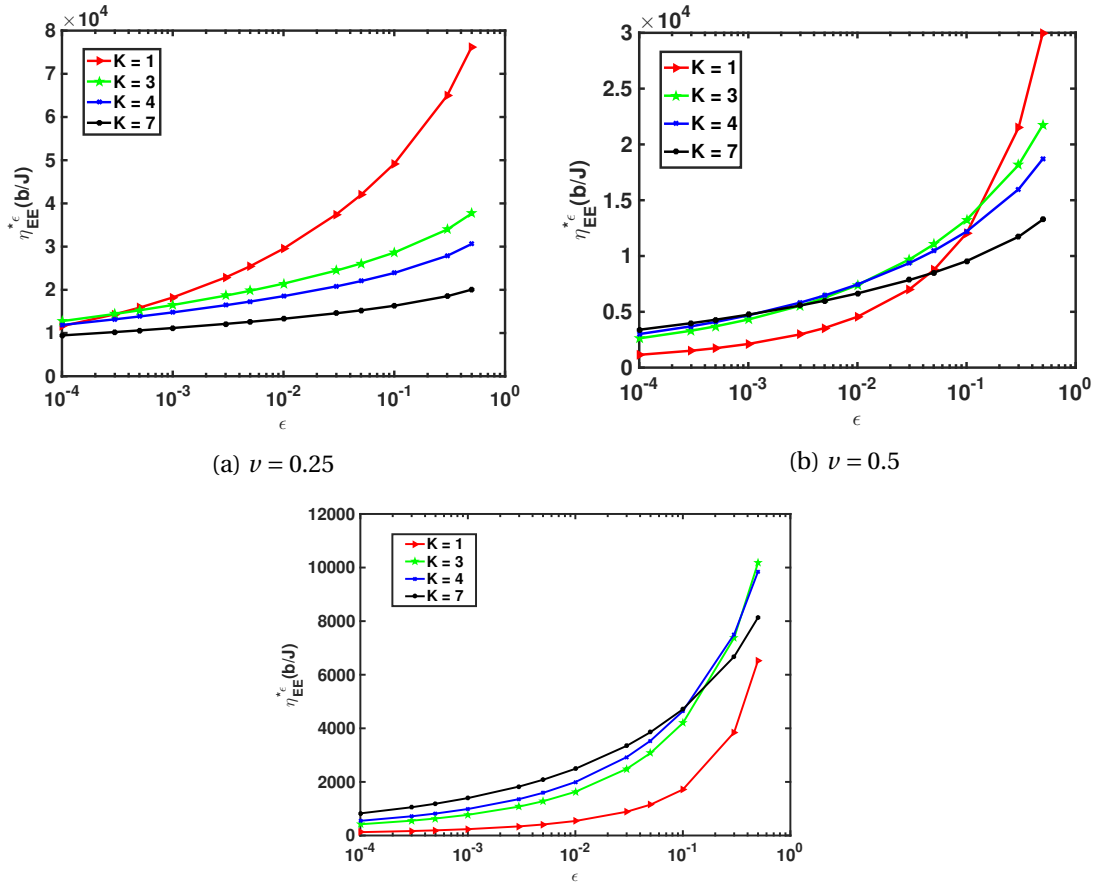

(a) $\nu = 0.25$

(b) $\nu = 0.5$

(c) $\nu = 0.85$

Figure 4.8 – Optimal ϵ-EE vs. ϵ

4.5 Conclusion

In this chapter, we have investigated the EE-SE tradeoff in homogeneous hexagonal interference-limited network using a practical power consumption model considering frequency reuse factors both with and without shadowing. We obtained a parametric expression of f-parameter by curve fitting to analyze the EE-SE tradeoff without shadowing. Then we proposed approximations for the CDF of SINR to evaluate the EE-SE tradeoff with shadowing, which are validated by Monte Carlo simulations. Our results showed that the EE-SE curves have a large linear part, due to the static power consumption, followed by a sharp decreasing EE, since the network is homogeneous and interference-limited. Moreover, a frequency reuse equal to 1 for regions close to the BS and higher reuse factors in region closer to the cell edge optimize the EE-SE tradeoff. However, $K = 1$ is the best only for higher values of ϵ, i.e. i.e. higher outage in the system, even at a moderate distance due to significant SINR decrease when shadowing is taken into account. Moreover, better ϵ-EE-SE is achieved as ϵ increases, but the value should be set according to the QoS to meet. However, it should be noted that we do not consider feedback on channel state from the users to the BSs, and hence the BSs can not adapt their transmission to the channel state.

The BSs are assumed to transmit in best effort leading to equity in user access to the resources. However, in reality users getting low throughput request again for resources since they are less served. This highlights the importance of resource management for cell-edge users which we did not take into account. Resource management based on the real traffic condition and user position will lead to different power allocation for the desired signal and the interfering signal. In this chapter, results are obtained assuming that the desired power and the interference power are same. The results may be different for different power allocation.

Chapter 5

EE-ASE tradeoff in a PPP network

5.1 Introduction

Higher ASE can be achieved when the communication between BS and users is in the same time-frequency resources [28]. Precoding must be used in downlink to mitigate the interference due to the communication in the same radio resources. Optimal precoder maximizing the network sum rate subject to a transmit power constraint is desired on the perspective of EE-ASE tradeoff. Achieving such precoder is a non-convex and non-trivial problem and therefore linear precoding techniques, e.g. MRT, ZF, SLNR, minimum mean square error (MMSE), are also of interest [148, 149]. Although the ZF precoder nulls the intra-cell interference [29, 30, 31], it is not designed to limit the inter-cell interference. Moreover, the ZF precoder imposes a restriction on the minimum number of transmit antennas at BS [32]. A generalized MMSE precoder for downlink multicell MU-MISO systems considering different average SNRs of users has been proposed in [150]. The authors have shown that MMSE achieves higher throughput compared to other linear precoders by performing Monte Carlo simulations. However, evaluating the performance of MMSE precoder is generally difficult to handle theoretically.

Authors in [33] have proposed SLNR as an optimization metric for designing precoder. SLNR does not impose any restriction on the number of BS antennas in contrast to ZF solution [33] and moreover noise is considered. However, the previous works based on SLNR do not consider a multi-cell environment and also ignore the network geometry while computing the SLNR precoder solution [33, 34, 32, 35]. In this chapter, we investigate the performance of the SLNR precoder for cellular network taking into account non-homogeneous average SNR due to the large scale fading, i.e. path loss, and also the interference created on the other-cell users. The

MMSE and SLNR precoders have been proved to be equivalent under symmetric scenario, i.e. all channels between BS and users have the same gain [34, 99]. Although the network geometry is non-symmetric in our work, we consider the SLNR precoder for its close-to-optimal performance and simplicity.

Hexagonal cellular network model has been extensively used by both academia and industry for long time. This is a useful model to represent well planned BS deployments. However, the locations of the BSs in cellular network are not so regular, and hexagonal grid cannot capture the randomness of the positions of the BSs. Besides, the model is not tractable when MU-MISO with precoding is considered. Although the positions of the BSs are not completely random, it is more tractable to consider that the BSs are positioned at random. PPP can capture such randomness completely leveraging the techniques from stochastic geometry. Hence, we consider a spatial PPP network model in this chapter.

Stochastic geometry has been used for the performance analysis of cellular networks intensively during the past decade with the work of Baccelli, Andrews or Haenggi among others [5, 1]. The authors of [29] have used the stochastic geometry tool to study the relation between ASE and different system parameters, e.g. BS density, number of BS antennas, considering a ZF precoder. The same authors have studied the relation between EE and the system parameters in [86] considering MRT precoder. Most of the previous works dealing with stochastic geometry to analyze the network performances have considered either a MRT or ZF precoder because of tractability [29, 36, 30, 31].

In this chapter, we derive approximations for ASE and EE in a MU-MISO cellular network with random topology when SLNR precoder is used, which has never been considered in literature to the best of our knowledge. The result is achieved by combining some fundamental results from RMT to PPP and tightness of the approximations for ASE and EE are validated by performing Monte Carlo simulations for a wide range of system parameters.[1] We also compare the EE-ASE tradeoff of the SLNR precoder with ZF precoder, which is commonly used in PPP networks.[2] Finally, based on the derived expressions of ASE and EE, we illustrate the effect of number of BS antennas and BS density, with constant user density and constant BS-user density ratio, on the ASE and EE when SLNR precoder is used in PPP cellular networks.

[1] This work has been accepted for the publication [J1], cf. 1.3.2
[2] This work has led to the publication [C2], cf. 1.3.2

5.2 System model

A downlink MU-MISO cellular network is considered where BSs are equipped with M transmit antennas and users have a single receive antenna. BSs and users are modelled by two independent PPPs with density λ_b and λ_u respectively and users are connected to the nearest BS. Some BSs do not transmit any signal, and are called 'inactive', since they do not have any user to serve due to the independent locations of BSs and users. All BSs have the same transmit power, which is equally divided among the active users in the cell. The whole system bandwidth is allocated to each user, and hence users experience both intra and inter-cell interferences. The linear power consumption model, introduced earlier in (3.17), is considered for BSs:

$$P_{\text{total}} = aP_t + MP_{\text{RF}} + c. \tag{5.1}$$

Rayleigh flat fading channels between BS and users are considered and perfect CSI is assumed to be available at each BS. The signal received by the k-th user from the typical 0-th BS is given by

$$y_k = \sqrt{\frac{P_t r_{0k}^{-\alpha}}{u_0}}\mathbf{h}_{0k}^H \mathbf{w}_{0k} x_{0k} + \sum_{(i,j)\in\mathscr{A}} \sqrt{\frac{P_t r_{ik}^{-\alpha}}{u_i}}\mathbf{h}_{ik}^H \mathbf{w}_{ij} x_{ij} + n_k, \tag{5.2}$$

where $\mathscr{A} = \big\{\{i,j\} \in \mathbb{N}^2 | i = 0 \wedge j \neq k \vee i \neq 0, \forall j\big\}$, r_{ik} is the distance from the i-th BS to the k-th user, $\{i,k\} \in \mathbb{N}^2$, u_i is the number of users in the i-th cell and n_k is the AWGN with zero mean and variance σ_n^2 for user k. Moreover, $\mathbf{h}_{ik} \sim \mathscr{CN}(0, \mathbf{I}_M)$ is an $M \times 1$ vector representing the complex Gaussian distributed channel between the i-th BS and the k-th user where $\mathbf{I}_M$ is an $M \times M$ identity matrix. In addition, $\mathbf{w}_{ij} \in \mathbb{C}^M$, x_{ij} are the precoding vector and the transmitted symbol respectively for the j-th user in the i-th cell with $\mathrm{E}[|x_{ij}|^2] = 1$. Note that $(\cdot)^H$ denotes the Hermitian (transpose-conjugate) operation.

Following the approach in [29], BSs are divided into subsets denoted as Φ_u, with $u \in [0, u_{\max}]$, and each BS in the subset Φ_u serves u users. The maximum number of users served simultaneously in a cell is set to $u_{\max}$ in order to control several factors, i.e. spatial multiplexing gain, interference, beamforming gain, etc., that determine the SDMA gain. The number of users in different cells is assumed to be independent, and each BS group Φ_u follows a homogeneous PPP distribution with density $\lambda_b p_N(u)$, where $p_N(u)$ is the probability mass function (PMF) of the number of active users in a cell. The calculation of $p_N(u)$ requires the exact size distribution of the Poisson-Voronoi typical cell, which has been given in [151]. However, since the expression is challenging to compute numerically, a curve-fitted equation has been proposed in [152]. Using

this equation, PMF of the number of active users in a cell can be expressed as in [29]:

$$p_N(u) = \begin{cases} \frac{\mu^\mu \Gamma(u+\mu)\rho^{-u}}{\Gamma(\mu)u!\left(\frac{1}{\rho}+\mu\right)^{u+\mu}} & 0 \le u \le u_{\max}-1 \\ \sum\limits_{n=u_{\max}}^{\infty} \frac{\mu^\mu \Gamma(n+\mu)\rho^{-n}}{\Gamma(\mu)n!\left(\frac{1}{\rho}+\mu\right)^{n+\mu}} & u = u_{\max} \end{cases} \tag{5.3}$$

where n is the number of users available in a cell, $\mu = 3.5$ is a constant obtained through data fitting [152], $\rho = \frac{\lambda_b}{\lambda_u}$ is the BS-user density ratio, and $\Gamma(\cdot)$ is the gamma function. When $n \le u_{\max}$, n users are served by BS, while BS randomly chooses $u_{\max}$ users to serve when $n > u_{\max}$. Due to the limitation of active users to $u_{\max}$, their locations become correlated, which is very challenging to handle. In order to make the problem tractable, the simplifying assumption that the set of active users is the sum of independent PPPs with density $\lambda_b u p_N(u)$ with $u \in [1, u_{\max}]$ is made. Since the sum of independent PPPs is another PPP, the set of active users is considered as a PPP with density $\lambda_{au} = \sum_{u=1}^{u_{\max}} \lambda_b u P_N(u)$. The network is considered to be a circular disc of radius R_a, and total number of active users in this network is N_{au} which is a r.v. in a given area. However, we have $\lim\limits_{R_a\to\infty} N_{au}(R_a) = \lim\limits_{R_a\to\infty} \lambda_{au}\pi R_a^2$ when the network size grows to infinity.

Power received by the typical k-th user at distance r_{0k} from the 0-th BS is

$$P_{0k} = \frac{P_t}{u_0} r_{0k}^{-\alpha} \left|\mathbf{h}_{0k}^H \mathbf{w}_{0k}\right|^2, \tag{5.4}$$

where the propagation constant L in (3.18) is one and $\left|\mathbf{h}_{0k}^H \mathbf{w}_{0k}\right|^2$ is the random channel power gain given by X. By grouping the interfering BSs into subsets, the SINR of the k-th user can be written as

$$\gamma(u_0) = \frac{\frac{P_t r_{0k}^{-\alpha}}{u_0}\left|\mathbf{h}_{0k}^H \mathbf{w}_{0k}\right|^2}{\sum\limits_{j\neq k} \frac{P_t r_{0k}^{-\alpha}}{u_0}\left|\mathbf{h}_{0k}^H \mathbf{w}_{0j}\right|^2 + \sum\limits_{u=1}^{u_{\max}} \sum\limits_{i\in\Phi_u\setminus\{0\}} \sum\limits_{j=1}^{u} \frac{P_t r_{ik}^{-\alpha}}{u}\left|\mathbf{h}_{ik}^H \mathbf{w}_{ij}\right|^2 + \sigma_n^2}. \tag{5.5}$$

According to Slivnyak's theorem illustrated in 2.1.5, $(\Phi_u \setminus \{0\})$ has the same statistics as Φ_u. At denominator, the first and second terms refer to the intra and inter-cell interferences respectively.

5.3 SLNR and ZF precoding schemes

In this section, expressions of the SLNR and ZF precoding vectors are presented in the context of a MU-MISO cellular network with random topology.

5.3.1 SLNR precoder

The SLNR is defined as the ratio of the received signal power at the desired user to the interference created by the desired signal on the other terminals, also known as leakage, plus the noise power of the desired user. For user k, SLNR can be expressed as

$$\text{SLNR} = \frac{\frac{P_t r_{0k}^{-\alpha}}{u_0}\mathbf{w}_{0k}^H \mathbf{h}_{0k}\mathbf{h}_{0k}^H \mathbf{w}_{0k}}{\sum\limits_{j\neq k}\frac{P_t r_{0j}^{-\alpha}}{u_0}\mathbf{w}_{0k}^H \mathbf{h}_{0j}\mathbf{h}_{0j}^H \mathbf{w}_{0k} + \sigma_n^2} = \frac{r_{0k}^{-\alpha}\mathbf{w}_{0k}^H \mathbf{h}_{0k}\mathbf{h}_{0k}^H \mathbf{w}_{0k}}{\mathbf{w}_{0k}^H \bar{\mathbf{H}}_{0k}\bar{\mathbf{D}}_{0k}\bar{\mathbf{H}}_{0k}^H \mathbf{w}_{0k} + \frac{\sigma_n^2 u_0}{P_t}}, \tag{5.6}$$

where $\bar{\mathbf{H}}_{0k} = \left[\mathbf{h}_{01}, \cdots, \mathbf{h}_{0(k-1)}, \mathbf{h}_{0(k+1)}, \cdots, \mathbf{h}_{0N_{au}}\right]$ and $\bar{\mathbf{D}}_{0k} = \text{diag}\left(r_{01}^{-\alpha}, \cdots, r_{0(k-1)}^{-\alpha}, r_{0(k+1)}^{-\alpha}, \cdots, r_{0N_{au}}^{-\alpha}\right)$ represent the concatenated fading channels and a square diagonal matrix filled by the path losses from the 0-th BS to the active users in the network, except the k-th user. With average power constraint, the SLNR maximization for user k is:

$$\begin{aligned}\mathbf{w}_{0k} = &\arg \max_{\mathbf{w}_{0k}\in\mathbb{C}^{M\times 1}} \frac{\mathbf{w}_{0k}^H \mathbf{h}_{0k}\mathbf{h}_{0k}^H \mathbf{w}_{0k}}{\mathbf{w}_{0k}^H \left(\bar{\mathbf{H}}_{0k}\bar{\mathbf{D}}_{0k}\bar{\mathbf{H}}_{0k}^H + \frac{\sigma_n^2 u_0}{P_t\|\mathbf{w}_{0k}\|^2}\mathbf{I}_M\right)\mathbf{w}_{0k}} \\ &\text{subject to } \mathrm{E}\left[\|\mathbf{w}_{0k}\|^2\right] = 1\end{aligned} \tag{5.7}$$

where $\|\cdot\|$ represents the L_2 vector norm. When $M \to \infty$, the optimization problem in (5.7) can be proved to be equivalent to

$$\begin{aligned}\mathbf{w}_{0k} = &\arg \max_{\mathbf{w}_{0k}\in\mathbb{C}^{M\times 1}} \frac{\mathbf{w}_{0k}^H \mathbf{h}_{0k}\mathbf{h}_{0k}^H \mathbf{w}_{0k}}{\mathbf{w}_{0k}^H \left(\bar{\mathbf{H}}_{0k}\bar{\mathbf{D}}_{0k}\bar{\mathbf{H}}_{0k}^H + \frac{\sigma_n^2 u_0}{P_t}\mathbf{I}_M\right)\mathbf{w}_{0k}} \\ &\text{subject to } \mathrm{E}\left[\|\mathbf{w}_{0k}\|^2\right] = 1.\end{aligned} \tag{5.8}$$

Indeed, defining $\mathbf{w}_{0k} = [w_{0k1}, w_{0k2}, \cdots, w_{0kM}]^T$, we can write

$$\mathrm{E}\left[\|\mathbf{w}_{0k}\|^2\right] = \mathrm{E}\left[\sum_i^M w_{0ki}^2\right] = \sum_i^M \mathrm{E}\left[w_{0ki}^2\right] = M\mathrm{E}\left[w_{0ki}^2\right] = 1, \tag{5.9}$$

where the final step in (5.9) is obtained considering that w_{0ki} are iid with the same second order moment. Let the random variable $x_i = M w_{0ki}^2$ with the mean value independent of M and equal to 1, i.e. the mean value of w_{0ki}^2 decreases with M. Then, according to the law of large numbers

(LLN),

$$\|\mathbf{w}_{0k}\|^2 = \frac{1}{M}\sum_{i}^{M} x_i \xrightarrow{\text{LLN}} \mathrm{E}[x_i] = 1. \tag{5.10}$$

For (5.10) be true, the variance of x_i should be finite, which is assumed to be true and seems a reasonable assumption. From (5.9) and (5.10), we can write $\lim_{M\to\infty} \|\mathbf{w}_{0k}\|^2 = \mathrm{E}[\|\mathbf{w}_{0k}\|^2]$ and hence replace the problem in (5.7) by the problem in (5.8).

Using the generalized Rayleigh quotient theorem, the solution of (5.8) is the eigenvector corresponding to the maximum eigenvalue [153]:

$$\mathbf{w}_{0k} \propto \text{maxeigenvect}\left(\bar{\mathbf{H}}_{0k}\bar{\mathbf{D}}_{0k}\bar{\mathbf{H}}_{0k}^H + \frac{\sigma_n^2 u_0}{P_t}\mathbf{I}_M\right)^{-1}\mathbf{h}_{0k}\mathbf{h}_{0k}^H. \tag{5.11}$$

The resulting SLNR is equal to the maximum eigenvalue $\lambda_{\max}$ [34]. Any vector $\mathbf{g}_{0k}$, which is in the eigenspace corresponding to $\lambda_{\max}$, satisfies the following eigenvector equation:

$$\left(\bar{\mathbf{H}}_{0k}\bar{\mathbf{D}}_{0k}\bar{\mathbf{H}}_{0k}^H + \frac{\sigma_n^2 u_0}{P_t}\mathbf{I}_M\right)^{-1}\mathbf{h}_{0k}\mathbf{h}_{0k}^H\mathbf{g}_{0k} = \lambda_{\max}\mathbf{g}_{0k}. \tag{5.12}$$

Inserting a nonzero complex scalar $\delta_{0k} = \mathbf{h}_{0k}^H\mathbf{g}_{0k}$ into (5.12), $\mathbf{g}_{0k}$ can be written as

$$\mathbf{g}_{0k} = \frac{\delta_{0k}}{\lambda_{\max}}\left(\bar{\mathbf{H}}_{0k}\bar{\mathbf{D}}_{0k}\bar{\mathbf{H}}_{0k}^H + \frac{\sigma_n^2 u_0}{P_t}\mathbf{I}_M\right)^{-1}\mathbf{h}_{0k}. \tag{5.13}$$

Imposing the power constraint, solution to (5.8) is

$$\mathbf{w}_{0k} = \frac{\left(\bar{\mathbf{H}}_{0k}\bar{\mathbf{D}}_{0k}\bar{\mathbf{H}}_{0k}^H + \frac{\sigma_n^2 u_0}{P_t}\mathbf{I}_M\right)^{-1}\mathbf{h}_{0k}}{\sqrt{\mathrm{E}_{\bar{\mathbf{H}}_{0k},\bar{\mathbf{D}}_{0k},\mathbf{h}_{0k}}\left[\left\|\left(\bar{\mathbf{H}}_{0k}\bar{\mathbf{D}}_{0k}\bar{\mathbf{H}}_{0k}^H + \frac{\sigma_n^2 u_0}{P_t}\mathbf{I}_M\right)^{-1}\mathbf{h}_{0k}\right\|^2\right]}}. \tag{5.14}$$

Monte Carlo simulations have been performed on the CDF of SLNR when the precoding vector $\mathbf{w}_{0k}$ is as in (5.14) and when it is obtained by solving (5.8) and imposing an instantaneous power constraint, i.e. $\|\mathbf{w}_{0k}\|^2 = 1$ which is equivalent to remove the expectation in the denominator of (5.14). Simulations have been conducted considering several PPP network realizations and channel fading, and the CDF of SLNR is evaluated for a typical user located at center of the network. Parameters for the plots are set to $M = 10$, $\alpha = 4$, $\sigma_n^2 = -97.5$ dBm, $\lambda_u = 5\cdot 10^{-4}$ m^{-2},

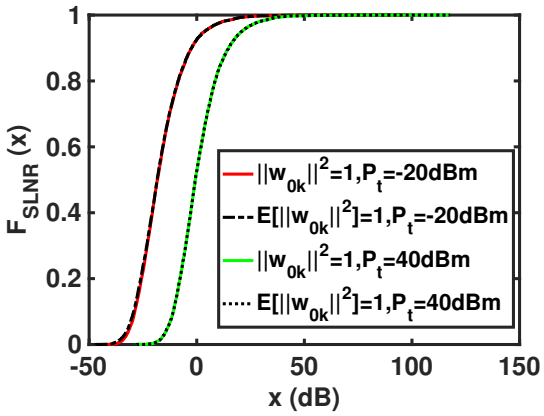

Figure 5.1 – CDF of the SLNR at $M = 10$

$\rho = 0.0077$. A perfect match of the CDFs with the instantaneous and the average power constraint is observed in Fig. 5.1 when $M = 10$. This suggests that $\mathrm{E}[\|\mathbf{w}_{0k}\|^2]$ can be used as a good approximation of $\|\mathbf{w}_{0k}\|^2$ even for M as small as 10.

The SLNR precoder causes a significant network overhead since each BS needs the CSI for all the active users in the network. However, considering the leakage to the users that are far away into the SLNR expression should have very little impact. Therefore, focus can be provided only on those users to whom much leakage is caused. It can be assumed that that each BS collects local CSI from the users in its own cell and non-local CSI from the users to whom a considerable leakage is created. This will results in a significant decrease in the network overhead due to the requirement of the CSI of all the active users in the network by each BS.

5.3.2 ZF precoder

ZF precoder is defined such that $\mathbf{H}_0^H \mathbf{G}_0 = \mathbf{I}_{u_0}$ [154], where $\mathbf{H}_0 = \left[\mathbf{h}_{01}, \cdots, \mathbf{h}_{0k}, \cdots, \mathbf{h}_{0u_0}\right] \in \mathbb{C}^{M \times u_0}$ and $\mathbf{G}_0 \in \mathbb{C}^{M \times u_0}$ respectively represent the concatenated channels and non-normalized precoding vectors for the users in cell 0. Non-normalized precoding matrix $\mathbf{G}_0$ can be chosen as the pseudo-inverse of $\mathbf{H}_0$, which for $u_0 \leq M$ can be written as [118]

$$\mathbf{G}_0 = \mathbf{H}_0 \left[\mathbf{H}_0^H \mathbf{H}_0\right]^{-1}. \tag{5.15}$$

Normalized precoding vector for the k-th user is given by

$$\mathbf{w}_{0k} = \frac{[\mathbf{G}_0]_k}{\|[\mathbf{G}_0]_k\|}, \tag{5.16}$$

where $[\mathbf{G}_0]_k$ is the k-th column of $\mathbf{G}_0$. In case of the ZF precoder, each BS requires CSI only from the users in the own cell.

5.4 Performance metrics

We provide the expressions of ASE and EE using stochastic system model.

5.4.1 Area spectral efficiency

Ergodic throughput of a cell with u_0 active users can be written as [155]

$$R_{\mathrm{BS}}(u_0) = u_0 R_u(u_0), \tag{5.17}$$

where $R_u(u_0)$ is the ergodic rate of a typical user when there are u_0 active users in the cell. The ergodic throughput of a typical BS averaged over the number of active users can be written as

$$R_{\mathrm{BS}} = \mathrm{E}_{u_0}\left[u_0 R_u(u_0)\right] = \sum_{u_0=1}^{u_{\max}} u_0 R_u(u_0) p_N(u_0). \tag{5.18}$$

Using (5.18), ASE in b/s/Hz/u.a. can be written as

$$\eta_{\mathrm{ASE}} = \lambda_b \sum_{u_0=1}^{u_{\max}} u_0 R_u(u_0) p_N(u_0). \tag{5.19}$$

Three different random processes, i.e. two independent PPPs governing users and BSs locations, and fading channels are taken into account in the system model. To calculate the ergodic rate of the k-th user, we first average the rate over the SINR conditioned on distance to the connected BS and then average over this random quantity. Therefore, the ergodic rate of the k-th user with u_0 users in the cell is

$$R_u(u_0) = \mathrm{E}_{r_{0k}}\left[\mathrm{E}_{\gamma}\left[\log_2\left(1+\gamma(u_0)\right)|_{r_{0k}}\right]\right], \tag{5.20}$$

where E_{γ} and $\mathrm{E}_{r_{0k}}$ denote the expectations over SINR, and the distance of the k-th user from the connected BS respectively. Calculation of (5.20) can be done using coverage probability [5] or moment generating function approaches [156]. Both these methods necessitate finding the distribution of the terms $\left|\mathbf{h}_{0k}^{H}\mathbf{w}_{0k}\right|^2$, $\left|\mathbf{h}_{0k}^{H}\mathbf{w}_{0j}\right|^2$ and $\left|\mathbf{h}_{ik}^{H}\mathbf{w}_{ij}\right|^2$, which are difficult to obtain.

Using the Jensen's inequality, we first search for an upper bound of $R_u(u_0)$,

$$R_u(u_0) \leq \mathrm{E}_{r_{0k}}\left[\log_2\left(1+\mathrm{E}_{\gamma}\left[\gamma(u_0)|_{r_{0k}}\right]\right)\right] = \hat{R}_u(u_0). \tag{5.21}$$

Secondly, $\mathrm{E}_{\gamma}\left[\gamma(u_0)|r_{0k}\right]$ is assumed to be close to the ratio of the average quantities in (5.5) as it has been done in [157] and is given by

$$\mathrm{E}_{\gamma}\left[\gamma(u_0)|r_{0k}\right] \simeq \frac{\mathrm{E}_{\tilde{\mathbf{H}}_{0k},\tilde{\mathbf{D}}_{0k},\mathbf{h}_{0k}}\left[\frac{P_t r_{0k}^{-\alpha}}{u_0}\left|\mathbf{h}_{0k}^{H}\mathbf{w}_{0k}\right|^2|_{r_{0k}}\right]}{\mathrm{E}_{\tilde{\mathbf{H}}_{0j},\tilde{\mathbf{D}}_{0jk},\mathbf{h}_{0j}}\left[\sum\limits_{j\neq k}\frac{P_t r_{0k}^{-\alpha}}{u_0}\left|\mathbf{h}_{0k}^{H}\mathbf{w}_{0j}\right|^2|_{r_{0k}}\right]+\mathrm{E}_{\tilde{\mathbf{H}}_{ij},\tilde{\mathbf{D}}_{ij},\mathbf{h}_{ij}}\left[\sum\limits_{u=1}^{u_{\max}}\sum\limits_{i\in\Phi_u\setminus\{0\}}\frac{P_t r_{ik}^{-\alpha}}{u}\sum\limits_{j=1}^{u}\left|\mathbf{h}_{ik}^{H}\mathbf{w}_{ij}\right|^2|_{r_{0k}}\right]+\sigma_n^2}. \tag{5.22}$$

It has been verified by simulation that $\mathrm{E}_{\gamma}\left[\gamma(u_0)|r_{0k}\right]$ and the approximation in (5.22) are close to each other. While the numerator in (5.22) represents the average desired power, the first and second terms at denominator refer to the average intra and inter-cell interference powers respectively. Note that all these average powers are calculated conditioned on r_{0k}. Upper bound of $R_u(u_0)$ can be written as

$$\hat{R}_u(u_0) = \int_{r_{0k}\geq 0}^{\infty}\log_2\left(1+\mathrm{E}_{\gamma}\left[\gamma(u_0)|r_{0k}\right]\right)f_{r_{0k}}(r_{0k})\,dr_{0k}, \tag{5.23}$$

where $f_{r_{0k}}(r_{0k})$ is the PDF of the distance of the k-th user from its connected BS, and is given by [5]

$$f_{r_{0k}}(r_{0k}) = e^{-\lambda_b \pi r_{0k}^2} 2\pi\lambda_b r_{0k}. \tag{5.24}$$

With (5.19), an upper bound of ASE can be written as

$$\hat{\eta}_{\mathrm{ASE}} = \lambda_b \sum_{u_0=1}^{u_{\max}} u_0 \hat{R}_u(u_0)\, p_N(u_0). \tag{5.25}$$

5.4.2 Energy efficiency

EE is another important performance metric for cellular networks, which is defined as the ratio of ASE to the average power consumption per u.a. To determine the average power consumption per u.a., only non-transmission power consumption is considered for inactive BSs. Therefore, the average power consumption per u.a. can be written as

$$P_A = \lambda_b\Big(1 - p_N(0)\Big)\Big(aP_t + MP_{\mathrm{RF}}\Big) + \lambda_b c \tag{5.26}$$

and hence EE is

$$\eta_{\mathrm{EE}} = \frac{\eta_{\mathrm{ASE}}}{P_A}, \tag{5.27}$$

which is obtained using (5.19) and (5.26). In a same way, upper bound of EE is

$$\hat{\eta}_{\mathrm{EE}} = \frac{\hat{\eta}_{\mathrm{ASE}}}{P_A}, \tag{5.28}$$

which is obtained using (5.25) and (5.26). The computation of ASE and EE requires to calculate an approximation of $\mathrm{E}_\gamma\big[\gamma(u_0)|r_{0k}\big]$ as suggested in (5.22). The simulation results in Section 5.6 will validate the approximation done on the average SINR.

5.5 Calculation of $\mathrm{E}_\gamma\big[\gamma(u_0)|r_{0k}\big]$

In this section, we provide four theorems to evaluate $\mathrm{E}_\gamma\big[\gamma(u_0)|r_{0k}\big]$. The first two theorems are used to calculate the average desired power and the last two ones are applied to calculate the inter-cell interference power. The third theorem is also used to determine the intra-cell interference power. All these theorems are obtained for the asymptotic regime, which is defined as follow

Definition 5.1. *(Asymptotic regime) Let R_a be the radius of the circular area centered at BS of interest and $\gamma_{au} \in \mathbb{R}^+$ a constant. The asymptotic regime (a.r.) refers to the condition $\lim_{N_{au},M\to+\infty} \frac{N_{au}}{M} = \gamma_{au}$ with $\lim_{R_a\to+\infty} \frac{N_{au}(R_a)}{\lambda_{au}\pi R_a^2} = 1$ and will be referred as $\overset{a.r.}{\sim}$ in the rest of the thesis.*

5.5.1 Average desired power conditioned on r_{0k}

Using (5.14), we can write

$$\left|\mathbf{h}_{0k}^H\mathbf{w}_{0k}\right|^2 = \frac{\left|\mathbf{h}_{0k}^H\left(\bar{\mathbf{H}}_{0k}\bar{\mathbf{D}}_{0k}\bar{\mathbf{H}}_{0k}^H + \frac{\sigma_n^2 u_0}{P_t}\mathbf{I}_M\right)^{-1}\mathbf{h}_{0k}\right|^2}{\mathrm{E}_{\bar{\mathbf{H}}_{0k},\bar{\mathbf{D}}_{0k},\mathbf{h}_{0k}}\left[\left\|\left(\bar{\mathbf{H}}_{0k}\bar{\mathbf{D}}_{0k}\bar{\mathbf{H}}_{0k}^H + \frac{\sigma_n^2 u_0}{P_t}\mathbf{I}_M\right)^{-1}\mathbf{h}_{0k}\right\|^2\right]}. \tag{5.29}$$

We manipulate (5.29) in order to apply Theorem 2.4 and obtain

$$\left|\mathbf{h}_{0k}^H\mathbf{w}_{0k}\right|^2 = \frac{\left|\mathbf{h}_{0k}^H\left(\frac{1}{M}\bar{\mathbf{H}}_{0k}M^{\frac{\alpha}{2}}\bar{\mathbf{D}}_{0k}\bar{\mathbf{H}}_{0k}^H + \frac{M^{\frac{\alpha}{2}-1}\sigma_n^2 u_0}{P_t}\mathbf{I}_M\right)^{-1}\mathbf{h}_{0k}\right|^2}{\mathrm{E}_{\bar{\mathbf{H}}_{0k},\bar{\mathbf{D}}_{0k},\mathbf{h}_{0k}}\left[\left\|\left(\frac{1}{M}\bar{\mathbf{H}}_{0k}M^{\frac{\alpha}{2}}\bar{\mathbf{D}}_{0k}\bar{\mathbf{H}}_{0k}^H + \frac{M^{\frac{\alpha}{2}-1}\sigma_n^2 u_0}{P_t}\mathbf{I}_M\right)^{-1}\mathbf{h}_{0k}\right\|^2\right]}. \tag{5.30}$$

The singular value decomposition (SVD) of the $M\times(N_{au}-1)$ matrix $\sqrt{M^{\frac{\alpha}{2}-1}}\bar{\mathbf{H}}_{0k}\bar{\mathbf{D}}_{0k}^{\frac{1}{2}}$ is $\bar{\mathbf{U}}_{0k}\bar{\Sigma}_{0k}\bar{\mathbf{V}}_{0k}^H$ where $\bar{\mathbf{U}}_{0k}\in\mathbb{C}^{M\times M}$ and $\bar{\mathbf{V}}_{0k}\in\mathbb{C}^{(N_{au}-1)\times(N_{au}-1)}$ are unitary matrices implying $\bar{\mathbf{U}}_{0k}^H\bar{\mathbf{U}}_{0k} = \bar{\mathbf{U}}_{0k}\bar{\mathbf{U}}_{0k}^H = \mathbf{I}_M$, $\bar{\mathbf{V}}_{0k}^H\bar{\mathbf{V}}_{0k} = \bar{\mathbf{V}}_{0k}\bar{\mathbf{V}}_{0k}^H = \mathbf{I}_{N_{au}-1}$. Moreover, $\bar{\Sigma}_{0k}$ is an $M\times(N_{au}-1)$ rectangular diagonal matrix with non-negative real numbers on the diagonal, which are the singular values of $\sqrt{M^{\frac{\alpha}{2}-1}}\bar{\mathbf{H}}_{0k}\bar{\mathbf{D}}_{0k}^{\frac{1}{2}}$. By using the SVD of $\sqrt{M^{\frac{\alpha}{2}-1}}\bar{\mathbf{H}}_{0k}\bar{\mathbf{D}}_{0k}^{\frac{1}{2}}$, we can write

$$\frac{1}{M}\bar{\mathbf{H}}_{0k}M^{\frac{\alpha}{2}}\bar{\mathbf{D}}_{0k}\bar{\mathbf{H}}_{0k}^H = \bar{\mathbf{U}}_{0k}\bar{\Sigma}_{0k}\bar{\mathbf{V}}_{0k}^H\bar{\mathbf{V}}_{0k}\bar{\Sigma}_{0k}^H\bar{\mathbf{U}}_{0k}^H = \bar{\mathbf{U}}_{0k}\bar{\Sigma}_{0k}\bar{\Sigma}_{0k}^H\bar{\mathbf{U}}_{0k}^H. \tag{5.31}$$

The RHS of (5.31) is the eigen decomposition of $\frac{1}{M}\bar{\mathbf{H}}_{0k}M^{\frac{\alpha}{2}}\bar{\mathbf{D}}_{0k}\bar{\mathbf{H}}_{0k}^H$ and the non-zero elements of $\bar{\Sigma}_{0k}$ are the square roots of the non-zero eigenvalues of $\frac{1}{M}\bar{\mathbf{H}}_{0k}M^{\frac{\alpha}{2}}\bar{\mathbf{D}}_{0k}\bar{\mathbf{H}}_{0k}^H$. Considering this eigen decomposition and writing $\bar{\mathbf{\Lambda}}_{0k} = \bar{\Sigma}_{0k}\bar{\Sigma}_{0k}^H$, (5.30) can be expressed as

$$\begin{aligned}\left|\mathbf{h}_{0k}^H\mathbf{w}_{0k}\right|^2 &= \frac{\left|\mathbf{h}_{0k}^H\left(\bar{\mathbf{U}}_{0k}\left(\bar{\mathbf{\Lambda}}_{0k} + \frac{M^{\frac{\alpha}{2}-1}\sigma_n^2 u_0}{P_t}\mathbf{I}_M\right)\bar{\mathbf{U}}_{0k}^H\right)^{-1}\mathbf{h}_{0k}\right|^2}{\mathrm{E}_{\bar{\mathbf{U}}_{0k},\bar{\mathbf{\Lambda}}_{0k},\mathbf{h}_{0k}}\left[\left\|\left(\bar{\mathbf{U}}_{0k}\left(\bar{\mathbf{\Lambda}}_{0k} + \frac{M^{\frac{\alpha}{2}-1}\sigma_n^2 u_0}{P_t}\mathbf{I}_M\right)\bar{\mathbf{U}}_{0k}^H\right)^{-1}\mathbf{h}_{0k}\right\|^2\right]} \\ &= \frac{\left|\mathbf{h}_{0k}^H\bar{\mathbf{U}}_{0k}\left(\bar{\mathbf{\Lambda}}_{0k} + \frac{M^{\frac{\alpha}{2}-1}\sigma_n^2 u_0}{P_t}\mathbf{I}_M\right)^{-1}\bar{\mathbf{U}}_{0k}^H\mathbf{h}_{0k}\right|^2}{\mathrm{E}_{\bar{\mathbf{U}}_{0k},\bar{\mathbf{\Lambda}}_{0k},\mathbf{h}_{0k}}\left[\mathbf{h}_{0k}^H\bar{\mathbf{U}}_{0k}\left(\bar{\mathbf{\Lambda}}_{0k} + \frac{M^{\frac{\alpha}{2}-1}\sigma_n^2 u_0}{P_t}\mathbf{I}_M\right)^{-2}\bar{\mathbf{U}}_{0k}^H\mathbf{h}_{0k}\right]}.\end{aligned} \tag{5.32}$$

Writing $\mathbf{t}_{0k} = \bar{\mathbf{U}}_{0k}^{H}\mathbf{h}_{0k}$, (5.32) can be expressed as

$$\left|\mathbf{h}_{0k}^{H}\mathbf{w}_{0k}\right|^2 = \frac{\left|\mathbf{t}_{0k}^{H}\left(\bar{\mathbf{\Lambda}}_{0k} + \frac{M^{\frac{\alpha}{2}-1}\sigma_n^2 u_0}{P_t}\mathbf{I}_M\right)^{-1}\mathbf{t}_{0k}\right|^2}{\mathrm{E}_{\mathbf{t}_{0k},\bar{\mathbf{\Lambda}}_{0k}}\left[\mathbf{t}_{0k}^{H}\left(\bar{\mathbf{\Lambda}}_{0k} + \frac{M^{\frac{\alpha}{2}-1}\sigma_n^2 u_0}{P_t}\mathbf{I}_M\right)^{-2}\mathbf{t}_{0k}\right]}. \tag{5.33}$$

With $\mathbf{t}_{0k} = [t_{0k1}, t_{0k2}, \cdots, t_{0kM}]^T$ and $\bar{\mathbf{\Lambda}}_{0k} = \mathrm{diag}\left(\bar{\lambda}_{0k1}, \bar{\lambda}_{0k2}, \cdots, \bar{\lambda}_{0kM}\right)$, (5.33) can be written as

$$\left|\mathbf{h}_{0k}^{H}\mathbf{w}_{0k}\right|^2 = \frac{\left(\sum_{l=1}^{M}\frac{|t_{0kl}|^2}{\bar{\lambda}_{0kl}+\frac{M^{\frac{\alpha}{2}-1}\sigma_n^2 u_0}{P_t}}\right)^2}{\mathrm{E}_{\mathbf{t}_{0k},\bar{\mathbf{\Lambda}}_{0k}}\left[\sum_{l=1}^{M}\frac{|t_{0kl}|^2}{\left(\bar{\lambda}_{0kl}+\frac{M^{\frac{\alpha}{2}-1}\sigma_n^2 u_0}{P_t}\right)^2}\right]}. \tag{5.34}$$

Since $\mathbf{w}_{0k}$ does not include r_{0k}, the expectation of $\left|\mathbf{h}_{0k}^{H}\mathbf{w}_{0k}\right|^2$ conditioned on r_{0k} is the same as its unconditional expectation. Therefore, using (5.34), we can write

$$\mathrm{E}_{\bar{\mathbf{H}}_{0k},\bar{\mathbf{D}}_{0k},\mathbf{h}_{0k}}\left[\left|\mathbf{h}_{0k}^{H}\mathbf{w}_{0k}\right|^2|_{r_{0k}}\right] = \frac{\mathrm{E}_{\mathbf{t}_{0k},\bar{\mathbf{\Lambda}}_{0k}}\left[\left(\sum_{l=1}^{M}\frac{|t_{0kl}|^2}{\bar{\lambda}_{0kl}+\frac{M^{\frac{\alpha}{2}-1}\sigma_n^2 u_0}{P_t}}\right)^2\right]}{\mathrm{E}_{\mathbf{t}_{0k},\bar{\mathbf{\Lambda}}_{0k}}\left[\sum_{l=1}^{M}\frac{|t_{0kl}|^2}{\left(\bar{\lambda}_{0kl}+\frac{M^{\frac{\alpha}{2}-1}\sigma_n^2 u_0}{P_t}\right)^2}\right]}. \tag{5.35}$$

The expression of $\mathbf{w}_{0k}$ in (5.14) allows us to write (5.35) since the expectation of denominator is already present in (5.30). Numerator of (5.35) can be expressed as

$$\begin{aligned}\mathrm{E}_{\mathbf{t}_{0k},\bar{\mathbf{\Lambda}}_{0k}}\left[\left(\sum_{l=1}^{M}\frac{|t_{0kl}|^2}{\bar{\lambda}_{0kl}+\frac{M^{\frac{\alpha}{2}-1}\sigma_n^2 u_0}{P_t}}\right)^2\right] = \\ \left(\mathrm{E}_{\mathbf{t}_{0k},\bar{\mathbf{\Lambda}}_{0k}}\left[\sum_{l=1}^{M}\frac{|t_{0kl}|^2}{\bar{\lambda}_{0kl}+\frac{M^{\frac{\alpha}{2}-1}\sigma_n^2 u_0}{P_t}}\right]\right)^2 + \mathrm{var}_{\mathbf{t}_{0k},\bar{\mathbf{\Lambda}}_{0k}}\left[\sum_{l=1}^{M}\frac{|t_{0kl}|^2}{\bar{\lambda}_{0kl}+\frac{M^{\frac{\alpha}{2}-1}\sigma_n^2 u_0}{P_t}}\right].\end{aligned} \tag{5.36}$$

We introduce two theorems to calculate (5.35). While Theorem 5.1 is used to calculate the first term in the RHS of (5.36), Theorem 5.2 is used to calculate the second term in the RHS of (5.36) and the denominator in (5.35).

Theorem 5.1. *Considering the* 0*-th BS,*

$$\mathrm{E}_{\mathbf{t}_{0k},\bar{\mathbf{\Lambda}}_{0k}}\left[\frac{1}{M}\sum_{l=1}^{M}\frac{|t_{0kl}|^2}{\bar{\lambda}_{0kl}+\frac{M^{\frac{\alpha}{2}-1}\sigma_n^2 u_0}{P_t}}\right] \overset{a.r.}{\sim} \bar{m}_{0k}(z) \tag{5.37}$$

with $\bar{m}_{0k}(z)$ *is the unique, non-negative real solution of the following equation:*

$$\frac{\pi\csc\left(\frac{2\pi}{\alpha}\right)}{\bar{m}_{0k}^{-\frac{2}{\alpha}}(z)\alpha}-\frac{z\bar{m}_{0k}(z)}{2\pi\lambda_{au}}-\frac{\bar{m}_{0k}(z)}{\alpha-2}\left(\left(\frac{\pi\lambda_{au}}{\gamma_{au}}\right)^{-\frac{\alpha}{2}}+\bar{m}_{0k}(z)\right)^{\frac{2}{\alpha}-1}$$
$$\times\,{}_2F_1\left(1-\frac{2}{\alpha},1-\frac{2}{\alpha},2-\frac{2}{\alpha},\frac{\left(\frac{\pi\lambda_{au}}{\gamma_{au}}\right)^{\frac{\alpha}{2}}\bar{m}_{0k}(z)}{1+\left(\frac{\pi\lambda_{au}}{\gamma_{au}}\right)^{\frac{\alpha}{2}}\bar{m}_{0k}(z)}\right)=\frac{1}{2\pi\lambda_{au}}, \tag{5.38}$$

where $z=-\frac{M^{\frac{\alpha}{2}-1}\sigma_n^2 u_0}{P_t}$, csc *is the cosecant function, and* ${}_2F_1(a,b,c,z)$ *is the Gauss hypergeometric function [158].*

Proof. See Appendix A.1. □

Theorem 5.2. *Considering the* 0*-th BS,*

$$\mathrm{var}_{\mathbf{t}_{0k},\bar{\mathbf{\Lambda}}_{0k}}\left[\frac{1}{\sqrt{M}}\sum_{l=1}^{M}\frac{|t_{0kl}|^2}{\bar{\lambda}_{0kl}+\frac{M^{\frac{\alpha}{2}-1}\sigma_n^2 u_0}{P_t}}\right]\overset{a.r.}{\sim}\mathrm{E}_{\mathbf{t}_{0k},\bar{\mathbf{\Lambda}}_{0k}}\left[\frac{1}{M}\sum_{l=1}^{M}\frac{|t_{0kl}|^2}{\left(\bar{\lambda}_{0kl}+\frac{M^{\frac{\alpha}{2}-1}\sigma_n^2 u_0}{P_t}\right)^2}\right]\overset{a.r.}{\sim} m'_{0k}(z),$$

where $m'_{0k}(z)$ *is the differentiation of* $\bar{m}_{0k}(z)$ *w.r.t.* z *and expressed as*

$$m'_{0k}(z)=\bar{m}_{0k}(z)\left(\frac{4\pi^2\lambda_{au}csc\left(\frac{2\pi}{\alpha}\right)}{\bar{m}_{0k}^{1-\frac{2}{\alpha}}(z)\alpha^2}-z+Q\right)^{-1}, \tag{5.39}$$

with $z=-\frac{M^{\frac{\alpha}{2}-1}\sigma_n^2 u_0}{P_t}$ *and*

$$Q=\frac{2\pi\lambda_{au}\bar{m}_{0k}(z)\left(\frac{\pi\lambda_{au}}{\gamma_{au}}\right)^{\alpha-1}}{2\alpha-2}\left(1+\bar{m}_{0k}(z)\left(\frac{\pi\lambda_{au}}{\gamma_{au}}\right)^{\frac{\alpha}{2}}\right)^{\frac{2}{\alpha}-2}{}_2F_1\left(2-\frac{2}{\alpha},1-\frac{2}{\alpha},3-\frac{2}{\alpha},\frac{\left(\frac{\pi\lambda_{au}}{\gamma_{au}}\right)^{\frac{\alpha}{2}}\bar{m}_{0k}(z)}{1+\left(\frac{\pi\lambda_{au}}{\gamma_{au}}\right)^{\frac{\alpha}{2}}\bar{m}_{0k}(z)}\right)$$
$$-\frac{2\pi\lambda_{au}\left(\frac{\pi\lambda_{au}}{\gamma_{au}}\right)^{\frac{\alpha}{2}-1}}{\alpha-2}\left(1+\bar{m}_{0k}(z)\left(\frac{\pi\lambda_{au}}{\gamma_{au}}\right)^{\frac{\alpha}{2}}\right)^{\frac{2}{\alpha}-1}{}_2F_1\left(1-\frac{2}{\alpha},1-\frac{2}{\alpha},2-\frac{2}{\alpha},\frac{\left(\frac{\pi\lambda_{au}}{\gamma_{au}}\right)^{\frac{\alpha}{2}}\bar{m}_{0k}(z)}{1+\left(\frac{\pi\lambda_{au}}{\gamma_{au}}\right)^{\frac{\alpha}{2}}\bar{m}_{0k}(z)}\right).$$

Proof. See Appendix A.2. □

Using (5.35), (5.36), and Theorems 5.1 and 5.2, the average desired signal power conditioned on r_{0k} can be expressed as

$$\mathrm{E}_{\tilde{\mathbf{H}}_{0k},\tilde{\mathbf{D}}_{0k},\mathbf{h}_{0k}}\left[\frac{P_t r_{0k}^{-\alpha}}{u_0}\left|\mathbf{h}_{0k}^H\mathbf{w}_{0k}\right|^2|_{r_{0k}}\right]\overset{a.r.}{\sim}\frac{P_t r_{0k}^{-\alpha}}{u_0}\left(1+\frac{M\bar{m}_{0k}^2(z)}{m'_{0k}(z)}\right). \tag{5.40}$$

5.5.2 Average inter-cell interference power conditioned on r_{0k}

We introduce Theorem 5.3 to calculate the average inter-cell interference power from the i-th BS conditioned on r_{ik} and r_{0k}.

Theorem 5.3. *Considering the i-th interfering BS,*

$$\mathrm{E}_{\tilde{\mathbf{H}}_{ij},\tilde{\mathbf{D}}_{ijk},\mathbf{h}_{ij}}\left[\left|\mathbf{h}_{ik}^H\mathbf{w}_{ij}\right|^2|_{r_{ik},r_{0k}}\right]\overset{a.r.}{\sim}\frac{1}{\left(1+M^{\frac{\alpha}{2}}r_{ik}^{-\alpha}\bar{m}_{ijk}(z)\right)^2}, \tag{5.41}$$

where $\bar{m}_{ijk}(z)$ is the unique, non-negative real solution of the following equation:

$$\frac{\pi\csc\left(\frac{2\pi}{\alpha}\right)}{\bar{m}_{ijk}^{-\frac{2}{\alpha}}(z)\alpha}-\frac{z\bar{m}_{ijk}(z)}{2\pi\lambda_{au}}-\frac{\bar{m}_{ijk}(z)}{\alpha-2}\left(\left(\frac{\pi\lambda_{au}}{\gamma_{au}}\right)^{-\frac{\alpha}{2}}+\bar{m}_{ijk}(z)\right)^{\frac{2}{\alpha}-1}$$
$$\times{}_2F_1\left(1-\frac{2}{\alpha},1-\frac{2}{\alpha},2-\frac{2}{\alpha},\frac{\left(\frac{\pi\lambda_{au}}{\gamma_{au}}\right)^{\frac{\alpha}{2}}\bar{m}_{ijk}(z)}{1+\left(\frac{\pi\lambda_{au}}{\gamma_{au}}\right)^{\frac{\alpha}{2}}\bar{m}_{ijk}(z)}\right)=\frac{1}{2\pi\lambda_{au}} \tag{5.42}$$

with $z=-\frac{M^{\frac{\alpha}{2}-1}\sigma_n^2 u_i}{P_t}$.

Proof. See Appendix A.3. □

From Theorem 5.3 and by averaging over r_{ik}, we state

Theorem 5.4. *The average inter-cell interference power conditioned on r_{0k} is*

$$\mathrm{E}_{\bar{\mathbf{H}}_{ij},\bar{\mathbf{D}}_{ij},\mathbf{h}_{ij}}\left[\sum_{u=1}^{u_{\max}}\sum_{i\in\Phi_u\setminus\{0\}}\frac{P_t r_{ik}^{-\alpha}}{u}\sum_{j=1}^{u}\left|\mathbf{h}_{ik}^H\mathbf{w}_{ij}\right|^2|_{r_{0k}}\right]\overset{a.r.}{\sim}\sum_{u=1}^{u_{\max}}\Big(f_1(u)-f_2(u,r_{0k})\Big).$$

where

$$f_1(u)=\frac{2\pi\lambda_b p_N(u)P_t M^{1-\frac{\alpha}{2}}\bar{m}_{ijk}^{\frac{\alpha+2}{\alpha}}(z)\,{}_2F_1\left(\frac{2}{\alpha},\frac{\alpha+2}{\alpha};2+\frac{2}{\alpha};1\right)}{(\alpha+2)\bar{m}_{ijk}^2(z)}$$

and

$$f_2(u,r_{0k})=\frac{2\pi\lambda_b p_N(u)P_t M^{1-\frac{\alpha}{2}}\,{}_2F_1\left(\frac{2}{\alpha},\frac{\alpha+2}{\alpha};2+\frac{2}{\alpha};\frac{1}{\bar{m}_{ijk}(z)M^{\frac{\alpha}{2}}r_{0k}^{-\alpha}+1}\right)}{\left(\frac{1}{\bar{m}_{ijk}(z)}+M^{\frac{\alpha}{2}}r_{0k}^{-\alpha}\right)^{\frac{\alpha+2}{\alpha}}(\alpha+2)\bar{m}_{ijk}^2(z)}.$$

Proof. See Appendix A.4. □

5.5.3 Average intra-cell interference power conditioned on r_{0k}

Since $\mathbf{h}_{0k}^H\mathbf{w}_{0j}$ has the same distribution as $\mathbf{h}_{ik}^H\mathbf{w}_{ij}$, $\mathrm{E}_{\bar{\mathbf{H}}_{0j},\bar{\mathbf{D}}_{0jk},\mathbf{h}_{0j}}\left[\left|\mathbf{h}_{0k}^H\mathbf{w}_{0j}\right|^2|_{r_{0k}}\right]$ can be computed with (5.41) substituting r_{ik} and $\bar{m}_{ijk}(z)$ by r_{0k} and $\bar{m}_{0jk}(z)$ respectively. Hence, we can write

$$\mathrm{E}_{\bar{\mathbf{H}}_{0j},\bar{\mathbf{D}}_{0jk},\mathbf{h}_{0j}}\left[\left|\mathbf{h}_{0k}^H\mathbf{w}_{0j}\right|^2|_{r_{0k}}\right]\overset{a.r.}{\sim}\frac{1}{\left(1+M^{\frac{\alpha}{2}}r_{0k}^{-\alpha}\bar{m}_{0jk}(z)\right)^2}. \tag{5.43}$$

According to Lemma 2.3 for $z<0$, $\bar{m}_{0jk}(z)$ is equal to $\bar{m}_{0k}(z)$ for large M, which is the unique, non-negative real solution of (5.38). Since $\mathrm{E}_{\bar{\mathbf{H}}_{0j},\bar{\mathbf{D}}_{0jk},\mathbf{h}_{0j}}\left[\left|\mathbf{h}_{0k}^H\mathbf{w}_{0j}\right|^2|_{r_{0k}}\right]=\mathrm{E}_{\bar{\mathbf{H}}_{0j'},\bar{\mathbf{D}}_{0j'k},\mathbf{h}_{0j'}}\left[\left|\mathbf{h}_{0k}^H\mathbf{w}_{0j'}\right|^2|_{r_{0k}}\right]$ $\forall\, j\neq j'$ except k, inserting $\bar{m}_{0jk}(z)=\bar{m}_{0k}(z)$ and using (5.43), the average intra-cell interference power conditioned on r_{0k} can be written as

$$\mathrm{E}_{\bar{\mathbf{H}}_{0j},\bar{\mathbf{D}}_{0jk},\mathbf{h}_{0j}}\left[\sum_{j\neq k}\frac{P_t r_{0k}^{-\alpha}}{u_0}\left|\mathbf{h}_{0k}^H\mathbf{w}_{0j}\right|^2|_{r_{0k}}\right]\overset{a.r.}{\sim}\frac{P_t r_{0k}^{-\alpha}\frac{(u_0-1)}{u_0}}{\left(1+M^{\frac{\alpha}{2}}r_{0k}^{-\alpha}\bar{m}_{0k}(z)\right)^2}. \tag{5.44}$$

Using (5.40), Theorem 5.4 and (5.44), (5.22) can be written as

$$\mathrm{E}_{\gamma}\left[\gamma(u_0)|r_{0k}\right] \overset{a.r.}{\sim} \frac{\frac{P_t r_{0k}^{-\alpha}}{u_0}\left(1+\frac{M\bar{m}_{0k}^2(z)}{m'_{0k}(z)}\right)}{\frac{P_t r_{0k}^{-\alpha}\frac{(u_0-1)}{u_0}}{\left(1+M^{\frac{\alpha}{2}} r_{0k}^{-\alpha}\bar{m}_{0k}(z)\right)^2}+\sum_{u=1}^{u_{\max}}\left(f_1(u)-f_2(u,r_{0k})\right)+\sigma_n^2}. \tag{5.45}$$

Despite that the theorems presented above are derived in asymptotic regime, i.e. large N_{au} and M, they provide accurate predictions on ASE and EE even for moderate values of M as it will be discussed in the next section.

5.6 Evaluation of expressions of ASE and EE

In the section, tightness of the approximations for ASE and EE, i.e. (5.25) and (5.28), are verified by performing Monte Carlo simulations. The simulations are performed considering (5.19) and (5.27), and also the instantaneous power constraint on the precoding vector, i.e. $\|\mathbf{w}_{0k}\|^2 = 1$. Throughout the rest of this chapter, α and σ_n^2 are set to 4 and -97.5 dBm respectively. For the power consumption model, micro BSs are considered with $P_{\mathrm{RF}} = 35$ W, $c = 34$ W and $a = 3.125$ [85, 86].

A circular area, whose radius is such that the average number of users in the network is N_u, is considered for simulations. We set $N_u = 5000$ except for the case $\rho = 0.1$, where $N_u = 2500$ was used to reduce the simulation time. Besides, $u_{\max}$ and λ_u are equal to M and $5\cdot 10^{-4}$ m^{-2} respectively. For the approximation of ASE, the number of active users in the network is determined as $\lim_{R_a\to\infty} N_{au}(R_a) = \lim_{R_a\to\infty} \frac{\lambda_{au}}{\lambda_u} N_u(R_a)$ since $\lim_{R_a\to\infty} N_u(R_a) = \lim_{R_a\to\infty} \lambda_u \pi R_a^2$ and $\lim_{R_a\to\infty} N_{au}(R_a) = \lim_{R_a\to\infty} \lambda_{au}\pi R_a^2$. The users are positioned uniformly in the area, and the typical user is considered to be located at center of the network.

Figs. 5.2a and 5.2b draw ASE vs. P_t labelled on BS-user density ratio and number of BS antennas respectively. It is observed that ASE is increasing and converging towards a limit when P_t exceeds 20 dBm. This is because the network is homogeneous (same transmit power) and interference limited, hence ASE saturates when noise power becomes negligible w.r.t. to the interference power. The results also demonstrate that higher ASE can be achieved by increasing the BS-user density ratio keeping user density constant or increasing the number of BS antennas.

EE vs. P_t is drawn on Figs. 5.3a and 5.3b for different BS-user density ratio and number of BS antennas respectively. It is observed that EE is first increasing when P_t is increased. However, since ASE converges towards a limit for P_t around 20 dBm, EE decreases for further increase

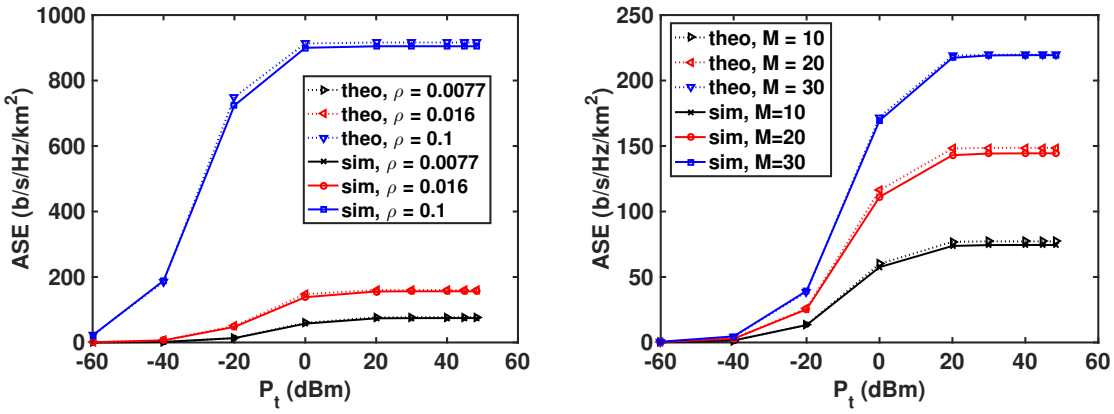

(a) $M = 10$, $\lambda_u = 5 \cdot 10^{-4}$ m^{-2} (b) $\rho = 0.0077$, $\lambda_u = 5 \cdot 10^{-4}$ m^{-2}

Figure 5.2 – ASE vs. BS transmit power

of P_t. Although Fig. 5.3b suggests that increasing the number of antennas slightly improves EE over a wide range of transmit power, it is not always energy-efficient to deploy more BSs at P_t around 20 dBm, as observed in Fig. 5.3a. Although a higher number of antennas induces more RF circuit power, i.e. P_{RF}, this is not dominant over the increase of ASE over the range of P_t taken into account. On the other hand, ASE increases with BS density, but also the power consumption per u.a., i.e. P_A. In low P_t regime, noise-to-signal ratio (NSR) dominates over ISR, and is lower for $\rho = 0.1$ compared to other values of ρ, i.e. $\rho = 0.016$ and $\rho = 0.0077$. Hence, the increase in ASE dominates over the increase in P_A for $\rho = 0.1$ when P_t is low and induces a higher EE compared to $\rho = 0.016$ and $\rho = 0.0077$. However, P_A finally becomes dominant over the increase of ASE for $\rho = 0.1$ around 20 dBm and then causing the EE decrease.

Figs. 5.4a and 5.4b plot the EE-ASE tradeoff labelled on the BS-user density ratio and number of antennas respectively. The EE-ASE tradeoff has a large linear part before a sharp decrease when ASE is increased, as also observed in Chapter 4 for a hexagonal network. The linear behavior is due to the significant consumption of the RF circuit and non-transmission powers, i.e. P_{RF} and c respectively. Moreover, since ASE converges towards a limit while EE decreases when P_t is increased, a sharp decrease of EE is observed for a slight improvement of ASE, as it has been also observed for regular hexagonal network in Chapter 4. The results also demonstrate that $\rho = 0.1$ allows to achieve the best ASE without loosing too much EE compared to other values of ρ. In a same way, $M = 30$ achieves the best ASE without loosing EE compared to $M = 10$ or 20. However, optimal EE is not achieved always with the highest valued parameters. We study the effect of

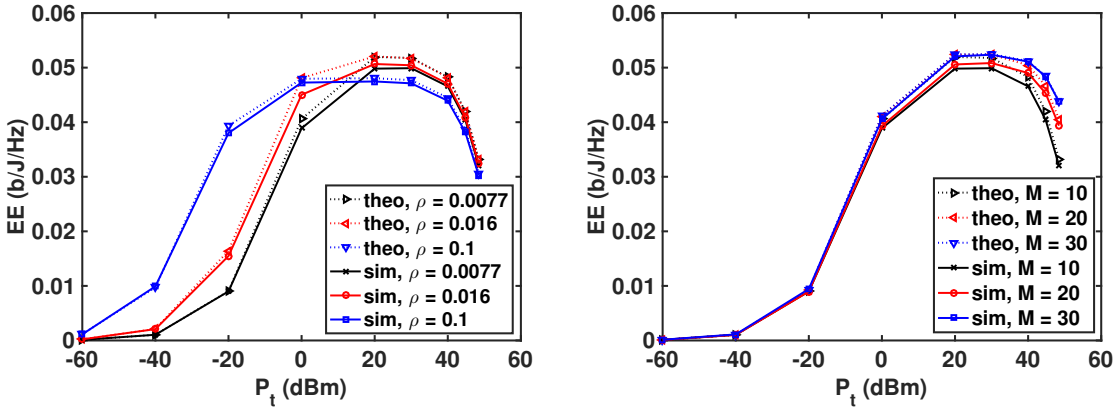

(a) $M = 10$, $\lambda_u = 5 \cdot 10^{-4}$ m^{-2} (b) $\rho = 0.0077$, $\lambda_u = 5 \cdot 10^{-4}$ m^{-2}

Figure 5.3 – EE vs. BS transmit power

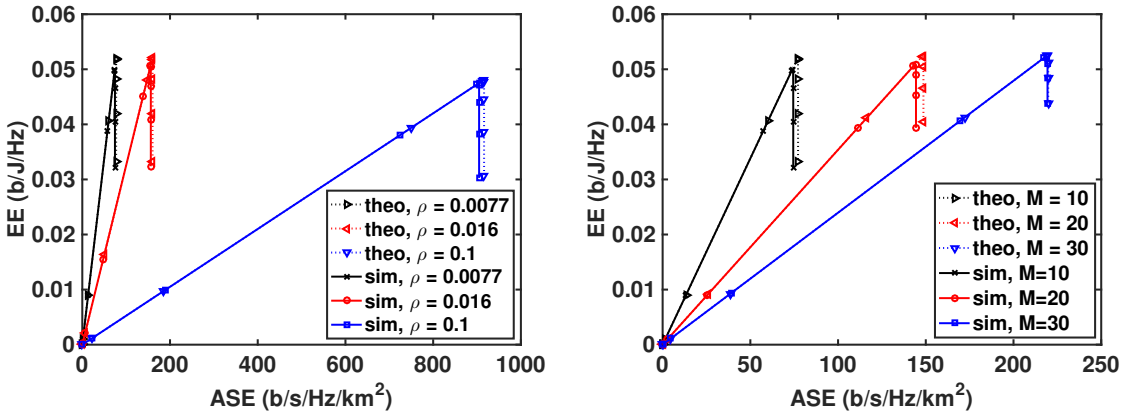

(a) $M = 10$, $\lambda_u = 5 \cdot 10^{-4}$ m^{-2} (b) $\rho = 0.0077$, $\lambda_u = 5 \cdot 10^{-4}$ m^{-2}

Figure 5.4 – EE vs. ASE

system parameters on ASE and EE in details in Section. 5.8.

Last but not least, our theoretical findings are very tight compared to the simulations results. The maximum value of the relative error considering all the simulations is about 3%. This small relative error indicates a good match between the simulations and the analytical expressions suggesting that the analytical expressions of ASE and EE can be used as a good approximation of exact values even for M and N_{au} as small as 10 and 2500 respectively. Moreover, despite the fact that the analytical expressions for ASE and EE developed from Theorem 5.1 to 5.4 are relatively

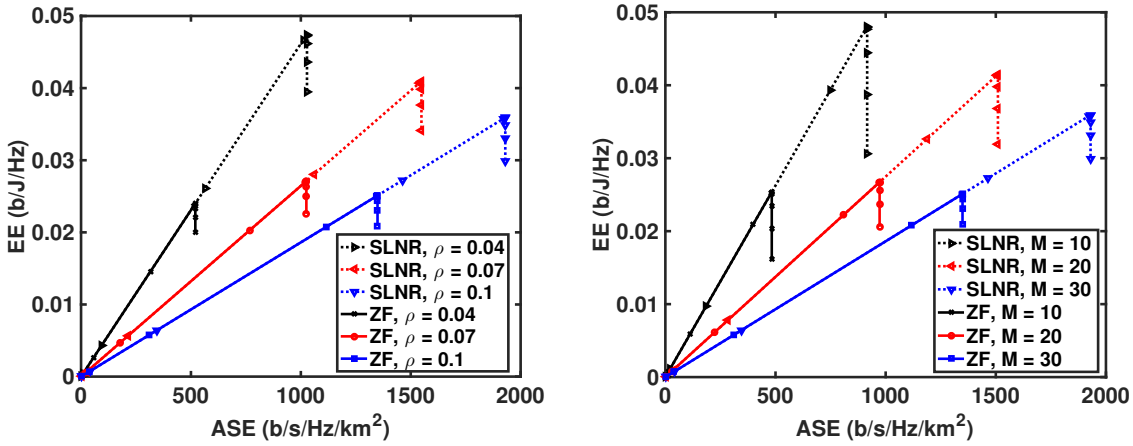

(a) $M = 30$, $\lambda_u = 5 \cdot 10^{-4}$ m^{-2} (b) $\rho = 0.1$, $\lambda_u = 5 \cdot 10^{-4}$ m^{-2}

Figure 5.5 – Comparison of the EE-ASE tradeoff of SLNR and ZF precoder

heavy, they are easily computable numerically which is, by far, faster than performing Monte Carlo simulations. Therefore, we use these expressions instead of running extensive Monte Carlo simulations in the remaining of the chapter when SLNR precoder is used.

5.7 Comparison with ZF precoder

We perform Monte Carlo simulations to obtain the EE-ASE tradeoff for the well known ZF precoder, i.e. (5.16), and compare the results with SLNR precoder, as shown in Figs. 5.5a and 5.5b. The figures are labelled on BS-user density ratio, with $M = 30$, and number of antennas, with $\rho = 0.1$, respectively. The parameters for the plots are set as $N_u = 5000$, $u_{\max} = M$ and $\lambda_u = 5 \cdot 10^{-4}$ m^{-2} unless otherwise mentioned. It can be seen that SLNR precoder has a significant performance gain compared to ZF precoder in terms of achievable EE and ASE.

Higher ASE implies a better SINR for the SLNR precoder compared to ZF. This is due to the fact that although ZF precoder nulls the intra-cell interference, it does not account the leakage to other-cell users. Moreover, the total cancellation of the intra-cell interference by ZF precoding is done at the price of a decrease in the received desired signal power [159]. On the other hand, the multi-cell SLNR precoder achieves a tradeoff between maximizing the received desired signal power of the intended user and minimizing the interference leakage to all other users in order to maximize the SLNR.

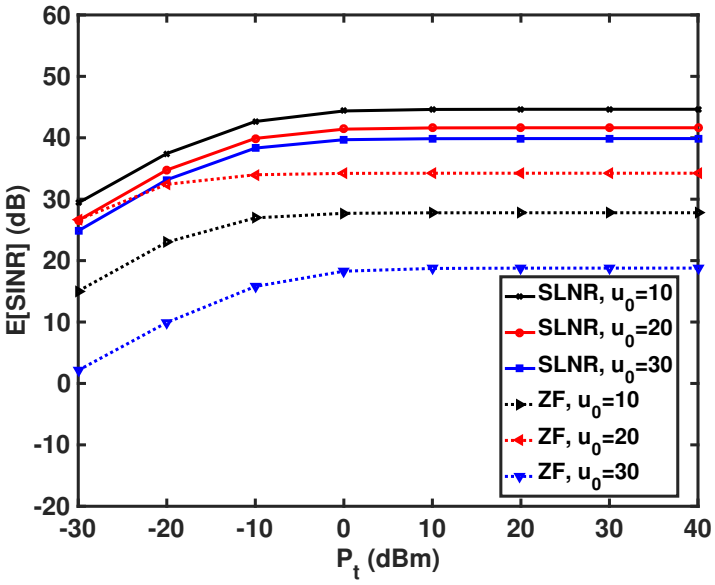

Figure 5.6 – Comparison of the mean received SINR of ZF and SLNR precoder for different u_0 with $M = 30$ and $\rho = 0.04$

This fact results in better SINR when SLNR precoder is used as it can also be seen in Fig. 5.6. However, the gain of SLNR over ZF precoder is less for $u_0 = 20$ compared to 10 and 30. The reason is that the maximum ASE for ZF precoder is achieved when the number of active usere in a cell is close to $\frac{3}{5}$M [155]. On the other hand, maximum ASE for SLNR precoder is achieved when the number of active usere in a cell is close to 3M, as will be shown in 5.8.1.

5.8 Effect of system parameters

Numerical results are provided in this section to investigate the influence of different system parameters on the performance of the system, i.e. ASE and EE, when SLNR precoder is used.

5.8.1 Effect of $u_{\max}$ on ASE

Number of active users per cell plays a significant role on the performance of SDMA since it affects the spatial multiplexing gain, the aggregated interference, and the beamforming gain for each user. The BS-user density ratio, i.e. ρ, and the maximum number of active users allowed in a cell, i.e. $u_{\max}$, determine the number of active users per cell, and hence the performance gain

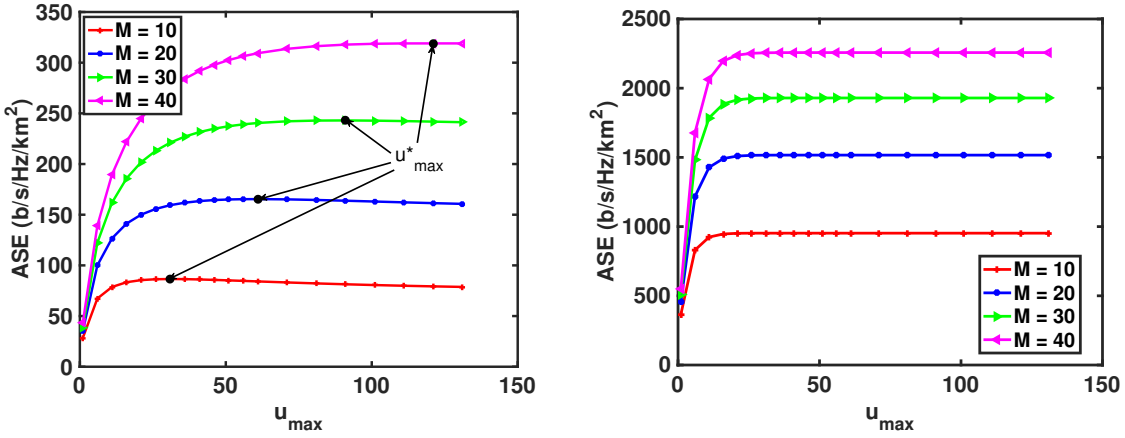

(a) $\rho = 0.0077$ (b) $\rho = 0.1$

Figure 5.7 – ASE vs. $u_{\max}$ at $N_u = 5000$, $\lambda_u = 5 \cdot 10^{-4}$ m^{-2} and $P_t = 40$ dBm

of the SDMA.

Figs. 5.7a and 5.7b illustrate ASE vs. $u_{\max}$ labelled on M for $\rho = 0.0077$ and 0.1 respectively, with $N_u = 5000$, $\lambda_u = 5 \cdot 10^{-4}$ m^{-2} and $P_t = 40$ dBm. BSs serve all the users available in a cell, i.e. n, when $n \leq u_{\max}$, while BS randomly chooses $u_{\max}$ users to serve when $n > u_{\max}$. Therefore, the number of active users does not change with $u_{\max}$ when it is sufficiently large compared to n, and this leads to a constant ASE afterwards.

PMF of the number of active users, i.e. p_N, with $u_{\max} = \infty$ or equivalently the PMF of the number of available users in a cell is plotted in Fig. 5.8. It is observed that the maximum of the PMF is shifted to higher value of u when $\rho = 0.0077$ compared to $\rho = 0.1$. This implies that the probability of having higher number of available users is higher when ρ is small. Hence, the value of $u_{\max}$ after which the number of active users remain constant, is very large for $\rho = 0.0077$, while the value is very small for $\rho = 0.1$.

As observed in Figs. 5.7a and 5.7b, ASE first increases rapidly with $u_{\max}$ due to the spatial multiplexing gain obtained from serving more users. When ρ is small, as in Fig. 5.7a, the number of active users increases until a large value of $u_{\max}$ resulting in higher interference and less beamforming gain for each user reducing the performance gain of SDMA. There is an optimal value of $u_{\max}$ denoted as $u^*_{\max}$ after which ASE decreases slightly and reaches to a constant value. Moreover, the value of $u^*_{\max}$ is close to $3M$. On the other hand, ASE becomes constant for a smaller $u_{\max}$ when ρ is large without causing the decrease in ASE, as in Fig. 5.7b.

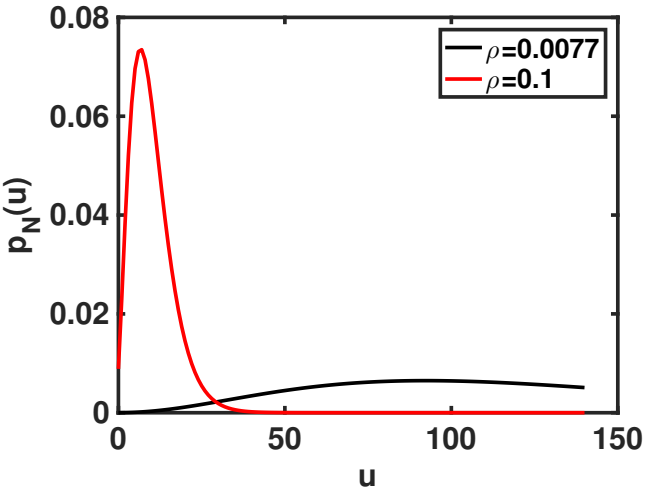

Figure 5.8 – $p_N(u)$ vs. u with $u_{\max} = \infty$

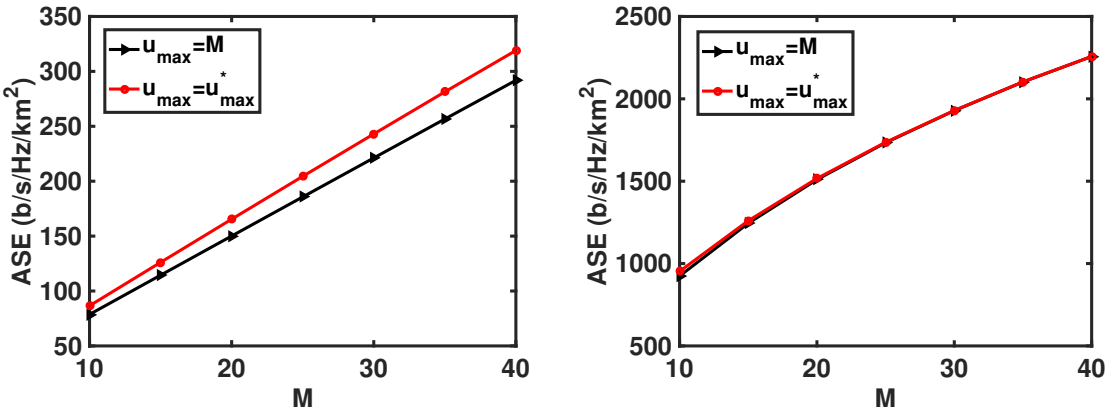

(a) $\rho = 0.0077$ (b) $\rho = 0.1$

Figure 5.9 – ASE vs. number of BS antennas at $N_u = 5000$, $\lambda_u = 5 \cdot 10^{-4}$ m^{-2} and $P_t = 40$ dBm

5.8.2 Effect of M on ASE and EE

We compare ASE for $u_{\max} = u^*_{\max}$ and $u_{\max} = M$ when $\rho = 0.0077$ and 0.1, in Figs. 5.9a and 5.9b respectively. As observed in Fig. 5.9a, when BS density is much lower than the user density, i.e. $\rho = 0.0077$, ASE grows linearly with M both when $u_{\max} = M$ and $u^*_{\max}$. This is due to the fact that the number of active users per cell in this case is sufficiently large to allow higher spatial multiplexing gain provided by the higher number of antennas. Moreover, the gain for $u_{\max} = u^*_{\max}$

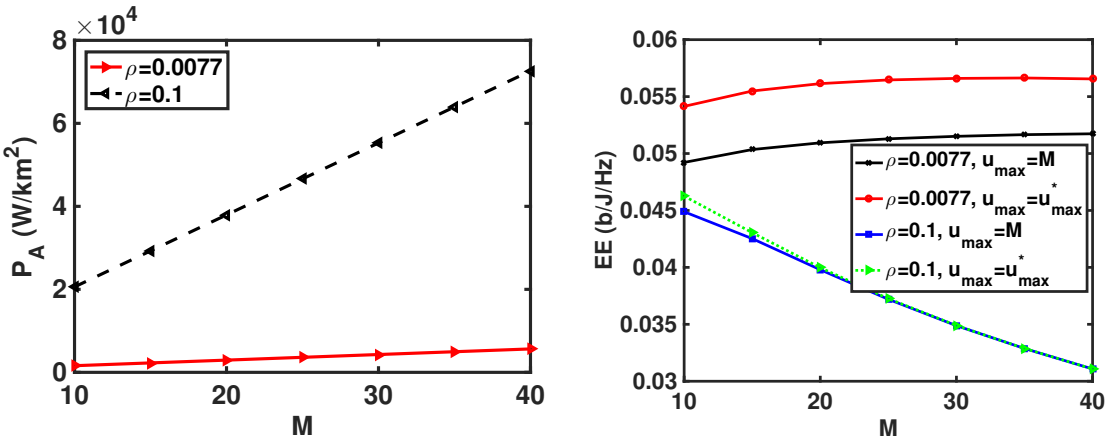

(a) P_A vs. M (b) EE vs. M

Figure 5.10 – Variation of average power consumption per u.a. and EE with number of BS antennas at $N_u = 5000$, $\lambda_u = 5 \cdot 10^{-4}$ m^{-2} and $P_t = 40$ dBm

compared to $u_{\max} = M$ increases with M, as shown in Fig. 5.9a.

On the other hand, when BS density is not much lower than the user density, i.e. $\rho = 0.1$, ASE does not increase linearly with M for both $u_{\max} = u^*_{\max}$ and $u_{\max} = M$. The reason is that the number of active users per cell becomes smaller compared to the number of BS antennas as M increases diminishing the spatial multiplexing gain provided by higher number of antennas. Moreover, ASE is the same for $u_{\max} = u^*_{\max}$ and $u_{\max} = M$.

In addition to ASE, EE depends on the average power consumption per u.a., i.e. P_A, as can be seen from (5.28). The gain in terms of ASE for higher number of antennas is associated with more P_A, which always increases linearly with M, as illustrated by (5.26) and observed in Fig. 5.10a. Since ASE does not increase linearly with M when $\rho = 0.1$, Fig 5.9b, but P_A does, EE significantly decreases with M at $\rho = 0.1$, Fig. 5.10b. Moreover, although ASE at $\rho = 0.1$ is much higher than ASE at $\rho = 0.0077$, P_A is also much higher at $\rho = 0.1$. Hence, EE at $\rho = 0.1$ is lower than EE at $\rho = 0.0077$.

5.8.3 Effect of BS density with constant λ_u on ASE and EE

We further plot ASE vs. ρ labelled on M in Fig. 5.11 with $N_u = 5000$, $\lambda_u = 5 \cdot 10^{-4}$ m^{-2}, $u_{\max} = M$, $P_t = 40$ dBm. Since the user density is constant, an increase in ρ implies that the BS density also increases. It is observed that the rate of increase of ASE is more constant for $M = 10$ compared to $M = 30$. The rate of increase declines for $M = 30$ as ρ increases since the number of active users

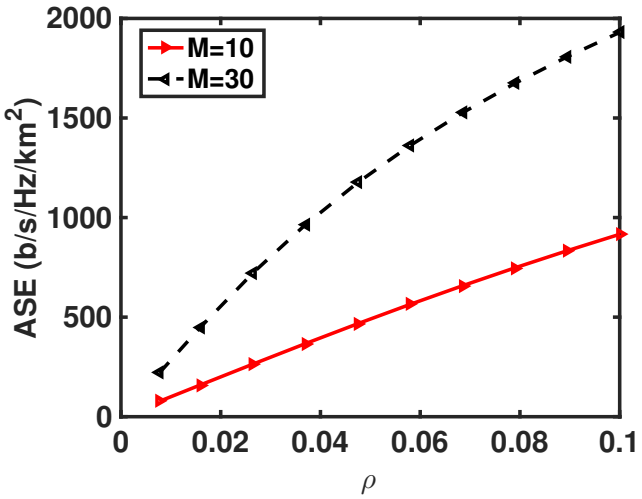

Figure 5.11 – ASE vs. BS-user density ratio at $N_u = 5000$, $\lambda_u = 5 \cdot 10^{-4}$ m^{-2}, $u_{\max} = M$ and $P_t = 40$ dBm

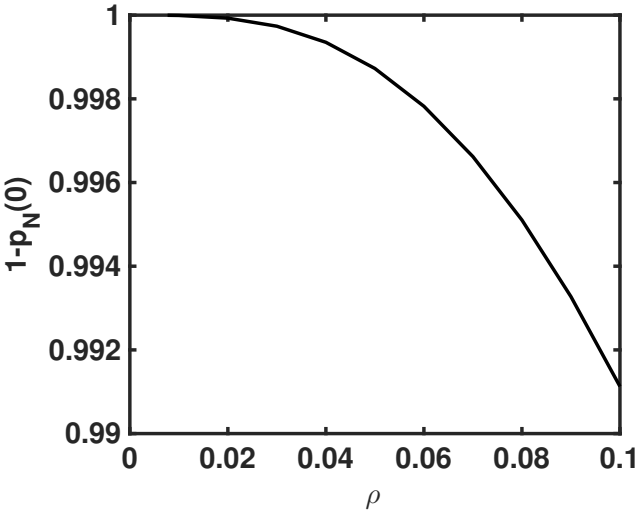

Figure 5.12 – BS activity probability vs. ρ

per cell becomes smaller compared to the number antennas limiting the spatial multiplexing gain.

The gain in terms of ASE for higher number of BSs is associated with more P_A, which depends on $\big(1 - p_N(0)\big)$, as can be seen from (5.26). For the range of ρ considered, $\big(1 - p_N(0)\big) \approx 1$, as

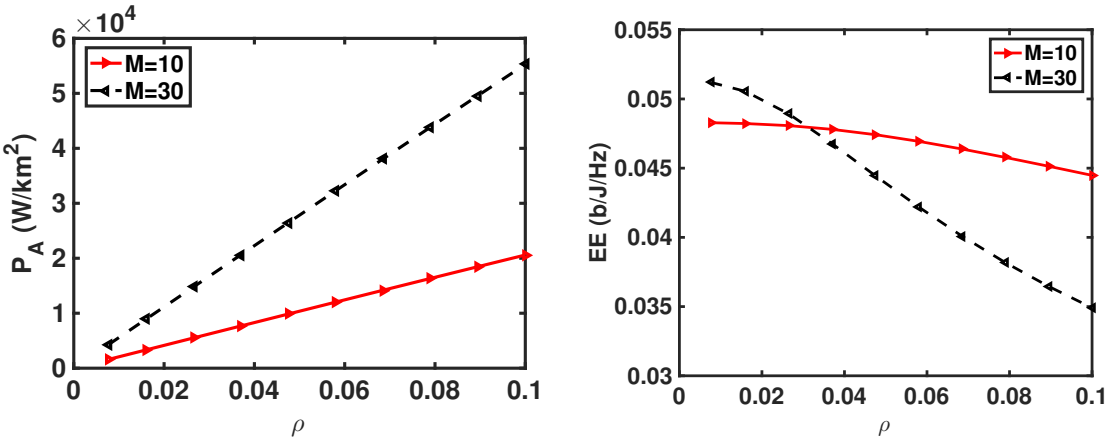

(a) P_A vs. ρ (b) EE vs. ρ

Figure 5.13 – Variation of average power consumption per u.a. and EE with BS-user density ratio at $\lambda_u = 5 \cdot 10^{-4}$ m^{-2} and $P_t = 40$ dBm

shown in Fig. 5.12. This leads to a linear increase of P_A with ρ, as it can be observed in Fig. 5.13a. The decreasing rate of increase in ASE with ρ for $M = 30$ in Fig. 5.11 leads to a significant decrease in EE with ρ, as shown in Fig. 5.13b.

5.8.4 Effect of BS density with constant ρ on ASE and EE

Figs. 5.14a and 5.14b draw the ASE vs. λ_b labelled on number of BS antennas, i.e. M, and transmit power, i.e. P_t, when BS-user density ratio, i.e. ρ, is 0.0077 and 1 respectively. The parameters for the plots are $N_u = 5000$ and $u_{\max} = M$. We see that increasing λ_b keeping ρ constant increases ASE. The results also demonstrate that while ASE increases linearly with λ_b when $P_t = 40$dBm, the rate of increase becomes higher slightly with λ_b at $P_t = -20$dBm. This is because ASE depends on upper bound of ergodic rate, i.e. $\hat{R}_u$, and the PMF of the number of active users in a cell, i.e. $p_N(u)$, as can be seen in (5.25). Since ρ is fixed, $p_N(u)$ is constant as can be seen from (5.3).

On the other hand, when P_t is sufficiently large leading to interference limited scenario, i.e. $P_t = 40$ dBm, $\hat{R}_u$ does not change with λ_b, as shown in Fig. 5.15. The reason is that the BS activity probability, i.e. $1 - p_N(0)$, does not change with BS density since ρ is constant. Therefore, the effect of the increase of the received desired signal power on $\hat{R}_u$ is exactly counter-balanced by the increase in the received interference power. This leads to a constant increase of ASE with λ_b when P_t is sufficiently large to ignore the noise. Andrews *et al.* have shown that coverage probability considering a general fading does not depend on λ_b due to the same reason when

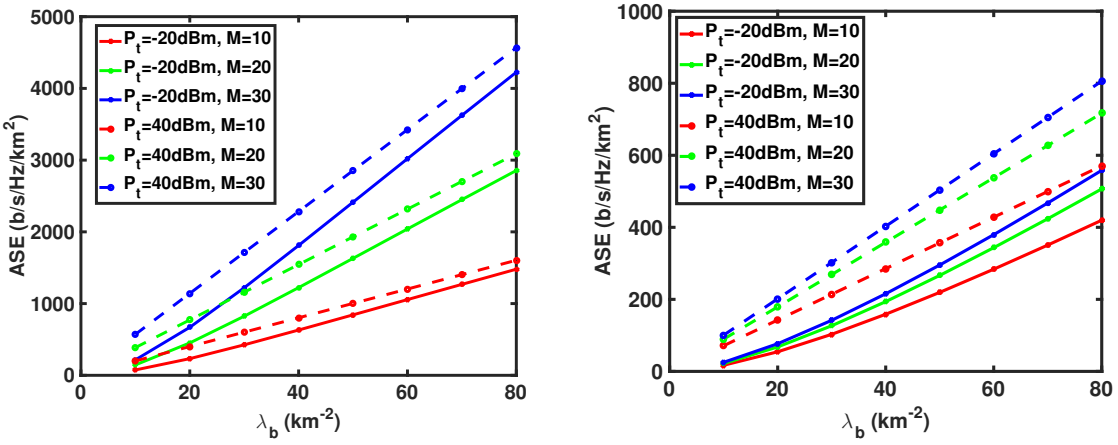

(a) $\rho = 0.0077$ (b) $\rho = 1$

Figure 5.14 – ASE vs. BS density at $N_u = 5000$ and $u_{\max} = M$

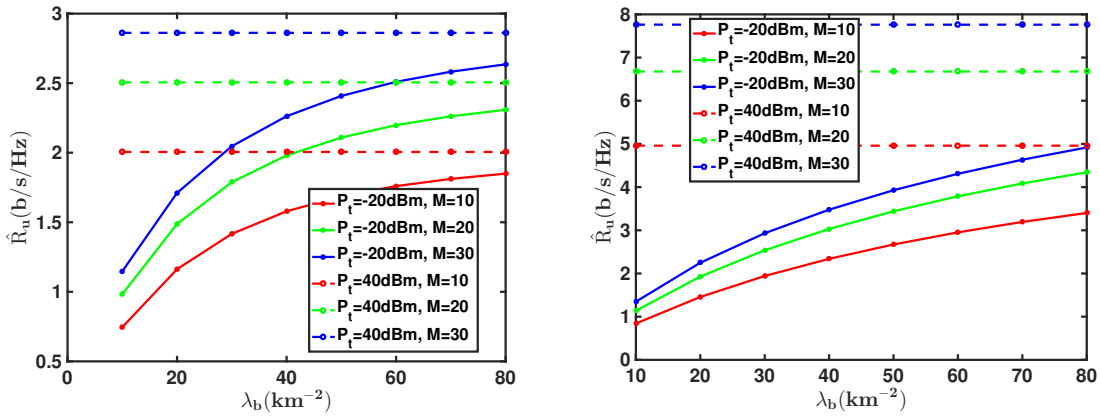

(a) $\rho = 0.0077$ (b) $\rho = 1$

Figure 5.15 – $\hat{R}_u$ vs. BS density at $N_u = 5000$, $u_{\max} = M$ and $u_0 = 10$

noise is ignored and all the BSs are active [5]. Mean received aggregated inter-cell interference power would not increase in the same scale as the mean received desired signal power when λ_b increases if the BS activity probability was changed. When P_t is low, e.g. -20 dBm, $\hat{R}_u$ increases with λ_b due to the decrease of NSR, and causes the increasing rate of ASE with BS density.

On the other hand, since $p_N(0)$ does not change with BS density when ρ is constant, P_A increases linearly with BS density, as it can be seen from (5.26). The constant increasing rate of ASE and P_A with BS density leads to a constant EE with BS density when $P_t = 40$ dBm, as can

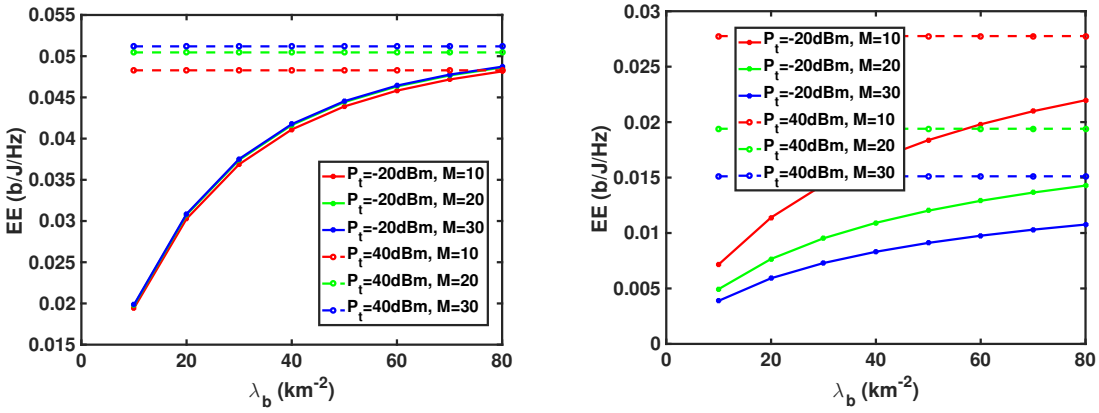

(a) $\rho = 0.0077$ (b) $\rho = 1$

Figure 5.16 – EE vs. BS density at $N_u = 5000$ and $u_{\max} = M$

be observed in Fig. 5.16. On the other hand, the increasing rate of ASE with BS density leads to an increasing EE with BS density at $P_t = -20$ dBm. However, $\hat{R}_u$ converges towards a limit as λ_b increases since the NSR becomes negligible compared to ISR. This will lead to a constant increase of ASE and a constant EE if λ_b is further increased even for $P_t = -20$ dBm.

It is also interesting to observe in Fig. 5.16b that higher number of BS antennas induces a loss in EE for $\rho = 1$, which is in contrast to $\rho = 0.0077$. The reason is that the spatial multiplexing gain provided by higher number of BS antennas cannot be achieved when ρ is large, i.e. $\rho = 1$. Therefore, the increase in P_A, due to the larger amount of RF circuit power consumption, dominates over the increase of ASE resulting in lower EE for higher BS antennas at $\rho = 1$.

5.9 Conclusions

We have introduced a theoretical framework for approaching the upper bound of ASE in asymptotic regime for PPP networks when SLNR precoder is used by means of random matrix theory and stochastic geometry. The theoretical expression of the EE-ASE tradeoff has been found to be tight with the results obtained through Monte Carlo simulations, even for moderate values of the number of antennas and users in the network, and for a wide range of system parameters. The results have shown that EE increases linearly as a function of ASE due to the important amount of power wasted in static circuitry. A sharp decrease of EE is observed when transmit power is increased beyond a certain level because of the saturation of ASE at this power. We also compared the performance of the SLNR precoder with ZF precoder. Our results have shown that

there is a performance gain over ZF precoder in terms of EE-ASE tradeoff when SLNR precoder is used.

We also investigated the effect of the maximum number of active users allowed in a cell, number of BS antennas, and BS density with a constant user density and constant BS-user density ratio. Numerical results have shown that deploying more BSs or BS antennas increases ASE. However, the performance gain depends on the BS-user density ratio and the number of BS antennas when user density is fixed. As long as the BS-user density ratio is small or equivalently the average number of users per cell is large compared to the number of antennas, ASE grows linearly with the number of antennas or BS density. The gain diminishes with the number of antennas or BS density if the BS-user density is large compared to the number of antennas.

Since the average power consumption per u.a. increases linearly with the number of antennas, the sub-linear increase in ASE for higher BS-user density ratio induces significant loss in EE when the number of antennas is increased. On the other hand, the BS activity probability decreases with the BS density when user density is fixed. However, the average area power consumption per u.a. increases linearly with BS density when the increased non-transmission power dominate over the transmission power. EE decreases significantly with BS density when ASE sub-linearly increases for higher number of antennas.

When BS density is increased keeping the BS-user density constant, ergodic rate of a user in the noise limited region, i.e. small transmit power, increases. This leads to a higher rate of increase in ASE and a sub-linear increase in EE with BS density. However, when the network is interference limited, the ergodic rate of a typical user converges to a constant value resulting in a linear increase in ASE and a constant EE with BS density. Therefore, ASE can be improved by deploying more BSs without sacrificing EE and also the ergodic rate of the users as the user density increases.

In this chapter, transmit power is assumed to be equally shared among the active users in a cell. Resource management based on the real traffic condition and user position will lead to different power allocation as already mentioned in Chapter 4. Joint distribution of the rates of the active users needs to be taken into account when the allocated resources are not equally shared among the active users.

Chapter 6

Conclusions and future works

6.1 Conclusions

Reusing the frequency bandwidth over relatively small geographical areas is one of the most promising strategies to increase SE and EE. The major concern in this case is CCI potentially decreasing SE and EE. In addition to the higher bandwidth, densification of the networks, by deploying small cells and multiple antennas at BSs, is also considered as a potential technique to increase ASE. Due to the large amount of circuit power consumption, the total energy consumption of the wireless networks increases causing a decrease in EE. In this thesis, we have characterized the achievable EE-SE region in a hexagonal cellular network considering several frequency reuse factors as well as shadowing. The EE-ASE region has been also studied in a MU-MISO cellular network with SLNR precoder, when BSs and users are modelled as PPP.

In the beginning, we provided the mathematical tools from stochastic geometry and random matrix theory which were later used in this thesis. We also conducted a brief survey on the performance metrics and energy-efficient research approaches from literature. Besides, the most commonly used models for network architecture, BS power consumption and propagation loss, which are also used in this thesis, have been described. Moreover, the linear precoders, e.g. MRT, ZF, SLNR, have been illustrated using a vector representation.

We have also revisited the EE-SE tradeoff for an AWGN channel. It was observed that EE decreases with SE when the static circuit power consumption is ignored. However, a linear part also exists in the EE-SE tradeoff curves where EE increases with SE when static circuit power consumption is taken into account. We have studied the effect of the PA factor and static circuit power consumption on the EE-SE tradeoff. The results demonstrated that both optimal EE and

SE decrease as the PA factor increases. Besides, although higher optimal SE is achieved when the static power consumption is increased, the optimal EE becomes lower.

Although Kelif *et al.* derived a closed form expression of ISR using the fluid model allowing a tractable derivation of EE-SE tradeoff in hexagonal cellular networks [14], the expression for ISR was limited to frequency reuse factor equal to one. We have characterized the EE-SE region in hexagonal cellular network for different frequency reuse factors both with and without shadowing. A downlink regular hexagonal cellular network with TDMA, FDMA or OFDMA type of access among the users in a cell has been considered in this work. Both BSs and users have been equipped with a single antenna.

We have obtained a parametric expression of ISR, as function of the normalized distance of the user and path loss exponent, for different frequency reuse factors with curve fitting approach. The parametric expressions of ISR have allowed us to derive the EE-SE tradeoff for several frequency reuse factors when path loss dependent channel modelling is considered. On the other hand, we have proposed ϵ-SE and ϵ-EE to characterize the EE-SE tradeoff when shadowing is considered since the capacity in Shannon's sense is not defined with shadowing consideration. We have obtained an analytical expression of CDF of SINR allowing to study the EE-SE tradeoff when shadowing is taken into account, and validated the expression of CDF by Monte Carlo simulations.

Consequently, we have investigated the EE-SE region with and without shadowing for different frequency reuse factors for a user at various distances. The effect of ϵ on the EE-SE tradeoff has also been investigated for the shadowing case. The EE-SE tradeoff curves have been observed to have a large linear part as seen also for the AWGN channel due to the domination of the consumption of static power over the transmit power. However, EE later started decreasing with SE due to the transmit power domination leading to an optimal EE. Since SE converges towards a limit for a given transmit power in the interference limited network, there is little SE improvement beyond the optimal point and EE decreases sharply when the transmit power is further increased.

The results have also demonstrated that a frequency reuse factor equal to 1 for regions close to BS and higher reuse factors in region closer to the cell edge optimizes the EE-SE tradeoff. Moreover, better EE-SE tradeoff can be achieved with higher ϵ or outage in the system when shadowing is considered. Besides, $K = 1$ allowed the best optimal EE-SE tradeoff only for higher values of ϵ even at a moderate distance since SINR decreases more significantly in shadowing environment for $K = 1$.

Then we have introduced a theoretical framework for obtaining the upper bound of ASE in

asymptotic regime in a MU-MISO cellular network with random topology when SLNR precoder is used, and derived EE from a linear power consumption model afterwards. The results were achieved by applying some fundamental results from RMT to PPP. Although the PPP model is extensively used in literature, the previous works have considered either the MRT or the ZF precoder due to tractability. The theoretical expressions of ASE and EE for the SLNR precoder have been found to be tight with the exact results obtained through Monte Carlo simulations, even for moderate values of the number of antennas and users in the network, and for a wide range of system parameters. Hence, the expressions can be used for the performance analysis of a real network saving the time to run extensive Monte Carlo simulations in addition to providing useful insights.

The results have shown that EE increases linearly with ASE due to the significant amount of static circuit power consumption, and decreases sharply when transmit power is increased beyond a certain level because of the saturation of ASE in the interference-limited network. We have also compared the performance of SLNR and ZF precoders. Our results have shown that there is a performance gain over ZF precoder in terms of EE-ASE tradeoff due to better SINR for the SLNR precoder. The reason is that although ZF precoder nulls the intra-cell interference, it does not account the leakage to other-cell users. Moreover, it decreases the received desired signal power. On the other hand, the multi-cell SLNR precoder achieves a tradeoff between maximizing the received desired signal power of the intended user and minimizing the interference leakage to all other users. This fact results in better SINR when SLNR precoder is used.

We have also investigated the effect of maximum number of active users allowed in a cell on ASE. Numerical results have shown that ASE first increases rapidly due to the spatial multiplexing gain obtained from serving more users. However, ASE converges to a constant value when the maximum number of active users is higher than a particular value, which is higher for a smaller BS-user density ratio.

We also studied the effect of number of BS antennas, and BS density with a constant user density on ASE and EE. The results have illustrated that deploying more BSs or BS antennas increases ASE, but the performance gain depends on the BS-user density ratio and the number of BS antennas. ASE has been observed to grow linearly with number of antennas and BS density when the average number of users per cell is large enough to achieve the spatial multiplexing gain provided by MU-MISO. However, the gain diminishes with number of antennas and BS density if the BS-user density is large compared to the number of antennas.

On the other hand, although the average power consumption per u.a. always increases linearly with the number of antennas, it increases linearly with BS density only when the increased

non-transmission power dominates over the transmission power. Sublinear increase in ASE for higher BS density and higher number of antennas when number of antennas and BS density increases respectively induces a significant loss in EE.

Finally, we illustrated the effect of BS density with constant BS-user density ratio on ASE and EE. In the noise limited regime, ergodic rate of a user increases, leading to a higher rate of increase in ASE and an increasing EE with BS density. However, when the network becomes interference limited, ergodic rate of a typical user converges to a constant value resulting in a linear increase in ASE and a constant EE with BS density. Therefore, ASE can be improved by deploying more BSs without sacrificing EE and also the ergodic rate of the users as the user density increases.

6.2 Future works

There are numerous things which can be addressed in the future:

– We have characterized the achievable EE-SE region in a hexagonal cellular network considering several frequency reuse factors. But the BSs have been equipped with a single antenna. Multiple antennas at BSs can increase the achievable data rate and more general results considering MU-MIMO can be derived in the future.

– Turning off BSs is believed to be a promising solution to save energy and taken into account in literature by several authors dealing with stochastic geometry. However, the switching off BSs is done randomly without considering the actual load in the cells, which is not desired. BSs can be turned off based on the actual load and its impact on the EE-ASE tradeoff can be studied afterwards when SLNR precoder is used in a PPP network.

– Deployment of heterogeneous network consisting of various small BSs, i.e. micro, pico, femto, etc., underlaid in a macro cellular network can save a huge amount of energy when combined with switching off BSs and hence gaining a lot of interest by the researchers recently. In a heterogeneous network, different amount of transmit power is required by the cells with different size. In addition, resource management based on the real traffic condition and user position leads to different power allocation for the desired signal and the interfering signal. In this thesis, results are obtained assuming that the desired power and the interference power are same. However, these powers will be different for different power allocation scheme that can be considered in the future.

– In this thesis, we have considered regular hexagonal network model with fixed BS positions and PPP model where BSs are positioned completely at random. Regular hexagonal network is highly idealized and not very tractable. On the other hand, the assumption that BSs are positioned completely at random has turned the PPP model more tractable compared to the hexagonal network model, but this model is far from reality. In real networks, position of BSs is neither fixed like regular hexagonal network nor totally random as considered in PPP model. Andrews *et al.* have shown in [5] that the hexagonal network is optimistic and the PPP model is pessimistic in terms of coverage probability when compared with measurements from a real network. The works in this thesis can be extended in future by modelling the BSs by a point process that considers spatial correlation among the BSs without hampering the tractability.

– Deriving the theoretical expressions for the EE-ASE tradeoff in PPP networks using MMSE precoder is very challenging. The MMSE and SLNR precoders have been proved to be equivalent under symmetric scenario where all channels between BS and users have the same gain [34, 99]. However, finding the optimal parameters for the MMSE precoder in a non-symmetric scenario is generally hard. In future, theoretical expressions for the EE-ASE tradeoff in PPP networks can be developed using MMSE precoder and performance between the SLNR and MMSE precoder can be compared afterwards.

Appendix A

Appendix

A.1 Proof of Theorem 5.1

Let us first derive the CDF of $M^{\frac{\alpha}{2}} r_{0j}^{-\alpha}$, where r_{0j} denotes the distance from BS 0 to the j-th user. Note that $M^{\frac{\alpha}{2}} r_{0j}^{-\alpha}$, $\forall\, j \neq k$ are the diagonal components and also the eigenvalues of $M^{\frac{\alpha}{2}} \bar{\mathbf{D}}_{0k}$. Considering that BS 0 is positioned at the center of the network, the PDF of r_{0j} is [160]:

$$f_{r_{0j}}(x) = \frac{2x}{R_a^2}. \tag{A.1}$$

The CDF of $M^{\frac{\alpha}{2}} r_{0j}^{-\alpha}$ can be written as:

$$F^{M^{\frac{\alpha}{2}} r_{0j}^{-\alpha}}(\tau) = \mathrm{P}\left(M^{\frac{\alpha}{2}} r_{0j}^{-\alpha} < \tau\right) = \mathrm{P}\left(r_{0j}^{-\alpha} < \tau M^{-\frac{\alpha}{2}}\right). \tag{A.2}$$

Since $r_{0j}^{-\alpha}$ is a decreasing function of r_{0j}, using (A.1), (A.2) can be written as

$$\begin{aligned} F^{M^{\frac{\alpha}{2}} r_{0j}^{-\alpha}}(\tau) &= 1 - \mathrm{P}\left(r_{0j} < \left(\tau M^{-\frac{\alpha}{2}}\right)^{\frac{-1}{\alpha}}\right) \\ &= 1 - \int_0^{\tau^{\frac{-1}{\alpha}} M^{\frac{1}{2}}} \frac{2x}{R_a^2} dx \\ &= 1 - \frac{\tau^{\frac{-2}{\alpha}} M}{R_a^2}. \end{aligned} \tag{A.3}$$

Since $\lim_{R_a\to\infty} N_{au}(R_a) = \lim_{R_a\to\infty} \lambda_{au}\pi R_a^2$, using (A.3), we can write

$$\lim_{R_a\to\infty} F^{M^{\frac{\alpha}{2}} r_{0j}^{-\alpha}}(\tau) = \lim_{R_a\to\infty} \left(1 - \frac{\tau^{\frac{-2}{\alpha}} M}{\frac{N_{au}(R_a)}{\pi\lambda_{au}}}\right) \overset{a.r.}{\sim} \left(1 - \frac{\pi\lambda_{au}\tau^{\frac{-2}{\alpha}}}{\gamma_{au}}\right) = F_l^{M^{\frac{\alpha}{2}} r_{0j}^{-\alpha}}(\tau) \tag{A.4}$$

with $\left(\frac{\pi\lambda_{au}}{\gamma_{au}}\right)^{\frac{\alpha}{2}} < \tau < \infty$. Using (A.4), the derivative of $F_l^{M^{\frac{\alpha}{2}} r_{0j}^{-\alpha}}(\tau)$ can be written as

$$dF_l^{M^{\frac{\alpha}{2}} r_{0j}^{-\alpha}}(\tau) = \frac{2\pi\lambda_{au}}{\alpha\gamma_{au}}\tau^{-\frac{2}{\alpha}-1}d\tau. \tag{A.5}$$

The matrix (unitary) of eigenvectors $\bar{\mathbf{U}}_{0k}$ and the matrix of eigenvalues $\bar{\mathbf{\Lambda}}_{0k}$ are obtained from the eigen decomposition of $\frac{1}{M}\bar{\mathbf{H}}_{0k}M^{\frac{\alpha}{2}}\bar{\mathbf{D}}_{0k}\bar{\mathbf{H}}_{0k}^H$ that does not contain $\mathbf{h}_{0k}$. Since $\mathbf{t}_{0k} = \bar{\mathbf{U}}_{0k}^H\mathbf{h}_{0k}$, where $\mathbf{h}_{0k} \sim \mathscr{CN}(0,\mathbf{I}_M)$ then $\mathbf{t}_{0k} \sim \mathscr{CN}(0,\mathbf{I}_M)$ and hence $\mathbf{t}_{0k}$ is independent of $\bar{\mathbf{\Lambda}}_{0k}$. Since $|t_{0kl}|^2$ is exponentially distributed with mean 1, and also independent of $\bar{\lambda}_{0kl}$, we have

$$\begin{aligned}\mathrm{E}_{\mathbf{t}_{0k},\bar{\mathbf{\Lambda}}_{0k}}\left[\frac{1}{M}\sum_{l=1}^{M}\frac{|t_{0kl}|^2}{\bar{\lambda}_{0kl}+\frac{M^{\frac{\alpha}{2}-1}\sigma_n^2u_0}{P_t}}\right] &= \frac{1}{M}\sum_{l=1}^{M}\mathrm{E}\left[|t_{0kl}|^2\right]\mathrm{E}_{\bar{\lambda}_{0kl}}\left[\frac{1}{\bar{\lambda}_{0kl}+\frac{M^{\frac{\alpha}{2}-1}\sigma_n^2u_0}{P_t}}\right] \\ &= \frac{1}{M}\sum_{l=1}^{M}\mathrm{E}_{\bar{\lambda}_{0kl}}\left[\frac{1}{\bar{\lambda}_{0kl}+\frac{M^{\frac{\alpha}{2}-1}\sigma_n^2u_0}{P_t}}\right].\end{aligned} \tag{A.6}$$

According to Definition 2.6, ESD of $\frac{1}{M}\bar{\mathbf{H}}_{0k}M^{\frac{\alpha}{2}}\bar{\mathbf{D}}_{0k}\bar{\mathbf{H}}_{0k}^H$ can be expressed as

$$F^{\bar{\mathbf{\Lambda}}_{0k}}(x) = \frac{1}{M}\sum_{l=1}^{M}\mathbf{1}_{\bar{\lambda}_{0kl}\le x}(x). \tag{A.7}$$

The Stieltjes transform of $F^{\bar{\mathbf{\Lambda}}_{0k}}(x)$ on $\mathbb{C}\backslash\mathbb{R}^+$, according to Definition 2.9, is

$$m_{F^{\bar{\mathbf{\Lambda}}_{0k}}}(z) = \int_0^\infty \frac{1}{x-z}dF^{\bar{\mathbf{\Lambda}}_{0k}}(x). \tag{A.8}$$

Since the support of $F^{\bar{\mathbf{\Lambda}}_{0k}}$ is on the nonnegative real axis, $m_{F^{\bar{\mathbf{\Lambda}}_{0k}}}$ is continuous in the neighborhood of the negative real line, and can be evaluated at negative real values of z [45, 46]. $F^{\bar{\mathbf{\Lambda}}_{0k}}$ is random and depends on $\bar{\mathbf{H}}_{0k} \in \mathbb{C}^{M\times(N_{au}-1)}$ and $\bar{\mathbf{D}}_{0k} \in \mathbb{R}_+{}^{(N_{au}-1)\times(N_{au}-1)}$. The latter is independent of $\bar{\mathbf{H}}_{0k}$. Moreover, $\mathrm{E}\left[\bar{\mathbf{H}}_{0k11} - \mathrm{E}\left[\bar{\mathbf{H}}_{0k11}\right]\right]^2 = 1$ where $\bar{\mathbf{H}}_{0k11}$ denotes the element of the first column and first

row of the matrix $\bar{\mathbf{H}}_{0k}$ and $F^{M^{\frac{\alpha}{2}}\bar{\mathbf{D}}_{0k}} \overset{a.r.}{\sim} F_l^{M^{\frac{\alpha}{2}} r_{0j}^{-\alpha}}$ provided in (A.4). Hence according to Theorem 2.4, $F^{\bar{\mathbf{\Lambda}}_{0k}}$ converges in distribution to a non-random function $F_l^{\bar{\mathbf{\Lambda}}_{0k}}$, and Stieltjes transform of $F_l^{\bar{\mathbf{\Lambda}}_{0k}}$ denoted by $m_{F_l^{\bar{\mathbf{\Lambda}}_{0k}}}(z)$ satisfies

$$z m_{F_l^{\bar{\mathbf{\Lambda}}_{0k}}}(z) + 1 = m_{F_l^{\bar{\mathbf{\Lambda}}_{0k}}}(z)\gamma_{au} \int_0^{\infty} \frac{\tau dF_l^{M^{\frac{\alpha}{2}} r_{0j}^{-\alpha}}(\tau)}{1+\tau m_{F_l^{\bar{\mathbf{\Lambda}}_{0k}}}(z)}. \tag{A.9}$$

Since the elements of $\bar{\Lambda}_{0k}$ are non-negative, the integrand in (A.8) is bounded and positive for negative values of z. Hence, $F^{\bar{\Lambda}_{0k}} \to F_l^{\bar{\Lambda}_{0k}}$ implies $m_{F^{\bar{\Lambda}_{0k}}}(z) \to m_{F_l^{\bar{\Lambda}_{0k}}}(z)$ which is also non-random. Therefore, the term inside the sum in the RHS of (A.6) is $m_{F_l^{\bar{\Lambda}_{0k}}}(z)$ evaluated at $z = -\frac{M^{\frac{\alpha}{2}-1}\sigma_n^2 u_0}{P_t}$ in the asymptotic regime. Hence, (A.6) can be written as

$$\mathrm{E}_{\mathbf{t}_{0k},\bar{\mathbf{\Lambda}}_{0k}}\left[\frac{1}{M}\sum_{l=1}^{M}\frac{|t_{0kl}|^2}{\bar{\lambda}_{0kl}+\frac{M^{\frac{\alpha}{2}-1}\sigma_n^2 u_0}{P_t}}\right] \overset{a.r.}{\sim} m_{F_l^{\bar{\mathbf{\Lambda}}_{0k}}}(z). \tag{A.10}$$

Let us write $m_{F_l^{\bar{\Lambda}_{0k}}} = \bar{m}_{0k}$ for notational simplicity. By using (A.5), RHS of (A.9) can be expressed as

$$\begin{aligned}\bar{m}_{0k}(z)\gamma_{au}\int_0^{\infty}\frac{\tau dF_l^{M^{\frac{\alpha}{2}} r_{0j}^{-\alpha}}(\tau)}{1+\tau\bar{m}_{0k}(z)} &= \bar{m}_{0k}(z)\gamma_{au}\int_{\left(\frac{\pi\lambda_{au}}{\gamma_{au}}\right)^{\frac{\alpha}{2}}}^{\infty}\frac{\frac{2\pi\lambda_{au}\tau^{\frac{-2}{\alpha}}}{\alpha\gamma_{au}}}{1+\tau\bar{m}_{0k}(z)}d\tau \\ &= \frac{\bar{m}_{0k}(z)}{\frac{\alpha}{2\pi\lambda_{au}}}\int_{\left(\frac{\pi\lambda_{au}}{\gamma_{au}}\right)^{\frac{\alpha}{2}}}^{\infty}\frac{\tau^{\frac{-2}{\alpha}}}{1+\tau\bar{m}_{0k}(z)}d\tau.\end{aligned} \tag{A.11}$$

Applying lemma 1 from [161], (A.11) can be written as

$$\begin{aligned}\bar{m}_{0k}(z)\gamma_{au}\int_0^{\infty}\frac{\tau dF_l^{M^{\frac{\alpha}{2}} r_{0j}^{-\alpha}}(\tau)}{1+\tau\bar{m}_{0k}(z)} &= \frac{2\pi^2\lambda_{au}\bar{m}_{0k}^{\frac{2}{\alpha}}(z)csc\left(\frac{2\pi}{\alpha}\right)}{\alpha} - \frac{2\pi\lambda_{au}\bar{m}_{0k}(z)\left(\frac{\pi\lambda_{au}}{\gamma_{au}}\right)^{\frac{\alpha}{2}-1}}{\alpha-2}\times \\ &\left(1+\bar{m}_{0k}(z)\left(\frac{\pi\lambda_{au}}{\gamma_{au}}\right)^{\frac{\alpha}{2}}\right)^{\frac{2}{\alpha}-1}{}_2F_1\left(1-\frac{2}{\alpha},1-\frac{2}{\alpha},2-\frac{2}{\alpha},\frac{\left(\frac{\pi\lambda_{au}}{\gamma_{au}}\right)^{\frac{\alpha}{2}}\bar{m}_{0k}(z)}{1+\left(\frac{\pi\lambda_{au}}{\gamma_{au}}\right)^{\frac{\alpha}{2}}\bar{m}_{0k}(z)}\right).\end{aligned} \tag{A.12}$$

Substituting (A.12) into (A.9) provides

$$zm_{F_l^{\check{\Lambda}_{0k}}}(z)+1=\frac{2\pi^2\lambda_{au}\bar{m}_{0k}^{\frac{2}{\alpha}}(z)csc\left(\frac{2\pi}{\alpha}\right)}{\alpha}-\frac{2\pi\lambda_{au}\bar{m}_{0k}(z)\left(\frac{\pi\lambda_{au}}{\gamma_{au}}\right)^{\frac{\alpha}{2}-1}}{\alpha-2}\times$$
$$\left(1+\bar{m}_{0k}(z)\left(\frac{\pi\lambda_{au}}{\gamma_{au}}\right)^{\frac{\alpha}{2}}\right)^{\frac{2}{\alpha}-1}{}_2F_1\left(1-\frac{2}{\alpha},1-\frac{2}{\alpha},2-\frac{2}{\alpha},\frac{\left(\frac{\pi\lambda_{au}}{\gamma_{au}}\right)^{\frac{\alpha}{2}}\bar{m}_{0k}(z)}{1+\left(\frac{\pi\lambda_{au}}{\gamma_{au}}\right)^{\frac{\alpha}{2}}\bar{m}_{0k}(z)}\right). \quad \text{(A.13)}$$

After straightforward manipulations of (A.13), (5.38) is obtained and the proof is complete.

A.2 Proof of Theorem 5.2

Using the law of total variance [161, 48], we can write

$$\begin{aligned}\mathrm{var}_{\mathbf{t}_{0k},\bar{\mathbf{\Lambda}}_{0k}}\left[\frac{1}{\sqrt{M}}\sum_{l=1}^{M}\frac{|t_{0kl}|^2}{\bar{\lambda}_{0kl}+\frac{M^{\frac{\alpha}{2}-1}\sigma_n^2u_0}{P_t}}\right] &= \mathrm{E}_{\bar{\mathbf{\Lambda}}_{0k}}\left[\mathrm{var}_{\mathbf{t}_{0k}}\left[\frac{1}{\sqrt{M}}\sum_{l=1}^{M}\frac{|t_{0kl}|^2}{\bar{\lambda}_{0kl}+\frac{M^{\frac{\alpha}{2}-1}\sigma_n^2u_0}{P_t}}|_{\bar{\mathbf{\Lambda}}_{0k}}\right]\right]\\ &\quad+\mathrm{var}_{\bar{\mathbf{\Lambda}}_{0k}}\left[\mathrm{E}_{\mathbf{t}_{0k}}\left[\frac{1}{\sqrt{M}}\sum_{l=1}^{M}\frac{|t_{0kl}|^2}{\bar{\lambda}_{0kl}+\frac{M^{\frac{\alpha}{2}-1}\sigma_n^2u_0}{P_t}}|_{\bar{\mathbf{\Lambda}}_{0k}}\right]\right].\end{aligned}\tag{A.14}$$

Since $|t_{0kl}|^2$ are iid with both mean and variance equal to 1, (A.14) can be proved to be

$$\begin{aligned}&\mathrm{var}_{\mathbf{t}_{0k},\bar{\mathbf{\Lambda}}_{0k}}\left[\frac{1}{\sqrt{M}}\sum_{l=1}^{M}\frac{|t_{0kl}|^2}{\bar{\lambda}_{0kl}+\frac{M^{\frac{\alpha}{2}-1}\sigma_n^2u_0}{P_t}}\right]\\ &=\mathrm{E}_{\bar{\mathbf{\Lambda}}_{0k}}\left[\frac{1}{M}\sum_{l=1}^{M}\left(\frac{1}{\bar{\lambda}_{0kl}+\frac{M^{\frac{\alpha}{2}-1}\sigma_n^2u_0}{P_t}}\right)^2\mathrm{var}\left[|t_{0kl}|^2|_{\bar{\mathbf{\Lambda}}_{0k}}\right]\right]+\mathrm{var}_{\bar{\mathbf{\Lambda}}_{0k}}\left[\frac{1}{\sqrt{M}}\sum_{l=1}^{M}\frac{\mathrm{E}\left[|t_{0kl}|^2|_{\bar{\mathbf{\Lambda}}_{0k}}\right]}{\bar{\lambda}_{0kl}+\frac{M^{\frac{\alpha}{2}-1}\sigma_n^2u_0}{P_t}}\right]\\ &=\frac{1}{M}\sum_{l=1}^{M}\mathrm{E}_{\bar{\mathbf{\Lambda}}_{0k}}\left[\left(\frac{1}{\bar{\lambda}_{0kl}+\frac{M^{\frac{\alpha}{2}-1}\sigma_n^2u_0}{P_t}}\right)^2\right]+M\mathrm{var}_{\bar{\mathbf{\Lambda}}_{0k}}\left[\frac{1}{M}\sum_{l=1}^{M}\frac{1}{\bar{\lambda}_{0kl}+\frac{M^{\frac{\alpha}{2}-1}\sigma_n^2u_0}{P_t}}\right].\end{aligned}\tag{A.15}$$

Let,

$$\begin{aligned}S&=\mathrm{var}_{\bar{\mathbf{\Lambda}}_{0k}}\left[\frac{1}{M}\sum_{l=1}^{M}\frac{1}{\bar{\lambda}_{0kl}+\frac{M^{\frac{\alpha}{2}-1}\sigma_n^2u_0}{P_t}}\right]\\ &=\mathrm{var}_{\bar{\mathbf{\Lambda}}_{0k}}\left[\frac{1}{M}\mathrm{tr}\left(\left(\bar{\mathbf{\Lambda}}_{0k}+\frac{M^{\frac{\alpha}{2}-1}\sigma_n^2u_0}{P_t}\right)^{-1}\right)\right]\\ &=\int_0^{\infty}2x\mathrm{P}\left[\left|\frac{1}{M}\mathrm{tr}\left(\left(\bar{\mathbf{\Lambda}}_{0k}+\frac{M^{\frac{\alpha}{2}-1}\sigma_n^2u_0}{P_t}\right)^{-1}\right)-\mathrm{E}\left[\frac{1}{M}\mathrm{tr}\left(\left(\bar{\mathbf{\Lambda}}_{0k}+\frac{M^{\frac{\alpha}{2}-1}\sigma_n^2u_0}{P_t}\right)^{-1}\right)\right]\right|>x\right]dx\end{aligned}\tag{A.16}$$

Using Bayes rule and inserting $\tilde{\mathbf{\Lambda}}_{0k} = \left(\bar{\mathbf{\Lambda}}_{0k} + \frac{M^{\frac{\alpha}{2}-1}\sigma_n^2 u_0}{P_t}\right)^{-1}$, (A.16) can be written as

$$S = \int_0^\infty 2x \int \cdots \int \mathrm{P}\left[\left|\frac{1}{M}\mathrm{tr}\left(\tilde{\mathbf{\Lambda}}_{0k}\right) - \mathrm{E}\left[\frac{1}{M}\mathrm{tr}\left(\tilde{\mathbf{\Lambda}}_{0k}\right)\right]\right| > x \middle| \tilde{d}_{01}, \cdots, \tilde{d}_{0(k-1)}, \tilde{d}_{0(k+1)}, \tilde{d}_{0N_{au}}\right] \times$$
$$f_{\tilde{d}}(\tilde{d}_{01}, \cdots, \tilde{d}_{0(k-1)}, \tilde{d}_{0(k+1)}, \tilde{d}_{0N_{au}}) d\tilde{d}_{01} \cdots d\tilde{d}_{0(k-1)} d\tilde{d}_{0(k+1)} d\tilde{d}_{0N_{au}} dx, \tag{A.17}$$

with $\tilde{\mathbf{D}}_{0k} = M^{\frac{\alpha}{2}}\bar{\mathbf{D}}_{0k} = \mathrm{diag}\left(\tilde{d}_{01}, \cdots, \tilde{d}_{0(k-1)}, \tilde{d}_{0(k+1)}, \tilde{d}_{0N_{au}}\right)$.

Applying Corollary 1.8 in [162],

$$\mathrm{P}\left[\left|\frac{1}{M}\mathrm{tr}\left(\tilde{\mathbf{\Lambda}}_{0k}\right) - \mathrm{E}\left[\frac{1}{M}\mathrm{tr}\left(\tilde{\mathbf{\Lambda}}_{0k}\right)\right]\right| > x \middle| \tilde{d}_{01}, \cdots, \tilde{d}_{0(k-1)}, \tilde{d}_{0(k+1)}, \tilde{d}_{0N_{au}}\right] \leq 2e^{-\frac{M^2x^2}{2\delta_1\delta_2\delta_3}}, \tag{A.18}$$

where δ_1 is the Sobolev inequality constant for the distribution of the entries of $\tilde{\mathbf{H}}_{0k}$, $\delta_2 = \frac{27}{64\left(\frac{M^{\frac{\alpha}{2}-1}\sigma_n^2 u_0}{P_t}\right)^3}$ which is the square of the Lipschitz constant for the function $f(x) = \frac{1}{\frac{M^{\frac{\alpha}{2}-1}\sigma_n^2 u_0}{P_t} + x^2}$ and δ_3 is the largest $\tilde{d}_{0i}$ which is $M^{\frac{\alpha}{2}}\epsilon^{-\alpha}$ considering that ϵ is the close-in reference distance. Therefore, $\frac{1}{2\delta_1\delta_2\delta_3} \geq \frac{64\left(\frac{\sigma_n^2 u_0}{P_t}\right)^3 M^{\alpha-3}}{54\delta_1\epsilon^{-\alpha}}$ and (A.18) can be written as

$$\mathrm{P}\left[\left|\frac{1}{M}\mathrm{tr}\left(\tilde{\mathbf{\Lambda}}_{0k}\right) - \mathrm{E}\left[\frac{1}{M}\mathrm{tr}\left(\tilde{\mathbf{\Lambda}}_{0k}\right)\right]\right| > x \middle| \tilde{d}_{01}, \cdots, \tilde{d}_{0(k-1)}, \tilde{d}_{0(k+1)}, \tilde{d}_{0N_{au}}\right] \leq 2e^{\frac{-64\left(\frac{\sigma_n^2 u_0}{P_t}\right)^3 M^{\alpha-1}x^2}{54\delta_1\epsilon^{-\alpha}}} \tag{A.19}$$

Using (A.19), (A.17) can be expressed as

$$S \leq \int_0^\infty 2x \int \cdots \int 2e^{\frac{-64\left(\frac{\sigma_n^2 u_0}{P_t}\right)^3 M^{\alpha-1}x^2}{54\delta_1\epsilon^{-\alpha}}} f_{\tilde{d}}(\tilde{d}_{01}, \cdots, \tilde{d}_{0(k-1)}, \tilde{d}_{0(k+1)}, \tilde{d}_{0N_{au}}) d\tilde{d}_{01} \cdots d\tilde{d}_{0(k-1)} d\tilde{d}_{0(k+1)} d\tilde{d}_{0N_{au}} dx$$
$$\leq \int_0^\infty 4xe^{\frac{-64\left(\frac{\sigma_n^2 u_0}{P_t}\right)^3 M^{\alpha-1}x^2}{54\delta_1\epsilon^{-\alpha}}} dx = \frac{27\delta_1\epsilon^{-\alpha}M^{1-\alpha}}{16\left(\frac{\sigma_n^2 u_0}{P_t}\right)^3}. \tag{A.20}$$

As $M \to \infty$, $MS \to 0$ for $\alpha > 2$. Hence, (A.15) can be expressed as

$$\mathrm{var}_{\mathbf{t}_{0k}, \tilde{\mathbf{\Lambda}}_{0k}}\left[\frac{1}{\sqrt{M}}\sum_{l=1}^{M}\frac{|t_{0kl}|^2}{\bar{\lambda}_{0kl} + \frac{M^{\frac{\alpha}{2}-1}\sigma_n^2 u_0}{P_t}}\right] \underset{\sim}{a.r.} \frac{1}{M}\sum_{l=1}^{M} E_{\tilde{\mathbf{\Lambda}}_{0k}}\left[\left(\frac{1}{\bar{\lambda}_{0kl} + \frac{M^{\frac{\alpha}{2}-1}\sigma_n^2 u_0}{P_t}}\right)^2\right]. \tag{A.21}$$

Differentiation of $m_{F_l^{\bar{\mathbf{\Lambda}}_{0k}}}(z)$ w.r.t. z is

$$m'_{F_l^{\bar{\mathbf{\Lambda}}_{0k}}}(z) = \frac{d}{dz}\int_0^\infty \frac{dF_l^{\bar{\mathbf{\Lambda}}_{0k}}(x)}{x-z} = \int_0^\infty \frac{dF_l^{\bar{\mathbf{\Lambda}}_{0k}}(x)}{(x-z)^2}. \tag{A.22}$$

Using (A.22), we can write

$$\frac{1}{M}\sum_{l=1}^{M} E_{\bar{\mathbf{\Lambda}}_{0k}}\left[\left(\frac{1}{\bar{\lambda}_{0kl}+\frac{M^{\frac{\alpha}{2}-1}\sigma_n^2 u_0}{P_t}}\right)^2\right] \overset{a.r.}{\sim} m'_{0k}(z), \tag{A.23}$$

where $z = -\frac{M^{\frac{\alpha}{2}-1}\sigma_n^2 u_0}{P_t}$, and $m'_{F_l^{\bar{\mathbf{\Lambda}}_{0k}}}$ is denoted by m'_{0k} for notational simplicity, which can be obtained as expressed in (5.39) by differentiating (A.13) w.r.t. z. On the other hand, using the fact that $|t_{0kl}|^2$ is independent of $\frac{1}{\left(\bar{\lambda}_{0kl}+\frac{M^{\frac{\alpha}{2}-1}\sigma_n^2 u_0}{P_t}\right)^2}$, and $\mathrm{E}[|t_{0kl}|^2]=1$, we have

$$\begin{aligned}\mathrm{E}_{\mathbf{t}_{0k},\bar{\mathbf{\Lambda}}_{0k}}\left[\frac{1}{M}\sum_{l=1}^{M}\frac{|t_{0kl}|^2}{\left(\bar{\lambda}_{0kl}+\frac{M^{\frac{\alpha}{2}-1}\sigma_n^2 u_0}{P_t}\right)^2}\right] &= \frac{1}{M}\sum_{l=1}^{M}\mathrm{E}\left[|t_{0kl}|^2\right]\mathrm{E}_{\bar{\Lambda}_{0k}}\left[\frac{1}{\left(\bar{\lambda}_{0kl}+\frac{M^{\frac{\alpha}{2}-1}\sigma_n^2 u_0}{P_t}\right)^2}\right] \\ &= \frac{1}{M}\sum_{l=1}^{M}\mathrm{E}_{\bar{\Lambda}_{0k}}\left[\frac{1}{\left(\bar{\lambda}_{0kl}+\frac{M^{\frac{\alpha}{2}-1}\sigma_n^2 u_0}{P_t}\right)^2}\right].\end{aligned} \tag{A.24}$$

Combining (A.21), (A.23) and (A.24) completes the proof.

A.3 Proof of Theorem 5.3

We can write the precoder for the j-th user in the i-th cell as

$$\mathbf{w}_{ij} = \frac{\left(\bar{\mathbf{H}}_{ij}\bar{\mathbf{D}}_{ij}\bar{\mathbf{H}}_{ij}^H + \frac{\sigma_n^2 u_i}{P_t}\mathbf{I}_M\right)^{-1}\mathbf{h}_{ij}}{\sqrt{\mathrm{E}_{\bar{\mathbf{H}}_{ij},\bar{\mathbf{D}}_{ij},\mathbf{h}_{ij}}\left[\left\|\left(\bar{\mathbf{H}}_{ij}\bar{\mathbf{D}}_{ij}\bar{\mathbf{H}}_{ij}^H + \frac{\sigma_n^2 u_i}{P_t}\mathbf{I}_M\right)^{-1}\mathbf{h}_{ij}\right\|^2\right]}}, \tag{A.25}$$

where $\bar{\mathbf{H}}_{ij} = [\mathbf{h}_{i1}, \cdots, \mathbf{h}_{i(j-1)}, \mathbf{h}_{i(j+1)}, \cdots, \mathbf{h}_{iN_{au}}]$ and $\bar{\mathbf{D}}_{ij} = \mathrm{diag}\left(r_{i1}^{-\alpha}, \cdots, r_{i(j-1)}^{-\alpha}, r_{i(j+1)}^{-\alpha}, \cdots, r_{iN_{au}}^{-\alpha}\right)$ respectively represent the concatenated fading channels and a square diagonal matrix filled by the path losses from the i-th BS to all active users in the network, except the jth user. Using (A.25), we can write

$$\begin{aligned}
\left|\mathbf{h}_{ik}^H\mathbf{w}_{ij}\right|^2 &= \frac{\left|\mathbf{h}_{ik}^H\left(\bar{\mathbf{H}}_{ij}\bar{\mathbf{D}}_{ij}\bar{\mathbf{H}}_{ij}^H + \frac{\sigma_n^2 u_i}{P_t}\mathbf{I}_M\right)^{-1}\mathbf{h}_{ij}\right|^2}{\mathrm{E}_{\bar{\mathbf{H}}_{ij},\bar{\mathbf{D}}_{ij},\mathbf{h}_{ij}}\left[\left\|\left(\bar{\mathbf{H}}_{ij}\bar{\mathbf{D}}_{ij}\bar{\mathbf{H}}_{ij}^H + \frac{\sigma_n^2 u_i}{P_t}\mathbf{I}_M\right)^{-1}\mathbf{h}_{ij}\right\|^2\right]} \\
&= \frac{\left|\mathbf{h}_{ik}^H\left(\frac{1}{M}\bar{\mathbf{H}}_{ijk}M^{\frac{\alpha}{2}}\bar{\mathbf{D}}_{ijk}\bar{\mathbf{H}}_{ijk}^H + \frac{M^{\frac{\alpha}{2}-1}}{r_{ik}^{\alpha}}\mathbf{h}_{ik}\mathbf{h}_{ik}^H + \frac{M^{\frac{\alpha}{2}-1}\sigma_n^2 u_i}{P_t}\mathbf{I}_M\right)^{-1}\mathbf{h}_{ij}\right|^2}{\mathrm{E}_{\bar{\mathbf{H}}_{ij},\bar{\mathbf{D}}_{ij},\mathbf{h}_{ij}}\left[\left\|\left(\frac{1}{M}\bar{\mathbf{H}}_{ij}M^{\frac{\alpha}{2}}\bar{\mathbf{D}}_{ij}\bar{\mathbf{H}}_{ij}^H + \frac{M^{\frac{\alpha}{2}-1}\sigma_n^2 u_i}{P_t}\mathbf{I}_M\right)^{-1}\mathbf{h}_{ij}\right\|^2\right]},
\end{aligned} \tag{A.26}$$

with

$$\bar{\mathbf{H}}_{ijk} = [\mathbf{h}_{i1}, \cdots, \mathbf{h}_{i(j-1)}, \mathbf{h}_{i(j+1)}, \cdots, \mathbf{h}_{i(k-1)}, \mathbf{h}_{i(k+1)}, \cdots, \mathbf{h}_{iN_{au}}]$$

which is the concatenated fading channels from the i-th BS to all active users in the network except the j-th and the k-th user and

$$\bar{\mathbf{D}}_{ijk} = \mathrm{diag}\left(r_{i1}^{-\alpha}, \cdots, r_{i(j-1)}^{-\alpha}, r_{i(j+1)}^{-\alpha}, \cdots, r_{i(k-1)}^{-\alpha}, r_{i(k+1)}^{-\alpha}, \cdots, r_{iN_{au}}^{-\alpha}\right)$$

which is the a square diagonal matrix filled by the path losses from the i-th BS to all active users in the network except the j-th and the k-th user. Since $\left(\frac{1}{M}\bar{\mathbf{H}}_{ijk}M^{\frac{\alpha}{2}}\bar{\mathbf{D}}_{ijk}\bar{\mathbf{H}}_{ijk}^H + \frac{M^{\frac{\alpha}{2}-1}\sigma_n^2 u_i}{P_t}\mathbf{I}_M\right)$ and $\left(\frac{1}{M}\bar{\mathbf{H}}_{ijk}M^{\frac{\alpha}{2}}\bar{\mathbf{D}}_{ijk}\bar{\mathbf{H}}_{ijk}^H + \frac{M^{\frac{\alpha}{2}-1}}{r_{ik}^{\alpha}}\mathbf{h}_{ik}\mathbf{h}_{ik}^H + \frac{M^{\frac{\alpha}{2}-1}\sigma_n^2 u_i}{P_t}\mathbf{I}_M\right)$ are invertible matrix of size $M \times M$ with $\frac{M^{\frac{\alpha}{2}-1}}{r_{ik}^{\alpha}}$

be a scalar, $\mathbf{h}_{ik} \in \mathbb{C}^M$ be a vector, applying Lemma 2.1, (A.26) can be written as

$$\left|\mathbf{h}_{ik}^H \mathbf{w}_{ij}\right|^2 = \frac{\left| \frac{\mathbf{h}_{ik}^H \left(\frac{1}{M}\tilde{\mathbf{H}}_{ijk} M^{\frac{\alpha}{2}} \tilde{\mathbf{D}}_{ijk} \tilde{\mathbf{H}}_{ijk}^H + \frac{M^{\frac{\alpha}{2}-1}\sigma_n^2 u_i}{P_t} \mathbf{I}_M \right)^{-1} \mathbf{h}_{ij}}{1 + \frac{M^{\frac{\alpha}{2}-1}}{r_{ik}^{\alpha}} \mathbf{h}_{ik}^H \left(\frac{1}{M}\tilde{\mathbf{H}}_{ijk} M^{\frac{\alpha}{2}} \tilde{\mathbf{D}}_{ijk} \tilde{\mathbf{H}}_{ijk}^H + \frac{M^{\frac{\alpha}{2}-1}\sigma_n^2 u_i}{P_t} \mathbf{I}_M \right)^{-1} \mathbf{h}_{ik}} \right|^2}{\mathrm{E}_{\tilde{\mathbf{H}}_{ij}, \tilde{\mathbf{D}}_{ij}, \mathbf{h}_{ij}} \left[\left\| \left(\frac{1}{M}\tilde{\mathbf{H}}_{ij} M^{\frac{\alpha}{2}} \tilde{\mathbf{D}}_{ij} \tilde{\mathbf{H}}_{ij}^H + \frac{M^{\frac{\alpha}{2}-1}\sigma_n^2 u_i}{P_t} \mathbf{I}_M \right)^{-1} \mathbf{h}_{ij} \right\|^2 \right]}. \tag{A.27}$$

Since $\left(\frac{1}{M}\tilde{\mathbf{H}}_{ijk} M^{\frac{\alpha}{2}} \tilde{\mathbf{D}}_{ijk} \tilde{\mathbf{H}}_{ijk}^H + \frac{M^{\frac{\alpha}{2}-1}\sigma_n^2 u_i}{P_t} \mathbf{I}_M \right)^{-1}$ is independent of $\mathbf{h}_{ik}$ and the elements of $\mathbf{h}_{ik}$ are iid complex Gaussian with variance 1, applying Lemma 2.2 and using (A.27), we can write

$$\lim_{M\to\infty} \left|\mathbf{h}_{ik}^H \mathbf{w}_{ij}\right|^2 = \lim_{M\to\infty} \frac{\left| \frac{\mathbf{h}_{ik}^H \left(\frac{1}{M}\tilde{\mathbf{H}}_{ijk} M^{\frac{\alpha}{2}} \tilde{\mathbf{D}}_{ijk} \tilde{\mathbf{H}}_{ijk}^H + \frac{M^{\frac{\alpha}{2}-1}\sigma_n^2 u_i}{P_t} \mathbf{I}_M \right)^{-1} \mathbf{h}_{ij}}{1 + \frac{M^{\frac{\alpha}{2}-1}}{r_{ik}^{\alpha}} \mathrm{tr}\left(\left(\frac{1}{M}\tilde{\mathbf{H}}_{ijk} M^{\frac{\alpha}{2}} \tilde{\mathbf{D}}_{ijk} \tilde{\mathbf{H}}_{ijk}^H + \frac{M^{\frac{\alpha}{2}-1}\sigma_n^2 u_i}{P_t} \mathbf{I}_M \right)^{-1} \right)} \right|^2}{\mathrm{E}_{\tilde{\mathbf{H}}_{ij}, \tilde{\mathbf{D}}_{ij}, \mathbf{h}_{ij}} \left[\left\| \left(\frac{1}{M}\tilde{\mathbf{H}}_{ij} M^{\frac{\alpha}{2}} \tilde{\mathbf{D}}_{ij} \tilde{\mathbf{H}}_{ij}^H + \frac{M^{\frac{\alpha}{2}-1}\sigma_n^2 u_i}{P_t} \mathbf{I}_M \right)^{-1} \mathbf{h}_{ij} \right\|^2 \right]}. \tag{A.28}$$

Applying the eigen decomposition: $\frac{1}{M}\tilde{\mathbf{H}}_{ijk} M^{\frac{\alpha}{2}} \tilde{\mathbf{D}}_{ijk} \tilde{\mathbf{H}}_{ijk}^H = \tilde{\mathbf{U}}_{ijk} \tilde{\mathbf{\Lambda}}_{ijk} \tilde{\mathbf{U}}_{ijk}^H$ and $\frac{1}{M}\tilde{\mathbf{H}}_{ij} M^{\frac{\alpha}{2}} \tilde{\mathbf{D}}_{ij} \tilde{\mathbf{H}}_{ij}^H = \tilde{\mathbf{U}}_{ij} \tilde{\mathbf{\Lambda}}_{ij} \tilde{\mathbf{U}}_{ij}^H$, and inserting $\tilde{\mathbf{U}}_{ijk}^H \mathbf{h}_{ik} = \mathbf{t}_{ik}$, $\tilde{\mathbf{U}}_{ijk}^H \mathbf{h}_{ij} = \mathbf{t}_{Nij}$ and $\tilde{\mathbf{U}}_{ij}^H \mathbf{h}_{ij} = \mathbf{t}_{Dij}$, (A.28) can be written as

$$\lim_{M\to\infty} \left|\mathbf{h}_{ik}^H \mathbf{w}_{ij}\right|^2 = \lim_{M\to\infty} \frac{\left| \frac{M^{-\frac{\alpha}{2}} \mathbf{t}_{ik}^H \left(\tilde{\mathbf{\Lambda}}_{ijk} + \frac{M^{\frac{\alpha}{2}-1}\sigma_n^2 u_i}{P_t} \mathbf{I}_M \right)^{-1} \mathbf{t}_{Nij}}{M^{-\frac{\alpha}{2}} + \frac{r_{ik}^{-\alpha}}{M} \mathrm{tr}\left(\left(\tilde{\mathbf{\Lambda}}_{ijk} + \frac{M^{\frac{\alpha}{2}-1}\sigma_n^2 u_i}{P_t} \mathbf{I}_M \right)^{-1} \right)} \right|^2}{\mathrm{E}_{\mathbf{t}_{Dij}, \tilde{\mathbf{\Lambda}}_{ij}} \left[\mathbf{t}_{Dij}^H \left(\tilde{\mathbf{\Lambda}}_{ij} + \frac{M^{\frac{\alpha}{2}-1}\sigma_n^2 u_i}{P_t} \mathbf{I}_M \right)^{-2} \mathbf{t}_{Dij} \right]} \tag{A.29}$$

where $\mathbf{t}_{Dij} = [t_{Dij1}, \cdots, t_{DijM}]$ and $\tilde{\mathbf{\Lambda}}_{ij} = [\tilde{\lambda}_{ij1}, \cdots, \tilde{\lambda}_{ijM}]$. Therefore, the denominator of (A.29) can be expressed as

$$\mathrm{E}_{\mathbf{t}_{Dij}, \tilde{\mathbf{\Lambda}}_{ij}} \left[\mathbf{t}_{Dij}^H \left(\tilde{\mathbf{\Lambda}}_{ij} + \frac{M^{\frac{\alpha}{2}-1}\sigma_n^2 u_i}{P_t} \mathbf{I}_M \right)^{-2} \mathbf{t}_{Dij} \right] = \mathrm{E}_{\mathbf{t}_{Dij}, \tilde{\mathbf{\Lambda}}_{ij}} \left[\sum_{l=1}^{M} \frac{|t_{Dijl}|^2}{\left(\tilde{\boldsymbol{\lambda}}_{ijl} + \frac{M^{\frac{\alpha}{2}-1}\sigma_n^2 u_i}{P_t} \right)^2} \right] \tag{A.30}$$

Moreover, $\frac{1}{M}\text{tr}\left(\left(\bar{\mathbf{\Lambda}}_{ijk}+\frac{M^{\frac{\alpha}{2}-1}\sigma_n^2 u_i}{P_t}\mathbf{I}_M\right)^{-1}\right)$ can be represented by $m_{F^{\bar{\Lambda}_{ijk}}}\left(-\frac{M^{\frac{\alpha}{2}-1}\sigma_n^2 u_i}{P_t}\right)$ for large M. The CDF of the entries of $M^{\frac{\alpha}{2}}\bar{\mathbf{D}}_{ijk}$ can be proved to converge almost surely to (A.4) in the asymptotic regime considering that the infinite network is centered around the i-th BS. Furthermore, $\bar{\mathbf{H}}_{ijk}\in\mathbb{C}^{M\times(N_{au}-2)}$ contains iid complex entries with $\text{E}\left[\bar{\mathbf{H}}_{ijk11}-\text{E}\left[\bar{\mathbf{H}}_{ijk11}\right]\right]^2=1$. Therefore, according to the Theorem 2.4, ESD of $\frac{1}{M}\bar{\mathbf{H}}_{ijk}M^{\frac{\alpha}{2}}\bar{\mathbf{D}}_{ijk}\bar{\mathbf{H}}_{ijk}^H$, denoted as $F^{\bar{\mathbf{\Lambda}}_{ijk}}$ in the asymptotic regime converges to a non-random function $F_l^{\bar{\mathbf{\Lambda}}_{ijk}}$. Since the elements of $\bar{\Lambda}_{ijk}$ are non-negative, $F^{\bar{\Lambda}_{ijk}}\rightarrow F_l^{\bar{\Lambda}_{ijk}}$ implies $m_{F^{\bar{\Lambda}_{ijk}}}(z)\rightarrow m_{F_l^{\bar{\Lambda}_{ijk}}}(z)$ for negative values of z. Following the proof of Theorem 5.1, $m_{F_l^{\bar{\Lambda}_{ijk}}}(z)$ can be shown to be the unique, non-negative real solution of (5.42) where $z=-\frac{M^{\frac{\alpha}{2}-1}\sigma_n^2 u_i}{P_t}$, and $\bar{m}_{ijk}$ is used instead of $m_{F_l^{\bar{\Lambda}_{ijk}}}$ for notational simplicity. Therefore, inserting(A.30), (A.29) can be written as

$$\left|\mathbf{h}_{ik}^H\mathbf{w}_{ij}\right|^2\overset{a.r.}{\sim}\frac{\left|M^{\frac{-\alpha}{2}}\mathbf{t}_{ik}^H\left(\bar{\mathbf{\Lambda}}_{ijk}+\frac{M^{\frac{\alpha}{2}-1}\sigma_n^2 u_i}{P_t}\mathbf{I}_M\right)^{-1}\mathbf{t}_{Nij}\right|^2}{\left(M^{-\frac{\alpha}{2}}+r_{ik}^{-\alpha}\bar{m}_{ijk}\left(-\frac{M^{\frac{\alpha}{2}-1}\sigma_n^2 u_i}{P_t}\right)\right)^2\text{E}_{\mathbf{t}_{Dij},\bar{\mathbf{\Lambda}}_{ij}}\left[\sum_{l=1}^M\frac{|t_{Dijl}|^2}{\left(\bar{\lambda}_{ijl}+\frac{M^{\frac{\alpha}{2}-1}\sigma_n^2 u_i}{P_t}\right)^2}\right]}. \tag{A.31}$$

Moreover, the numerator of (A.31) can be expressed as

$$\begin{aligned}&\left|M^{\frac{-\alpha}{2}}\mathbf{t}_{ik}^H\left(\bar{\mathbf{\Lambda}}_{ijk}+\frac{M^{\frac{\alpha}{2}-1}\sigma_n^2 u_i}{P_t}\mathbf{I}_M\right)^{-1}\mathbf{t}_{Nij}\right|^2 \\ &=M^{-\alpha}\mathbf{t}_{ik}^H\left(\bar{\mathbf{\Lambda}}_{ijk}+\frac{M^{\frac{\alpha}{2}-1}\sigma_n^2 u_i}{P_t}\mathbf{I}_M\right)^{-1}\mathbf{t}_{Nij}\mathbf{t}_{Nij}^H\left(\bar{\mathbf{\Lambda}}_{ijk}+\frac{M^{\frac{\alpha}{2}-1}\sigma_n^2 u_i}{P_t}\mathbf{I}_M\right)^{-1}\mathbf{t}_{ik} \\ &=M^{-\alpha}\sum_{m=1}^M\sum_{\substack{n=1\\n\neq m}}^M\frac{t_{ikm}^H t_{Nijm}t_{Nijn}^H t_{ikn}}{\left(\bar{\lambda}_{ijkm}+\frac{M^{\frac{\alpha}{2}-1}\sigma_n^2 u_i}{P_t}\right)\left(\bar{\lambda}_{ijkn}+\frac{M^{\frac{\alpha}{2}-1}\sigma_n^2 u_i}{P_t}\right)}+M^{-\alpha}\sum_{l=1}^M\frac{|t_{ikl}|^2|t_{Nijl}|^2}{\left(\bar{\lambda}_{ijkl}+\frac{M^{\frac{\alpha}{2}-1}\sigma_n^2 u_i}{P_t}\right)^2},\end{aligned} \tag{A.32}$$

where $\mathbf{t}_{ik}=[t_{ik1},\cdots,t_{ikM}]$, $\mathbf{t}_{Nij}=\left[t_{Nij1},\cdots,t_{NijM}\right]$ and $\bar{\mathbf{\Lambda}}_{ijk}=\left[\bar{\lambda}_{ijk1},\cdots,\bar{\lambda}_{ijkM}\right]$. Both $\mathbf{t}_{ik}$ and $\mathbf{t}_{Nij}$ are complex Gaussian vectors with mean 0 and covariance matrix $\mathbf{I}_M$. Moreover, they are independent of $\bar{\mathbf{\Lambda}}_{ijk}$. Since $\mathbf{h}_{ik}$ and $\mathbf{h}_{ij}$ are independent, and $\mathbf{t}_{ik}=\bar{\mathbf{U}}_{ijk}^H\mathbf{h}_{ik}$, $\mathbf{t}_{Nij}=\bar{\mathbf{U}}_{ijk}^H\mathbf{h}_{ij}$, $\mathbf{t}_{Nij}$ and $\mathbf{t}_{ik}$ are also independent. Furthermore, the entries of $\mathbf{t}_{Nij}$ and $\mathbf{t}_{ik}$ are iid with mean 0.

Therefore, we can write

$$\sum_{m=1}^{M}\sum_{\substack{n=1\\n\neq m}}^{M}\mathrm{E}_{t,\lambda}\left[\frac{M^{-\alpha}t_{ikm}^{H}t_{Nijm}t_{Nijn}^{H}t_{ikn}}{\left(\bar{\lambda}_{ijkm}+\frac{M^{\frac{\alpha}{2}-1}\sigma_n^2u_i}{P_t}\right)\left(\bar{\lambda}_{ijkn}+\frac{M^{\frac{\alpha}{2}-1}\sigma_n^2u_i}{P_t}\right)}\right]$$
$$=\sum_{m=1}^{M}\sum_{\substack{n=1\\n\neq m}}^{M}\mathrm{E}_{t,\lambda}\left[\frac{M^{-\alpha}t_{ikm}^{H}t_{Nijm}t_{Nijn}^{H}}{\left(\bar{\lambda}_{ijkm}+\frac{M^{\frac{\alpha}{2}-1}\sigma_n^2u_i}{P_t}\right)\left(\bar{\lambda}_{ijkn}+\frac{M^{\frac{\alpha}{2}-1}\sigma_n^2u_i}{P_t}\right)}\right]\mathrm{E}\left[t_{ikn}\right]$$
$$=0. \tag{A.33}$$

Using (A.33) and (A.32), we can write

$$\mathrm{E}_{\mathbf{t}_{ik},\mathbf{t}_{Nij},\bar{\mathbf{\Lambda}}_{ijk}}\left[\left|M^{-\frac{\alpha}{2}}\mathbf{t}_{ik}^{H}\left(\bar{\mathbf{\Lambda}}_{ijk}+\frac{M^{\frac{\alpha}{2}-1}\sigma_n^2u_i}{P_t}\mathbf{I}_M\right)^{-1}\mathbf{t}_{Nij}\right|^2\right]$$
$$=\mathrm{E}_{\mathbf{t}_{ik},\mathbf{t}_{Nij},\bar{\mathbf{\Lambda}}_{ijk}}\left[\sum_{l=1}^{M}\frac{M^{-\alpha}|t_{ikl}|^2|t_{Nijl}|^2}{\left(\bar{\lambda}_{ijkl}+\frac{M^{\frac{\alpha}{2}-1}\sigma_n^2u_i}{P_t}\right)^2}\right]. \tag{A.34}$$

Using (A.34) and (A.31), mean of $\left|\mathbf{h}_{ik}^{H}\mathbf{w}_{ij}\right|^2$ conditioned on r_{0k} and r_{ik} can be written as

$$\mathrm{E}_{\bar{\mathbf{H}}_{ij},\bar{\mathbf{D}}_{ijk},\mathbf{h}_{ij}}\left[\left|\mathbf{h}_{ik}^{H}\mathbf{w}_{ij}\right|^2|_{r_{0k},r_{ik}}\right]\overset{a.r.}{\sim}\frac{\mathrm{E}_{\mathbf{t}_{ik},\mathbf{t}_{Nij},\bar{\mathbf{\Lambda}}_{ijk}}\left[\sum_{l=1}^{M}\frac{M^{-\alpha}|t_{ikl}|^2|t_{Nijl}|^2}{(\bar{\lambda}_{ijkl}-z)^2}\right]}{\left(M^{-\frac{\alpha}{2}}+r_{ik}^{-\alpha}\bar{m}_{ijk}(z)\right)^2\mathrm{E}_{\mathbf{t}_{Dij},\bar{\mathbf{\Lambda}}_{ij}}\left[\sum_{l=1}^{M}\frac{|t_{Dijl}|^2}{(\bar{\lambda}_{ijl}-z)^2}\right]}, \tag{A.35}$$

where $z=-\frac{M^{\frac{\alpha}{2}-1}\sigma_n^2u_i}{P_t}$. Note that $|t_{ikl}|^2$, $|t_{Nijl}|^2$, $(\bar{\lambda}_{ijkl}-z)^{-2}$ are independent to each other with $\mathrm{E}\left[|t_{ikl}|^2\right]=\mathrm{E}\left[|t_{Nijl}|^2\right]=1$. Moreover, $|t_{Dijl}|^2$ and $(\bar{\lambda}_{ijl}-z)^{-2}$ are independent to each other with $\mathrm{E}\left[|t_{Dijl}|^2\right]=1$. Therefore, (A.35) can be written as

$$\mathrm{E}_{\bar{\mathbf{H}}_{ij},\bar{\mathbf{D}}_{ijk},\mathbf{h}_{ij}}\left[\left|\mathbf{h}_{ik}^{H}\mathbf{w}_{ij}\right|^2|_{r_{0k},r_{ik}}\right]\overset{a.r.}{\sim}\frac{\mathrm{E}_{\bar{\mathbf{\Lambda}}_{ijk}}\left[M^{-\alpha}\sum_{l=1}^{M}\frac{1}{(\bar{\lambda}_{ijkl}-z)^2}\right]}{\left(M^{-\frac{\alpha}{2}}+r_{ik}^{-\alpha}\bar{m}_{ijk}(z)\right)^2\mathrm{E}_{\bar{\mathbf{\Lambda}}_{ij}}\left[\sum_{l=1}^{M}\frac{1}{(\bar{\lambda}_{ijl}-z)^2}\right]}. \tag{A.36}$$

Since $\frac{1}{M}\bar{\mathbf{H}}_{ij}M^{\frac{\alpha}{2}}\bar{\mathbf{D}}_{ij}\bar{\mathbf{H}}_{ij}^H = \frac{1}{M}\bar{\mathbf{H}}_{ijk}M^{\frac{\alpha}{2}}\bar{\mathbf{D}}_{ijk}\bar{\mathbf{H}}_{ijk}^H + M^{\frac{\alpha}{2}-1}r_{ik}^{-\alpha}\mathbf{h}_{ik}\mathbf{h}_{ik}^H$ where $\left(M^{\frac{\alpha}{2}-1}r_{ik}^{-\alpha}\mathbf{h}_{ik}\mathbf{h}_{ik}^H\right)$ is a rank-1 matrix with $\mathbf{h}_{ik}\in\mathbb{C}^M$, $\frac{1}{M}\bar{\mathbf{H}}_{ij}M^{\frac{\alpha}{2}}\bar{\mathbf{D}}_{ij}\bar{\mathbf{H}}_{ij}^H$ is the rank-1 perturbation of $\frac{1}{M}\bar{\mathbf{H}}_{ijk}M^{\frac{\alpha}{2}}\bar{\mathbf{D}}_{ijk}\bar{\mathbf{H}}_{ijk}^H$. Therefore, according to Lemma 2.3,

$$\lim_{M\to\infty}\operatorname{tr}\left(\left(\frac{1}{M}\bar{\mathbf{H}}_{ij}M^{\frac{\alpha}{2}}\bar{\mathbf{D}}_{ij}\bar{\mathbf{H}}_{ij}^H - z\mathbf{I}_M\right)^{-1}\right) = \lim_{M\to\infty}\operatorname{tr}\left(\left(\frac{1}{M}\bar{\mathbf{H}}_{ijk}M^{\frac{\alpha}{2}}\bar{\mathbf{D}}_{ijk}\bar{\mathbf{H}}_{ij}^H - z\mathbf{I}_M\right)^{-1}\right). \tag{A.37}$$

Since $\bar{\lambda}_{ijl}$ and $\bar{\lambda}_{ijkl}$ are the eigenvalues of $\frac{1}{M}\bar{\mathbf{H}}_{ij}M^{\frac{\alpha}{2}}\bar{\mathbf{D}}_{ij}\bar{\mathbf{H}}_{ij}^H$ and $\frac{1}{M}\bar{\mathbf{H}}_{ijk}M^{\frac{\alpha}{2}}\bar{\mathbf{D}}_{ijk}\bar{\mathbf{H}}_{ijk}^H$ respectively, (A.37) can be written as

$$\lim_{M\to\infty}\sum_{l=1}^{M}\left(\bar{\lambda}_{ijl}-z\right)^{-1} = \lim_{M\to\infty}\sum_{l=1}^{M}\left(\bar{\lambda}_{ijkl}-z\right)^{-1}. \tag{A.38}$$

Derivating (A.38) w.r.t z, we obtain

$$\lim_{M\to\infty}\sum_{l=1}^{M}\left(\bar{\lambda}_{ijl}-z\right)^{-2} = \lim_{M\to\infty}\sum_{l=1}^{M}\left(\bar{\lambda}_{ijkl}-z\right)^{-2}. \tag{A.39}$$

Using (A.39), (A.36) can be expressed as

$$\mathrm{E}_{\bar{\mathbf{H}}_{ij},\bar{\mathbf{D}}_{ijk},\mathbf{h}_{ij}}\left[\left|\mathbf{h}_{ik}^H\mathbf{w}_{ij}\right|^2|_{r_{0k},r_{ik}}\right] \overset{a.r.}{\sim} \frac{1}{\left(1+M^{\frac{\alpha}{2}}r_{ik}^{-\alpha}\bar{m}_{ijk}(z)\right)^2}. \tag{A.40}$$

This completes the proof.

A.4 Proof of Theorem 5.4

The mean inter-cell interference power conditioned on r_{0k} can be written as

$$\mathrm{E}_{\tilde{\mathbf{H}}_{ij},\tilde{\mathbf{D}}_{ij},\mathbf{h}_{ij}}\left[\sum_{u=1}^{u_{\max}}\sum_{i\in\Phi_u\setminus\{0\}}\frac{P_t r_{ik}^{-\alpha}}{u}\sum_{j=1}^{u}\left|\mathbf{h}_{ik}^H\mathbf{w}_{ij}\right|^2|_{r_{0k}}\right]$$
$$=\sum_{u=1}^{u_{\max}}\mathrm{E}_{r_{ik}}\left[\sum_{i\in\Phi_u\setminus\{0\}}\frac{P_t r_{ik}^{-\alpha}}{u}\sum_{j=1}^{u}\mathrm{E}_{\tilde{\mathbf{H}}_{ij},\tilde{\mathbf{D}}_{ijk},\mathbf{h}_{ij}}\left[\left|\mathbf{h}_{ik}^H\mathbf{w}_{ij}\right|^2|_{r_{ik},r_{0k}}\right]\right]. \tag{A.41}$$

$\mathrm{E}_{\tilde{\mathbf{H}}_{ij},\tilde{\mathbf{D}}_{ijk},\mathbf{h}_{ij}}\left[\left|\mathbf{h}_{ik}^H\mathbf{w}_{ij}\right|^2|_{r_{ik},r_{0k}}\right]=\mathrm{E}_{\tilde{\mathbf{H}}_{ij'},\tilde{\mathbf{D}}_{ij'k},\mathbf{h}_{ij'}}\left[\left|\mathbf{h}_{ik}^H\mathbf{w}_{ij'}\right|^2|_{r_{ik},r_{0k}}\right]\ \forall i,\ \forall j\neq j'$, and hence (A.41) can be written using Theorem 5.3 as

$$\mathrm{E}_{\tilde{\mathbf{H}}_{ij},\tilde{\mathbf{D}}_{ij},\mathbf{h}_{ij}}\left[\sum_{u=1}^{u_{\max}}\sum_{i\in\Phi_u\setminus\{0\}}\frac{P_t r_{ik}^{-\alpha}}{u}\sum_{j=1}^{u}\left|\mathbf{h}_{ik}^H\mathbf{w}_{ij}\right|^2|_{r_{0k}}\right]\overset{a.r.}{\sim}\sum_{u=1}^{u_{\max}}\mathrm{E}_{r_{ik}}\left[\sum_{i\in\Phi_u\setminus\{0\}}\frac{P_t r_{ik}^{-\alpha}}{\left(1+M^{\frac{\alpha}{2}}r_{ik}^{-\alpha}\bar{m}_{ijk}(z)\right)^2}\right]. \tag{A.42}$$

By using the Campbell's theorem, i.e. Theorem 2.1, for the PPP Φ_u, we can write

$$\mathrm{E}_{r_{ik}}\left[\sum_{i\in\Phi_u\setminus\{0\}}\frac{P_t r_{ik}^{-\alpha}}{\left(1+M^{\frac{\alpha}{2}}r_{ik}^{-\alpha}\bar{m}_{ijk}(z)\right)^2}\right]=2\pi\lambda_b p_N(u)\int_{r_{0k}}^{\infty}\frac{P_t r_{ik}^{1-\alpha}}{\left(1+M^{\frac{\alpha}{2}}r_{ik}^{-\alpha}\bar{m}_{ijk}(z)\right)^2}dr_{ik}. \tag{A.43}$$

Moreover letting $\tau=M^{\frac{\alpha}{2}}r_{ik}^{-\alpha}$, (A.43) can be written as

$$\mathrm{E}_{r_{ik}}\left[\sum_{i\in\Phi_u\setminus\{0\}}\frac{P_t r_{ik}^{-\alpha}}{\left(1+M^{\frac{\alpha}{2}}r_{ik}^{-\alpha}\bar{m}_{ijk}(z)\right)^2}\right]=2\pi\lambda_b p_N(u)\int_{M^{\frac{\alpha}{2}}r_{0k}^{-\alpha}}^{0}\frac{P_t(\tau^{-\frac{1}{\alpha}}M^{\frac{1}{2}})^{(1-\alpha)}\frac{-1}{\alpha}\tau^{-\frac{1}{\alpha}-1}M^{\frac{1}{2}}}{\left(1+\tau\bar{m}_{ijk}(z)\right)^2}d\tau$$
$$=-\frac{2\pi\lambda_b p_N(u)P_t M^{1-\frac{\alpha}{2}}}{\alpha}\int_{M^{\frac{\alpha}{2}}r_{0k}^{-\alpha}}^{0}\frac{\tau^{-\frac{2}{\alpha}}}{\left(1+\tau\bar{m}_{ijk}(z)\right)^2}d\tau$$
$$=f_1(u)-f_2(u,r_{0k}), \tag{A.44}$$

with $f_1(u)$ and $f_2(u,r_{0k})$ as in Theorem 5.4. Using (A.44), (A.42) can be written as,

$$\mathrm{E}_{\tilde{\mathbf{H}}_{ij},\tilde{\mathbf{D}}_{ij},\mathbf{h}_{ij}}\left[\sum_{u=1}^{u_{\max}}\sum_{i\in\Phi_u\setminus\{0\}}\frac{P_t r_{ik}^{-\alpha}}{u}\sum_{j=1}^{u}\left|\mathbf{h}_{ik}^H\mathbf{w}_{ij}\right|^2|_{r_{0k}}\right]\overset{a.r.}{\sim}\sum_{u=1}^{u_{\max}}\left(f_1(u)-f_2(u,r_{0k})\right). \tag{A.45}$$

and the proof is complete.

Bibliography

[1] M. Haenggi and R. K. Ganti, *Interference in large wireless networks*. Now Publishers Inc, 2009.

[2] S. Fletcher, "Green radio–sustainable wireless networks," *Mobile VCE Core*, vol. 5, 2009.

[3] L. Suarez, L. Nuaymi, and J.-M. Bonnin, "An overview and classification of research approaches in green wireless networks," *EURASIP journal on wireless communications and networking*, no. 1, pp. 1–18, 2012.

[4] T. S. Rappaport *et al.*, *Wireless communications: principles and practice*. Prentice Hall PTR New Jersey, 1996, vol. 2.

[5] J. G. Andrews, F. Baccelli, and R. K. Ganti, "A tractable approach to coverage and rate in cellular networks," *IEEE Transactions on Communications*, vol. 59, no. 11, pp. 3122–3134, 2011.

[6] G. Auer, V. Giannini, C. Desset, I. Godor, P. Skillermark, M. Olsson, M. Imran, D. Sabella, M. Gonzalez, O. Blume, and A. Fehske, "How much Energy is Needed to Run a Wireless Network?" *IEEE Transactions on Wireless Communications*, vol. 18, no. 5, pp. 40–49, October 2011.

[7] E. Björnson, E. Jorswieck *et al.*, "Optimal resource allocation in coordinated multi-cell systems," *Foundations and Trends® in Communications and Information Theory*, vol. 9, no. 2–3, pp. 113–381, 2013.

[8] Z. Hasan, H. Boostanimehr, and V. K. Bhargava, "Green cellular networks: A survey, some research issues and challenges," *IEEE Communications surveys & tutorials*, vol. 13, no. 4, pp. 524–540, 2011.

[9] M. Imran and E. Katranaras, "Energy efficiency analysis of the reference systems, areas of improvements and target breakdown. ICT-EARTH Project, Deliverable D2. 3, EC-IST Office, Brussels, Belgium (January 2011)."

[10] G. Y. Li, Z. Xu, C. Xiong, C. Yang, S. Zhang, Y. Chen, and S. Xu, "Energy-efficient wireless communications: tutorial, survey, and open issues," *IEEE Wireless Communications*, vol. 18, no. 6, pp. 28–35, 2011.

[11] L. M. Correia, D. Zeller, O. Blume, D. Ferling, Y. Jading, I. Gódor, G. Auer, and L. Van Der Perre, "Challenges and enabling technologies for energy aware mobile radio networks," *IEEE Communications Magazine*, vol. 48, no. 11, pp. 66–72, 2010.

[12] C. Li, J. Zhang, and K. Letaief, "Throughput and Energy Efficiency Analysis of Small Cell Networks with Multi-Antenna Base Stations," *IEEE Transactions on Wireless Communications*, vol. 13, no. 5, pp. 2505–2517, May 2014.

[13] E. Bjornson, L. Sanguinetti, and M. Kountouris, "Energy-efficient future wireless networks: A marriage between massive MIMO and small cells," in *IEEE 16th International Workshop on Signal Processing Advances in Wireless Communications (SPAWC)*, 2015, pp. 211–215.

[14] J.-M. Kelif, M. Coupechoux, and P. Godlewski, "A Fluid Model for Performance Analysis in Cellular Networks," *EURASIP Journal on Wireless Comm. and Networking*, no. 435189, pp. 1–11, August 2010.

[15] I. R. M. Association *et al.*, "Green Technologies: Concepts, Methodologies, Tools and Applications," *IGI Global*, 2011.

[16] G. Auer, O. Blume, V. Giannini, I. Godor, M. Imran, Y. Jading, E. Katranaras, M. Olsson, D. Sabella, P. Skillermark *et al.*, "D2. 3: Energy efficiency analysis of the reference systems, areas of improvements and target breakdown," *EARTH*, 2010.

[17] O. Blume *et al.*, "Most Promising Tracks of Green Network Technologies," INFSO-ICT-247733 EARTH, Tech. Rep., Dec. 2011.

[18] E. Belmega, S. Lasaulce, and M. Debbah, "A Survey on Energy-Efficient Communications," in *IEEE 21st International Symposium on Personal, Indoor and Mobile Radio Communications (PIMRC)*, September 2010, pp. 289–294.

[19] J. M. Gorce, D. Tsilimantos, P. Ferrand, and V. H. Poor, "Energy-Capacity Trade-off Bounds in a Downlink Typical Cell," in *IEEE 25th International Symposium on Personal Indoor and Mobile Radio Communications (PIMRC)*, September 2014, pp. 1–6.

[20] I. Humar, X. Ge, L. Xiang, M. Jo, M. Chen, and J. Zhang, "Rethinking Energy Efficiency Models of Cellular Networks with Embodied Energy," *IEEE Network*, vol. 25, no. 2, pp. 40–49, March 2011.

[21] J. Xu, L. Qui, and C. Yu, "Improving Network Energy Efficiency through Cooperative Idling in the Multi-Cell Systems," *EURASIP Journal on Wireless Comm. and Networking*, no. 165, pp. 1–18, November 2011.

[22] X. Weng, D. Cao, and Z. Niu, "Energy-Efficient Cellular Network Planning under Insufficient Cell Zooming," in *IEEE 73rd Conference on Vehicular Technology*, May 2011, pp. 1–5.

[23] M. Maaz, J. Lorandel, P. Mary, J.-C. Prévotet, and M. Hélard, "Energy efficiency analysis of hybrid-ARQ relay-assisted schemes in LTE-based systems," *EURASIP Journal on Wireless Communications and Networking*, no. 1, pp. 1–13, 2016.

[24] M. Imran, J. Alonso-Rubio, G. Auer, M. Boldi, M. Braglia, P. Fazekas, D. Ferling, A. Fehske, P. Frenger, R. Gupta *et al.*, "Most suitable efficiency metrics and utility functions," *EARTH Project Report*, pp. 1–89, 2011.

[25] C. Sun and C. Yang, "Energy efficiency analysis of one-way and two-way relay systems," *EURASIP Journal on Wireless Communications and Networking*, no. 1, pp. 1–18, 2012.

[26] V. G. Auer and O. Blume, "Energy efficiency analysis of the reference systems, areas of improvements and target breakdown (earth)," 2012.

[27] C. Desset, B. Debaillie, V. Giannini, A. Fehske, G. Auer, H. Holtkamp, W. Wajda, D. Sabella, F. Richter, M. J. Gonzalez *et al.*, "Flexible power modeling of LTE base stations," in *IEEE Wireless Communications and Networking Conference (WCNC)*, 2012, pp. 2858–2862.

[28] H. Q. Ngo, E. G. Larsson, and T. L. Marzetta, "Energy and spectral efficiency of very large multiuser MIMO systems," *IEEE Transactions on Communications*, vol. 61, no. 4, pp. 1436–1449, 2013.

[29] C. Li, J. Zhang, and K. Letaief, "Performance analysis of SDMA in multicell wireless networks," in *IEEE Global Communications Conference (GLOBECOM)*, 2013, pp. 3867–3872.

[30] A. K. Gupta, H. S. Dhillon, S. Vishwanath, and J. G. Andrews, "Downlink coverage probability in MIMO HetNets with flexible cell selection," in *IEEE Global Communications Conference (GLOBECOM)*, 2014, pp. 1534–1539.

[31] H. S. Dhillon, M. Kountouris, and J. G. Andrews, "Downlink MIMO HetNets: Modeling, ordering results and performance analysis," *IEEE Transactions on Wireless Communications*, vol. 12, no. 10, pp. 5208–5222, 2013.

[32] P. Cheng, M. Tao, and W. Zhang, "A new SLNR-based linear precoding for downlink multi-user multi-stream MIMO systems," *IEEE Communications Letters*, vol. 14, no. 11, pp. 1008–1010, 2010.

[33] M. Sadek, A. Tarighat, and A. H. Sayed, "A leakage-based precoding scheme for downlink multi-user MIMO channels," *IEEE Transactions on Wireless Communications*, vol. 6, no. 5, pp. 1711–1721, 2007.

[34] P. Patcharamaneepakorn, S. Armour, and A. Doufexi, "On the Equivalence Between SLNR and MMSE Precoding Schemes with Single-Antenna Receivers," *IEEE Communications Letters*, vol. 16, no. 7, pp. 1034–1037, July 2012.

[35] A. Tarighat, M. Sadek, and A. H. Sayed, "A multi user beamforming scheme for downlink MIMO channels based on maximizing signal-to-leakage ratios," in *IEEE International Conference on Acoustics, Speech, and Signal Processing (ICASSP'05)*, vol. 3, 2005.

[36] E. Bjornson, L. Sanguinetti, and M. Kountouris, "Designing wireless broadband access for energy efficiency: Are small cells the only answer?" in *IEEE International Conference on Communication Workshop (ICCW)*, 2015, pp. 136–141.

[37] Z. Ruifeng, J.-M. Gorce, and K. Jaffres-Runser, "Low Bound of Energy-Latency Trade-Off of Opportunistic Routing in Multi-Hop Networks," in *IEEE International Conference on Communications*, June 2009, pp. 1–6.

[38] M. Haenggi, *Stochastic geometry for wireless networks*. Cambridge University Press, 2012.

[39] T. D. Novlan, R. K. Ganti, J. G. Andrews, and A. Ghosh, "A new model for coverage with fractional frequency reuse in OFDMA cellular networks," in *IEEE Global Telecommunications Conference (GLOBECOM 2011)*, 2011, pp. 1–5.

[40] J. G. Andrews, F. Baccelli, and R. K. Ganti, "A new tractable model for cellular coverage," in *48th Annual Conference on Communication, Control, and Computing (Allerton)*, 2010, pp. 1204–1211.

[41] R. K. Ganti, F. Baccelli, and J. G. Andrews, "A new way of computing rate in cellular networks," in *IEEE International Conference on Communications (ICC)*, 2011, pp. 1–5.

[42] X. Zhang and M. Haenggi, "A stochastic geometry analysis of inter-cell interference coordination and intra-cell diversity," *IEEE Transactions on Wireless Communications*, vol. 13, no. 12, pp. 6655–6669, 2014.

[43] R. Couillet and M. Debbah, *Random matrix methods for wireless communications*. Cambridge University Press, 2011.

[44] V. A. Marčenko and L. A. Pastur, "Distribution of eigenvalues for some sets of random matrices," *Mathematics of the USSR-Sbornik*, vol. 1, no. 4, p. 457, 1967.

[45] S. Govindasamy, D. W. Bliss, and D. H. Staelin, "Spectral Efficiency in Single-Hop Ad-Hoc Wireless Networks with Interference Using Adaptive Antenna Arrays," *IEEE Journal on Selected Areas in Communications*, vol. 25, no. 7, pp. 1358–1369, September 2007.

[46] D. N. C. Tse and S. V. Hanly, "Linear multiuser receivers: effective interference, effective bandwidth and user capacity," *IEEE Transactions on Information Theory*, vol. 45, no. 2, pp. 641–657, Mar 1999.

[47] J. W. Silverstein, "Strong convergence of the empirical distribution of eigenvalues of large dimensional random matrices," *Journal of Multivariate Analysis*, vol. 55, no. 2, pp. 331–339, 1995.

[48] P. Li, D. Paul, R. Narasimhan, and J. Cioffi, "On the distribution of SINR for the MMSE MIMO receiver and performance analysis," *IEEE Transactions on Information Theory*, vol. 52, no. 1, pp. 271–286, 2006.

[49] J. W. Silverstein and Z. Bai, "On the empirical distribution of eigenvalues of a class of large dimensional random matrices," *Journal of Multivariate analysis*, vol. 54, no. 2, pp. 175–192, 1995.

[50] Z.-D. Bai and J. W. Silverstein, "No eigenvalues outside the support of the limiting spectral distribution of large-dimensional sample covariance matrices," *Annals of probability*, pp. 316–345, 1998.

[51] A. Müller, "Random matrix analysis of future multi cell mu-mimo networks," Ph.D. dissertation, Supélec, 2014.

[52] R. Couillet, M. Debbah, and J. W. Silverstein, "A Deterministic Equivalent for the Analysis of Correlated MIMO Multiple Access Channels," *IEEE Transactions on Information Theory*, vol. 57, no. 6, pp. 3493–3514, June 2011.

[53] S. Aleksic, M. Deruyck, W. Vereecken, W. Joseph, M. Pickavet, and L. Martens, "Energy efficiency of femtocell deployment in combined wireless/optical access networks," *Computer Networks*, vol. 57, no. 5, pp. 1217–1233, 2013.

[54] A. Fehske, G. Fettweis, J. Malmodin, and G. Biczok, "The global footprint of mobile communications: The ecological and economic perspective," *IEEE Communications Magazine*, vol. 49, no. 8, pp. 55–62, 2011.

[55] D. Zeller, M. Olsson, O. Blume, A. Fehske, D. Ferling, W. Tomaselli, and I. Gódor, "Sustainable wireless broadband access to the future Internet-The EARTH project," in *The Future Internet Assembly*. Springer, 2013, pp. 249–271.

[56] A. P. Bianzino, C. Chaudet, D. Rossi, and J.-L. Rougier, "A survey of green networking research," *IEEE Communications Surveys & Tutorials*, vol. 14, no. 1, pp. 3–20, 2012.

[57] P. M. Cox, R. A. Betts, C. D. Jones, S. A. Spall, and I. J. Totterdell, "Acceleration of global warming due to carbon-cycle feedbacks in a coupled climate model," *Nature*, vol. 408, no. 6809, pp. 184–187, 2000.

[58] C. E. Shannon, "A mathematical theory of communication," *ACM SIGMOBILE Mobile Computing and Communications Review*, vol. 5, no. 1, pp. 3–55, 2001.

[59] D. Tse and P. Viswanath, *Fundamentals of Wireless Communication*. Cambridge University Press, 2005.

[60] E. Telatar, "Capacity of Multi-antenna Gaussian Channels," *European transactions on telecommunications*, vol. 10, no. 6, pp. 585–595, 1999.

[61] D. N. C. Tse and S. V. Hanly, "Multiaccess fading channels. I. Polymatroid structure, optimal resource allocation and throughput capacities," *IEEE Transactions on Information Theory*, vol. 44, no. 7, pp. 2796–2815, 1998.

[62] W. Yu, W. Rhee, S. Boyd, and J. M. Cioffi, "Iterative water-filling for Gaussian vector multiple-access channels," *IEEE Transactions on Information Theory*, vol. 50, no. 1, pp. 145–152, 2004.

[63] L. Li and A. J. Goldsmith, "Capacity and optimal resource allocation for fading broadcast channels. I. Ergodic capacity," *IEEE Transactions on Information Theory*, vol. 47, no. 3, pp. 1083–1102, 2001.

[64] W. Yu and J. M. Cioffi, "Trellis precoding for the broadcast channel," in *IEEE Global Telecommunications Conference (GLOBECOM)*, vol. 2, 2001, pp. 1344–1348.

[65] S. Vishwanath, N. Jindal, and A. Goldsmith, "Duality, achievable rates, and sum-rate capacity of Gaussian MIMO broadcast channels," *IEEE Transactions on Information Theory*, vol. 49, no. 10, pp. 2658–2668, 2003.

[66] P. Viswanath and D. N. C. Tse, "Sum capacity of the vector Gaussian broadcast channel and uplink-downlink duality," *IEEE Transactions on Information Theory*, vol. 49, no. 8, pp. 1912–1921, 2003.

[67] H. Weingarten, Y. Steinberg, and S. Shamai, "The capacity region of the Gaussian multiple-input multiple-output broadcast channel," *IEEE transactions on information theory*, vol. 52, no. 9, pp. 3936–3964, 2006.

[68] W. Yu, "Uplink-downlink duality via minimax duality," *IEEE Transactions on Information Theory*, vol. 52, no. 2, pp. 361–374, 2006.

[69] K. S. Gilhousen, I. M. Jacobs, R. Padovani, A. J. Viterbi, L. A. Weaver, and C. E. Wheatley, "On the capacity of a cellular CDMA system," *IEEE transactions on vehicular technology*, vol. 40, no. 2, pp. 303–312, 1991.

[70] H. Hamdoun, P. Loskot, T. O'Farrell, and J. He, "Survey and applications of standardized energy metrics to mobile networks," *Annals of telecommunications-annales des télécommunications*, vol. 67, no. 3-4, pp. 113–123, 2012.

[71] T. Chen, H. Kim, and Y. Yang, "Energy efficiency metrics for green wireless communications," in *IEEE International Conference on Wireless Communications and Signal Processing (WCSP)*, 2010, pp. 1–6.

[72] T. Jiang and Y. Wu, "An overview: peak-to-average power ratio reduction techniques for OFDM signals," *IEEE Transactions on broadcasting*, vol. 54, no. 2, p. 257, 2008.

[73] D. T. A. . ECR Initiative, "Network and telecom equipment-energy and performance assessment test procedures and measurement methodology," Deutsche Telekom, Tech. Rep., 2010.

[74] G. Auer, V. Giannini, M. Olsson, M. J. Gonzalez, and C. Desset, "Framework for Energy Efficiency Analysis of Wireless Networks," in *2nd International Conference on Wireless VITAE*, February 2011, pp. 1–5.

[75] S. Verdú and S. Shamai, "Spectral efficiency of CDMA with random spreading," *IEEE Transactions on Information theory*, vol. 45, no. 2, pp. 622–640, 1999.

[76] S. Sandhu and O. Oyman, "Non-ergodic power-bandwidth tradeoff in linear multi-hop networks," in *IEEE International Symposium on Information Theory*, 2006, pp. 1514–1518.

[77] O. Oyman and S. Sandhu, "A Shannon-theoretic perspective on fading multihop networks," in *IEEE 40th Annual Conference on Information Sciences and Systems*, 2006, pp. 525–530.

[78] Y. Yao, X. Cai, and G. B. Giannakis, "On energy efficiency and optimum resource allocation of relay transmissions in the low-power regime," *IEEE Transactions on Wireless Communications*, vol. 4, no. 6, pp. 2917–2927, 2005.

[79] Y. Chen, S. Zhang, and S. Xu, "Characterizing energy efficiency and deployment efficiency relations for green architecture design," in *IEEE International Conference on Communications Workshops*, 2010, pp. 1–5.

[80] V. Rodoplu and T. H. Meng, "Bits-per-joule capacity of energy-limited wireless ad hoc networks," in *IEEE Global Telecommunications Conference (GLOBECOM)*, vol. 1, 2002, pp. 16–20.

[81] T. H. Meng and V. Rodoplu, "Growth of wireless ad hoc networks," in *IEEE Global Telecommunications Conference (GLOBECOM)*, vol. 5, 2003, pp. 2819–2823.

[82] V. Rodoplu and T. H. Meng, "Bits-per-joule capacity of energy-limited wireless networks," *IEEE Transactions on Wireless Communications*, vol. 6, no. 3, pp. 857–865, 2007.

[83] A. J. Fehske, P. Marsch, and G. P. Fettweis, "Bit per joule efficiency of cooperating base stations in cellular networks," in *IEEE Globecom Workshops*, 2010, pp. 1406–1411.

[84] H. Kwon and T. Birdsall, "Channel capacity in bits per joule," *IEEE Journal of Oceanic Engineering*, vol. 11, no. 1, pp. 97–99, 1986.

[85] C. Li, J. Zhang, and K. Letaief, "Throughput and energy efficiency analysis of small cell networks with multi-antenna base stations," *IEEE Transactions on Wireless Communications*, vol. 13, no. 5, pp. 2505–2517, 2014.

[86] C. Li, J. Zhang, and K. B. Letaief, "Energy efficiency analysis of small cell networks," in *IEEE International Conference on Communications (ICC)*, 2013, pp. 4404–4408.

[87] C. Han, T. Harrold, S. Armour, I. Krikidis, S. Videv, P. M. Grant, H. Haas, J. S. Thompson, I. Ku, C. X. Wang, T. A. Le, M. R. Nakhai, J. Zhang, and L. Hanzo, "Green radio: radio techniques to enable energy-efficient wireless networks," *IEEE Communications Magazine*, vol. 49, no. 6, pp. 46–54, June 2011.

[88] K. A. Anang, P. B. Rapajic, R. Wu, L. Bello, T. I. Eneh *et al.*, "Cellular system information capacity change at higher frequencies due to propagation loss and system parameters," *Progress In Electromagnetics Research B*, vol. 44, pp. 191–221, 2012.

[89] E. Pollakis, R. L. Cavalcante, and S. Stańczak, "Base station selection for energy efficient network operation with the majorization-minimization algorithm," in *IEEE 13th International Workshop on Signal Processing Advances in Wireless Communications (SPAWC)*, 2012, pp. 219–223.

[90] J. Gong, J. S. Thompson, S. Zhou, and Z. Niu, "Base station sleeping and resource allocation in renewable energy powered cellular networks," *IEEE Transactions on Communications*, vol. 62, no. 11, pp. 3801–3813, 2014.

[91] W. C. Lee, "Spectrum efficiency in cellular [radio]," *IEEE Transactions on Vehicular Technology*, vol. 38, no. 2, pp. 69–75, 1989.

[92] A. Guo and M. Haenggi, "Asymptotic deployment gain: A new approach to characterize coverage probability," in *IEEE International Conference on Communications (ICC)*, 2014, pp. 2093–2098.

[93] F. Aurenhammer, "Voronoi diagrams-a survey of a fundamental geometric data structure," *ACM Computing Surveys (CSUR)*, vol. 23, no. 3, pp. 345–405, 1991.

[94] S. Cui, A. J. Goldsmith, and A. Bahai, "Energy-constrained modulation optimization," *IEEE transactions on wireless communications*, vol. 4, no. 5, pp. 2349–2360, 2005.

[95] G. Miao, N. Himayat, Y. G. Li, and A. Swami, "Cross-layer optimization for energy-efficient wireless communications: a survey," *Wireless Communications and Mobile Computing*, vol. 9, no. 4, pp. 529–542, 2009.

[96] H. ElSawy, E. Hossain, and M. Haenggi, "Stochastic geometry for modeling, analysis, and design of multi-tier and cognitive cellular wireless networks: A survey," *IEEE Communications Surveys & Tutorials*, vol. 15, no. 3, pp. 996–1019, 2013.

[97] H. Inaltekin, M. Chiang, H. V. Poor, and S. B. Wicker, "On unbounded path-loss models: effects of singularity on wireless network performance," *IEEE Journal on Selected Areas in Communications*, vol. 27, no. 7, pp. 1078–1092, September 2009.

[98] M. Costa, "Writing on dirty paper (corresp.)," *IEEE transactions on information theory*, vol. 29, no. 3, pp. 439–441, 1983.

[99] E. Björnson, M. Bengtsson, and B. Ottersten, "Optimal multiuser transmit beamforming: A difficult problem with a simple solution structure," *IEEE Signal Processing Magazine*, vol. 31, no. 4, pp. 142–148, 2014.

[100] T. K. Lo, "Maximum ratio transmission," in *IEEE International Conference on Communications (ICC'99)*, vol. 2, 1999, pp. 1310–1314.

[101] E. Bjornson, R. Zakhour, D. Gesbert, and B. Ottersten, "Cooperative multicell precoding: Rate region characterization and distributed strategies with instantaneous and statistical CSI," *IEEE Transactions on Signal Processing*, vol. 58, no. 8, pp. 4298–4310, 2010.

[102] G. Ginis and J. M. Cioffi, "A multi-user precoding scheme achieving crosstalk cancellation with application to DSL systems," in *Thirty-Fourth Asilomar Conference on Signals, Systems and Computers*, vol. 2, 2000, pp. 1627–1631.

[103] C. Guthy, W. Utschick, and G. Dietl, "Low-complexity linear zero-forcing for the MIMO broadcast channel," *IEEE Journal of Selected Topics in Signal Processing*, vol. 3, no. 6, pp. 1106–1117, 2009.

[104] B. O. Lee, H. W. Je, I. Sohn, O.-S. Shin, and K. B. Lee, "Interference-aware decentralized precoding for multicell MIMO TDD systems," in *IEEE Global Telecommunications Conference*, 2008, pp. 1–5.

[105] R. Stridh, M. Bengtsson, and B. Ottersten, "System evaluation of optimal downlink beamforming with congestion control in wireless communication," *IEEE Transactions on Wireless Communications*, vol. 5, no. 4, pp. 743–751, 2006.

[106] K. Vandermot, Y. Rolain, G. Vandersteen, R. Pintelon, F. Ferranti, and T. Dhaene, "A power-scalable linearized model for RF power amplifiers starting from S-parameter measurements," in *IEEE MTT-S International Microwave Symposium (IMS)*, 2009, pp. 745–748.

[107] M. Youssef, F. Monteiro, A. Dandache, and C. Diou, "An effective and scalable multiuser architecture for the base station receiver," in *2nd International Conference on Signal Processing and Communication Systems (ICSPCS)*, 2008, pp. 1–5.

[108] F. H. Raab, P. Asbeck, S. Cripps, P. B. Kenington, Z. B. Popovic, N. Pothecary, J. F. Sevic, and N. O. Sokal, "Power amplifiers and transmitters for RF and microwave," *IEEE transactions on Microwave Theory and Techniques*, vol. 50, no. 3, pp. 814–826, 2002.

[109] K.-J. Cho, J.-H. Kim, and S. P. Stapleton, "A highly efficient Doherty feedforward linear power amplifier for W-CDMA base-station applications," *IEEE Transactions on Microwave Theory and Techniques*, vol. 53, no. 1, pp. 292–300, 2005.

[110] C. Han, T. Harrold, S. Armour, I. Krikidis, S. Videv, P. M. Grant, H. Haas, J. S. Thompson, I. Ku, C.-X. Wang *et al.*, "Green radio: radio techniques to enable energy-efficient wireless networks," *IEEE communications magazine*, vol. 49, no. 6, pp. 46–54, 2011.

[111] H. Claussen, L. T. Ho, and F. Pivit, "Effects of joint macrocell and residential picocell deployment on the network energy efficiency," in *IEEE 19th International Symposium on Personal, Indoor and Mobile Radio Communications*, 2008, pp. 1–6.

[112] O. Blume, H. Eckhardt, S. Klein, E. Kuehn, and W. M. Wajda, "Energy savings in mobile networks based on adaptation to traffic statistics," *Bell Labs Technical Journal*, vol. 15, no. 2, pp. 77–94, 2010.

[113] Y. Chen, S. Zhang, S. Xu, and G. Y. Li, "Fundamental trade-offs on green wireless networks," *IEEE Communications Magazine*, vol. 49, no. 6, pp. 30–37, 2011.

[114] S. Cui, A. J. Goldsmith, and A. Bahai, "Energy-efficiency of MIMO and cooperative MIMO techniques in sensor networks," *IEEE Journal on selected areas in communications*, vol. 22, no. 6, pp. 1089–1098, 2004.

[115] W. Liu, X. Li, and M. Chen, "Energy efficiency of MIMO transmissions in wireless sensor networks with diversity and multiplexing gains," in *IEEE International Conference on Acoustics, Speech, and Signal Processing (ICASSP)*, 2005, pp. 897–900.

[116] X. Li, M. Chen, and W. Liu, "Application of STBC-encoded cooperative transmissions in wireless sensor networks," *IEEE signal processing letters*, vol. 12, no. 2, pp. 134–137, 2005.

[117] B. Bougard, G. Lenoir, A. Dejonghe, L. Van der Perre, F. Catthoor, and W. Dehaene, "Smart-mimo: Energy-aware adaptive mimo-ofdm radio link control for wireless local area networks," in *IEEE Workshop on Signal Processing Systems Design and Implementation*, 2006, pp. 399–404.

[118] A. M. Alam, P. Mary, J.-Y. Baudais, and X. Lagrange, "Energy Efficiency-Area Spectral Efficiency Tradeoff in PPP Network with SLNR Precoder," in *The 17th IEEE International Workshop on Signal Processing Advances in Wireless Communications (SPAWC)*, vol. 17, 2016, p. 6.

[119] D. Cao, S. Zhou, C. Zhang, and Z. Niu, "Energy saving performance comparison of coordinated multi-point transmission and wireless relaying," in *IEEE Global Telecommunications Conference (GLOBECOM)*, 2010, pp. 1–5.

[120] P. Lettieri and M. B. Srivastava, "A QoS-aware, energy-efficient wireless node architecture," in *IEEE International Workshop on Mobile Multimedia Communications (MoMuC)*, 1999, pp. 252–261.

[121] G. Miao, N. Himayat, Y. Li, and D. Bormann, "Energy efficient design in wireless OFDMA," in *IEEE International Conference on Communications*, 2008, pp. 3307–3312.

[122] M. Gruber, O. Blume, D. Ferling, D. Zeller, M. A. Imran, and E. C. Strinati, "EARTH-energy aware radio and network technologies," in *IEEE 20th International Symposium on Personal, Indoor and Mobile Radio Communications*, 2009, pp. 1–5.

[123] M. Maaz, P. Mary, and M. Helard, "Energy Minimization in HARQ-I Relay-Assisted Networks with Delay-limited Users," *IEEE Transactions on Vehicular Technology*, vol. PP, no. 99, pp. 1–1, 2017.

[124] M. Ericson, "Total network base station energy cost vs. deployment," in *IEEE 73rd Vehicular Technology Conference (VTC)*, 2011, pp. 1–5.

[125] A. De Domenico, E. C. Strinati, and A. Capone, "Enabling green cellular networks: A survey and outlook," *Computer Communications*, vol. 37, pp. 5–24, 2014.

[126] Z. Niu, "TANGO: traffic-aware network planning and green operation," *IEEE Wireless Communications*, vol. 18, no. 5, pp. 25–29, 2011.

[127] E. Oh, K. Son, and B. Krishnamachari, "Dynamic base station switching-on/off strategies for green cellular networks," *IEEE transactions on wireless communications*, vol. 12, no. 5, pp. 2126–2136, 2013.

[128] I. Ashraf, F. Boccardi, and L. Ho, "Sleep mode techniques for small cell deployments," *IEEE Communications Magazine*, vol. 49, no. 8, pp. 72–79, 2011.

[129] Z. Niu, Y. Wu, J. Gong, and Z. Yang, "Cell zooming for cost-efficient green cellular networks," *IEEE communications magazine*, vol. 48, no. 11, pp. 74–79, 2010.

[130] B. Badic, T. O'Farrrell, P. Loskot, and J. He, "Energy efficient radio access architectures for green radio: large versus small cell size deployment," in *IEEE 70th Vehicular Technology Conference Fall (VTC 2009-Fall)*, 2009, pp. 1–5.

[131] T. A. Le and M. R. Nakhai, "Possible power-saving gains by dividing a cell into tiers of smaller cells," *Electronics letters*, vol. 46, no. 16, pp. 1163–1165, 2010.

[132] C. Khirallah, J. S. Thompson, and H. Rashvand, "Energy and cost impacts of relay and femtocell deployments in long-term-evolution advanced," *IET communications*, vol. 5, no. 18, pp. 2617–2628, 2011.

[133] D. Calin, H. Claussen, and H. Uzunalioglu, "On femto deployment architectures and macrocell offloading benefits in joint macro-femto deployments," *IEEE Communications Magazine*, vol. 48, no. 1, pp. 26–32, 2010.

[134] K. Dufková, J.-Y. Le Boudec, M. Popović, M. Bjelica, R. Khalili, and L. Kencl, "Energy consumption comparison between macro-micro and public femto deployment in a plausible LTE network," in *The 2nd International Conference on Energy-Efficient Computing and Networking*, 2011, pp. 67–76.

[135] M. Wang, X. Zhu, Z. Zeng, S. Wan, and W. Li, "System performance analysis of OFDMA-based femtocell networks," in *International Conference on Communication Technology and Application (ICCTA 2011)*, 2011, pp. 405–410.

[136] A. Amanna, "Green Communications," *Annotated Literature Review and Research Vision*, 2010.

[137] J. Palicot, "Cognitive radio: an enabling technology for the green radio communications concept," in *International Conference on Wireless Communications and Mobile Computing: Connecting the World Wirelessly*, 2009, pp. 489–494.

[138] C. Bae and W. E. Stark, "End-to-end energy–bandwidth tradeoff in multihop wireless networks," *IEEE Transactions on Information Theory*, vol. 55, no. 9, pp. 4051–4066, 2009.

[139] P. Vetter, T. Ayhan, K. Kanonakis, B. Lannoo, K. L. Lee, L. Lefevre, C. Monney, F. Saliou, and X. Yin, "Towards energy efficient wireline networks, an update from GreenTouch," in *18th OptoElectronics and Communications Conference held jointly with International Conference on Photonics in Switching (OECC/PS)*, June 2013, pp. 1–2.

[140] "Greentouch 2014-2015 annual report," http:s3-us-west-2.amazonaws.com/belllabs-microsite-greentouch/uploads/documents/GreenTouch_Annual_Report_2015_-_Final.pdf, accessed: 2017-02-09.

[141] I. Chih-Lin, C. Rowell, S. Han, Z. Xu, G. Li, and Z. Pan, "Toward green and soft: a 5G perspective," *IEEE Communications Magazine*, vol. 52, no. 2, pp. 66–73, 2014.

[142] J. G. Olivier, J. A. Peters, and G. Janssens-Maenhout, "Trends in global CO2 emissions 2012 report," 2012.

[143] D. Feng, C. Jiang, G. Lim, L. J. Cimini, G. Feng, and G. Y. Li, "A survey of energy-efficient wireless communications," *IEEE Communications Surveys & Tutorials*, vol. 15, no. 1, pp. 167–178, 2013.

[144] "Towards Energy proportional Network (TEPN)," http:www.tepn.cominlabs.ueb.eu/, accessed: 2016-12-22.

[145] V. Abhayawardhana, I. Wassell, D. Crosby, M. Sellars, and M. Brown, "Comparison of empirical propagation path loss models for fixed wireless access systems," in *IEEE 61st Vehicular Technology Conference (VTC 2005-Spring)*, vol. 1, 2005, pp. 73–77.

[146] L. Fenton, "The Sum of Log-Normal Probability Distributions in Scatter Transmission Systems," *IRE Transactions on Communications Systems*, vol. 8, no. 1, pp. 57–67, March 1960.

[147] D. B. Cheikh, J.-M. Kelif, M. Coupechoux, and P. Godlewski, "SIR Distribution Analysis in Cellular Networks Considering the Joint Impact of Path-Loss, Shadowing and Fast Fading," *EURASIP Journal on Wireless Comm. and Networking*, no. 137, pp. 1–10, October 2011.

[148] D. H. Nguyen and T. Le-Ngoc, "MMSE precoding for multiuser MISO downlink transmission with non-homogeneous user SNR conditions," *EURASIP Journal on Advances in Signal Processing*, no. 1, pp. 1–12, 2014.

[149] S. S. Christensen, R. Agarwal, E. De Carvalho, and J. M. Cioffi, "Weighted sum-rate maximization using weighted MMSE for MIMO-BC beamforming design," *IEEE Transactions on Wireless Communications*, vol. 7, no. 12, pp. 4792–4799, 2008.

[150] I. Sohn, H. Lee, and K. B. Lee, "Generalized MMSE beamforming for multicell MIMO systems with random user geometry and channel feedback latency," *EURASIP Journal on Wireless Communications and Networking*, vol. 2014, no. 1, pp. 1–10, 2014.

[151] P. Calka, "Precise formulae for the distributions of the principal geometric characteristics of the typical cells of a two-dimensional poisson-voronoi tessellation and a poisson line process," *Advances in Applied Probability*, vol. 35, no. 03, pp. 551–562, 2003.

[152] J.-S. Ferenc and Z. Néda, "On the size distribution of Poisson Voronoi cells," *Physica A: Statistical Mechanics and its Applications*, vol. 385, no. 2, pp. 518–526, 2007.

[153] G. H. Golub and C. F. Van Loan, *Matrix computations*. JHU Press, 2012, vol. 3.

[154] F. Boccardi and H. Huang, "Zero-forcing precoding for the MIMO broadcast channel under per-antenna power constraints," in *IEEE 7th Workshop on Signal Processing Advances in Wireless Communications (SPAWC)*, 2006, pp. 1–5.

[155] R. Wang, J. Zhang, S. Song, and K. B. Letaief, "Average throughput analysis of downlink cellular networks with multi-antenna base stations," in *IEEE 25th Annual International Symposium on Personal, Indoor, and Mobile Radio Communication (PIMRC)*, 2014, pp. 1892–1896.

[156] M. Di Renzo, A. Guidotti, and G. E. Corazza, "Average rate of downlink heterogeneous cellular networks over generalized fading channels: A stochastic geometry approach," *IEEE Transactions on Communications*, vol. 61, no. 7, pp. 3050–3071, 2013.

[157] L. Yu, W. Liu, and R. Langley, "SINR Analysis of the Subtraction-Based SMI Beamformer," *IEEE Transactions on Signal Processing*, vol. 58, no. 11, pp. 5926–5932, Nov 2010.

[158] M. Abramowitz and I. Stegun, *Handbook of mathematical functions: with formulas, graphs, and mathematical tables*. Courier Corporation, 1964, vol. 55.

[159] D. B. Cheikh, J.-M. Kelif, M. Coupechoux, and P. Godlewski, "Multicellular zero forcing precoding performance in Rayleigh and shadow fading," in *IEEE 73rd Vehicular Technology Conference (VTC Spring)*, 2011, pp. 1–5.

[160] J. Ma, Y. J. Zhang, X. Su, and Y. Yao, "On capacity of wireless ad hoc networks with MIMO MMSE receivers," *IEEE Transactions on Wireless Communications*, vol. 7, no. 12, pp. 5493–5503, December 2008.

[161] S. Govindasamy, D. W. Bliss, and D. H. Staelin, "Spectral Efficiency in Single-Hop Ad-Hoc Wireless Networks with Interference Using Adaptive Antenna Arrays," *IEEE Journal on Selected Areas in Communications*, vol. 25, no. 7, pp. 1358–1369, September 2007.

[162] A. Guionnet, O. Zeitouni *et al.*, "Concentration of the spectral measure for large matrices," *Electron. Comm. Probab*, vol. 5, pp. 119–136, 2000.

INSA de RENNES
Service des Formations

AVIS DU JURY SUR LA REPRODUCTION DE LA THESE SOUTENUE

Titre de la thèse:
Energy efficiency-spectral efficiency tradeoff in interference-limited wireless networks

Nom Prénom de l'auteur : ALAM AHMAD MAHBUBUL

Membres du jury :
- Monsieur DENEIRE Luc
- Monsieur DI RENZO Marco
- Monsieur LAGRANGE Xavier
- Monsieur MARY Philippe
- Monsieur GORCE Jean-Marie
- Madame BOUCHERET Marie-Laure
- Monsieur BAUDAIS Jean-Yves

Président du jury : ML Boucheret

Date de la soutenance : 30 Mars 2017

Reproduction de la these soutenue

Thèse pouvant être reproduite en l'état
~~Thèse pouvant être reproduite après corrections suggérées~~

Fait à Rennes, le 30 Mars 2017

Signature du président de jury

Le Directeur,

M'hamed DRISSI

INSTITUT NATIONAL des SCIENCES APPLIQUÉES · RENNES ·

Résumé

L'une des stratégies utilisée pour augmenter l'efficacité spectrale (ES) des réseaux cellulaires est de réutiliser la bande de fréquences sur des zones relativement petites. Le problème majeur dans ce cas est un plus grand niveau d'interférence, diminuant l'efficacité énergétique (EE). En plus d'une plus grande largeur de bande, la densification des réseaux (cellules de petite taille ou multi-utilisateur à entrées multiples et sortie unique, MU-EMSO), peut augmenter l'efficacité spectrale par unité de surface (ESuS). La consommation totale d'énergie des réseaux sans fil augmente en raison de la grande quantité de puissance de circuit consommée par les structures de réseau denses, réduisant l'EE. Dans cette thèse, la région EE-ES est caractérisé dans un réseau cellulaire hexagonal en considérant plusieurs facteurs de réutilisation de fréquences (FRF), ainsi que l'effet de masquage. La région EE-ESuS est étudiée avec des processus de Poisson ponctuels (PPP) pour modéliser un réseau MU-EMSO avec un précodeur à rapport signal sur fuite plus bruit (RSFB). Différentes densités de station de base (SB) et nombre d'antennes aux SB avec une consommation d'énergie statique sont considérées.

Nous caractérisons d'abord la région EE-SE dans le réseau cellulaire hexagonal pour différentes FRF, avec et sans masquage. Avec le masquage, la mesure de coupure ε-EE-ES est proposée pour évaluer les performances. Les courbes EEES présentent une grande partie linéaire, due à la consommation de puissance statique, suivie d'une forte diminution de l'EE, puisque le réseau est homogène et limité par les interférences. Les résultats montrent qu'un FRF de 1 pour les régions proches de la SB et des FRF plus élevés sur le bord de la cellule améliorent le point optimal du EE-ES. En outre, un FRF de 1 est le meilleur choix pour une valeur élevée de coupure en raison d'une réduction du rapport signal sur interférence plus bruit (RSIB).

Les précodeurs sont utilisés en liaison descendante des réseaux cellulaires MU-EMSO à accès multiple par division spatiale (AMDS) pour améliorer le RSIB. La géométrie stochastique a été utilisée intensivement pour analyser de tels systèmes complexes. Nous obtenons une expression analytique de l'ESuS en régime asymptotique, c.-à-d. nombre d'antennes et d'utilisateurs infinis, en utilisant des résultats de matrices aléatoires et de géométrie stochastique. Les SBs et les utilisateurs sont modélisés par deux PPP indépendants et le précodage RSFB est utilisé. L'EE est dérivée d'un modèle de consommation de puissance linéaire. Les simulations de Monte Carlo montrent que les expressions analytiques sont précises même pour un nombre faible d'antennes et d'utilisateurs. Les résultats montrent également que le précodeur RSFB offre de meilleurs performances que le précodeur forçage à zéro (FZ), qui est typiquement utilisé dans la literature. Les résultats numériques pour le précodeur RSFB montrent que déployer plus de SBs ou d'antennes aux BSs augmente l'ESuS, mais que le gain dépend du rapport des densités SB-utilisateurs et du nombre d'antennes lorsque la densité de l'utilisateur est fixe. L'EE augmente seulement lorsque l'augmentation de l'ESuS est plus importante que l'augmentation de la consommation d'énergie par unité de surface. D'autre part, lorsque la densité d'utilisateur augmente, l'ESuS dans la région limitée par les interférences peut être améliorée en déployant davantage de SB sans sacrifier l'EE et le débit ergodique des utilisateurs.

Abstract

One of the used strategies to increase the spectral efficiency (SE) of cellular network is to reuse the frequency bandwidth over relatively small areas. The major issue in this case is higher interference, decreasing the energy efficiency (EE). In addition to the higher bandwidth, densification of the networks (e.g. small cells or multi-user multiple input single output, MUMISO) potentially increases the area spectral efficiency (ASE). The total energy consumption of the wireless networks increases due to the large amount of circuit power consumed by the dense network structures, leading to the decrease of EE. In this thesis, the EE-SE achievable region is characterized in a hexagonal cellular network considering several frequency reuse factors (FRF), as well as shadowing. The EE-ASE region is also studied using Poisson point processes (PPP) to model the MUMISO network with signal-to-leakage-and-noise ratio (SLNR) precoder. Different base station (BS) densities and different number of BS antennas with static power consumption are considered.

The EE-SE region in a hexagonal cellular network for different FRF, both with and without shadowing is first characterized. When shadowing is considered in addition to the path loss, the ε-SE-EE tradeoff is proposed as an outage measure for performance evaluation. The EE-SE curves have a large linear part, due to the static power consumption, followed by a sharp decreasing EE, since the network is homogeneous and interference-limited. The results show that FRF of 1 for regions close to BS and higher FRF for regions closer to the cell edge improve the EE-SE optimal point. Moreover, better EE-SE tradeoff can be achieved with higher outage values. Besides, FRF of 1 is the best choice for very high outage value due to the significant signal-to-interference-plus-noise ratio (SINR) decrease.

In downlink, precoders are used in space division multiple access (SDMA) MU-MISO cellular networks to improve the SINR. Stochastic geometry has been intensively used to analyse such a complex system. A closed-form expression for ASE in asymptotic regime, i.e. number of antennas and number of users grow to infinity, has been derived using random matrix theory and stochastic geometry. BSs and users are modeled by two independent PPP and SLNR precoder is used at BS. EE is then derived from a linear power consumption model. Monte Carlo simulations show that the analytical expressions are tight even for moderate number of antennas and users. Moreover, the EE-ASE curves have a large linear part before a sharply decreasing EE, as observed for hexagonal network. The results also show that SLNR outperforms the zero-foring (ZF) precoder, which is typically used in literature. Numerical results for SLNR show that deploying more BS or a large number of BS antennas increase ASE, but the gain depends on the BS-user density ratio and on the number of antennas when user density is fixed. EE increases only when the increase in ASE dominates the increase of the power consumption per unit area. On the other hand, when the user density increases, ASE can be improved by deploying more BS without sacrificing EE and the ergodic rate of the users.

INSA RENNES

N° d'ordre : 17ISAR 06 / D17 -06

Institut National des Sciences Appliquées de Rennes

20, Avenue des Buttes de Coëmes • CS 70839 • F-35708 Rennes Cedex 7

Tel : 02 23 23 82 00 - Fax : 02 23 23 83 96